



Diana Martins Bordalo

Licenciada em Biologia

Fate map of zebrafish left-right organizer

Dissertação para obtenção do Grau de Mestre em
Genética Molecular e Biomedicina

Orientador: Prof^a Doutora Susana Lopes, Investigadora Principal,
Centro de Estudos de Doenças Crónicas da Faculdade de Ciências
Médicas

Co-orientador: Prof^a Doutora Leonor Saúde, Investigadora Principal

Júri:

Presidente: Prof^a Doutora Paula Maria Theriaga

Mendes Bernardes Gonçalves

Arguentes: Prof^a Doutora Rita Leonor Alvares

Cabral Figueiredo Fior Sousa Soares

Fate map of zebrafish left-right organizer

Copyright © Diana Martins Bordalo, Faculdade de Ciências e Tecnologia, Universidade Nova de Lisboa.

A Faculdade de Ciências e Tecnologia e a Universidade Nova de Lisboa têm o direito, perpétuo e sem limites geográficos, de arquivar e publicar esta dissertação através de exemplares impressos reproduzidos em papel ou de forma digital, ou por qualquer outro meio conhecido ou que venha a ser inventado, e de a divulgar através de repositórios científicos e de admitir a sua cópia e distribuição com objectivos educacionais ou de investigação, não comerciais, desde que seja dado crédito ao autor e editor.

*“Education is an admirable thing, but it is well to remember from time to time that
nothing that is worth knowing can be taught.”*

Oscar Wilde

Acknowledgements

Primeiramente gostaria de agradecer à professora Rita Fior, não só por me fazer apaixonar por biologia do desenvolvimento, como por ter desencadeado esta tese quando me apresentou à Susana Lopes. Agradecer à Leonor Saúde pela sua orientação ao longo deste ano, mas queria agradecer especialmente à Susana Lopes por me ter guiado e por me ter feito crescer como cientista e pessoa. Claramente uma das melhores orientadoras que já tive, nunca desiste das pessoas e apoia-nos no que for preciso. Não te consigo agradecer o suficiente, mas posso dar-te casa quando me fores visitar ao EMBL. A todo o grupo do IMM (Instituto de Medicina Molecular) por me fazerem sentir em casa, mesmo que só lá tenha estado uma semana. À Raquel por me ter mostrado os cantos à casa, à Hanna e à Rita pelo convívio e desabafos, à Judit por transmitir sempre uma imensa felicidade, nem que mais não seja convertida em iguarias espanholas. Ao Pedro pela calma contagiante, à Bárbara pelas boas gargalhas dada a sua extravagante personalidade e à Mónica pelo seu lado tão humano que se reflecte em tudo o que faz. Em particular à Petra, que é uma pessoa que me fascina e que eu admiro, pela maneira como encara o mundo e as pessoas. Por me ter ensinado tanto, às vezes com tão poucas palavras.

Ao meu gato pelo seu serviço infalível de despertador às 7h30 da manhã, que me permitiu manter um bom ritmo de trabalho. E também por me ajudar a converter frustrações da tese em mimos. Ao meu colega de casa permanente, que mesmo de terras italianas, todos os dias me alegra o coração. E também, por cada vez que ele regressa a Portugal, me trazer um abraço apertado, carregado de saudade, que faz desaparecer todo o stress e preocupação. Obrigada a toda a família, que torna a distância mais pequena. Claro que jamais me podia esquecer das meninas mulheres, que arrasto comigo à praticamente 10 anos. A Monike, que mesmo lá de longe da Hungria, se farta de perguntar pela minha tese e de me mandar postais, um muito obrigada. Nesta situação em particular, devo um especial obrigado à Lúcia. Obrigada por toda a inspiração que me transmitiste com a tua tese, o teu perfeccionismo e a tua persistência. Obrigada pela directa partilhada na noite anterior à entrega da tese, e por estares no backstage da defesa. Estas duas Arrastonas são uma contribuição na minha vida que faço questão de manter. Ao meu pai que sempre me disse, como um dogma e certeza absoluta, “está tranquila, tudo vai correr bem”. Que me enche de mimos à distância e ao perto, e eu adoro mesmo que lhe chame “meles”. E à Anita, por tomar bem conta dela e de mim. Obrigada por me lembrarem constantemente como uma família unida é feita com os que estão presentes e com as memórias dos que já passaram. Dank je wel André, por seres um enorme apoio para a minha mãe. E em especial à minha mãe, que com todos os desafios que surgiram, encarou-os de frente, armada de um sorriso e uma tremenda força de vontade, fazendo-se deles sua amiga. Parte desses desafios, muito em breve ultrapassados, tornaram-na mais forte e foi essa força e vivacidade que ela me transmitiu durante este longo percurso. Mãe, quando dizes que não percebes como é que tens “uma filha assim”, olha-te ao espelho; observa e percebe.

Abstract

The organizer is a ciliated signalling transient organ, responsible for the patterning of embryo tissues during embryonic development. In higher vertebrates, such as mouse and chick, this organizer (the node and the Hensen's node, respectively) performs dorsalventral and anteriorposterior axis definition, as well as left-right patterning of the internal organs. In lower vertebrates, such as frog and zebrafish, there is a separate specialized organ for left-right purposes called the Gastrocoel Roof Plate (GRP) and Kupffer's Vesicle (KV), respectively.

It is known that mouse and chick organizer cells give rise to structures like floor plate, notochord, hypochord and somites. Frog GRP originates all these but floor plate. In zebrafish, at 13-14 somite stage (ss) the KV finished its left-right patterning but what happens to this organizer' cells is still poorly studied.

This research attempts to understand the fate and behaviour of the KV cells. We followed the fate of KV cells by live imaging and by tight time-courses with fixed larvae. We assessed in detail their proliferative and death profile, as well as cilia length progression from 9-10 ss until 29-30 ss.

We conclude that the KV cells mostly follow the evolutionarily conserved fates described for other organizers. These cells mainly incorporate the notochord and hypochord; few cells incorporate the floor plate and the somites. As a novelty, it is also hypothesized that the hypural cell fate may be among the KV cell fates.

Keywords: Kupffer's vesicle, fates, floor plate, notochord, hypochord, somite, cilia.

Resumo

O organizador é o órgão temporário ciliado responsável pela padronização dos vários tecidos que constituem o embrião. Em vertebrados superiores, tal como ratinho e galinha, o organizador para além de estabelecer os eixos dorsoventral e anteroposterior, também estabelece o eixo esquerda direita dos órgãos internos. Em vertebrados inferiores, tal como sapo e peixe zebra existe uma outra estrutura especializada na padronização esquerda direita, chamada chão do gastrocele (GRP) e a vesícula de Kupffer (KV), respectivamente.

Sabe-se que em ratinho e galinha o organizador dá origem a estruturas como chão do tubo neural, notocorda, hipocorda e sómitos. O GRP do sapo, origina todas estas estruturas à excepção do chão do tubo neural. Em peixe zebra, no estágio de 13-14 sómitos (ss) a vesícula de Kupffer está a finalizar a sua função na padronização esquerda direita, mas o que acontece às células que constituem este organizador está muito pouco estudado.

Esta investigação prendeu-se pelo objectivo de perceber o destino e comportamento das células da KV. Usando imagiologia em live e complementação com técnicas moleculares, podemos aferir em detalhe o destino destas células, o seu perfil proliferativo e apoptótico, bem como a progressão do tamanho ciliar dos 9-10 ss até aos 29-30 ss.

Concluimos que a maioria as células da KV segue um destino evolucionariamente conservado entre organizadores, incorporando a notocorda e a hipocorda, em número reduzido há também a integração no chão do tubo neural e nos sómitos. Foi também admitida a hipótese do destino de algumas destas células ser como hipural.

Palavras-chave: Vesícula de Kupffer, destinos celulares, chão do tubo neural, notocorda, hipocorda, somitos, cílios.

Contents

| | |
|--|-------------|
| ACKNOWLEDGEMENTS | V |
| ABSTRACT | VI |
| RESUMO | VII |
| CONTENTS | VIII |
| LIST OF FIGURES | XI |
| LIST OF TABLES | XIV |
| INTRODUCTION | 1 |
| 1. EMBRYONIC DEVELOPMENT | 1 |
| 2. LEFT-RIGHT ORGANIZER | 7 |
| 2.1 <i>Left-Right Asymmetry</i> | 9 |
| 2.1.1 Hypothesis and Models | 10 |
| 2.1.2 Problems with Asymmetry..... | 10 |
| 2.2 <i>Organizer's fates</i> | 11 |
| 3. ZEBRAFISH LEFT-RIGHT ORGANIZER | 13 |
| 3.1 Development of Kupffer's Vesicle..... | 14 |
| 3.2 Development of posterior body..... | 16 |
| AIMS | 21 |
| MATERIALS AND METHODS | 23 |
| 1. ZEBRAFISH HUSBANDRY AND MAINTENANCE | 23 |
| 2. LIVE IMAGING AND MICROSCOPY | 24 |
| 2.1 <i>Two-Photon Microscope – Migration studies</i> | 24 |

| | | |
|--------|--|-----------|
| 2.1.1 | Whole Mount..... | 24 |
| 2.1.2 | Image Acquisition | 24 |
| 2.2 | <i>Andor Spinning Disk – Cell Ablation</i> | 25 |
| 2.2.1 | Whole Mount..... | 25 |
| 2.2.2 | Cell laser Ablation | 25 |
| 2.3 | <i>Confocal Microscopy – Fixed Samples</i> | 26 |
| 3. | MOLECULAR TECHNIQUES..... | 27 |
| 3.1 | <i>Fixation of Embryos</i> | 27 |
| 3.2 | <i>In situ Hybridization</i> | 27 |
| 3.2.1. | Probe information and Synthesis..... | 28 |
| 3.2.2. | Protocol description..... | 29 |
| 3.3 | <i>Immunostaining</i> | 31 |
| 3.4 | <i>In situ Hybridization combined with Immunostaining</i> | 32 |
| 3.5 | <i>TUNEL Assay</i> | 33 |
| 3.6 | <i>TUNEL followed by immunostaining</i> | 34 |
| 4. | DATA ANALYSIS | 34 |
| 4.1 | <i>Fiji / Image J software</i> | 34 |
| 4.2 | <i>Huygens Professional software</i> | 35 |
| 4.3 | <i>Imaris Software</i> | 35 |
| | RESULTS | 37 |
| 1. | LIVE IMAGING REVEALED THAT KV CELLS INCORPORATE THE NOTOCHORD, HYPOCHORD, FLOOR PLATE AND TAIL MESENCHYME | 37 |
| 2. | COMPLEMENTARY INFORMATION FROM FIXED SAMPLES..... | 48 |
| 2.1 | <i>Kupffer’s vesicle cells undergo proliferation and programmed cell death</i> | 48 |
| 2.1.1 | KV cell proliferation occurs between 21-22 and 25-26 somite stage | 49 |
| 2.1.2 | Kupffer’s vesicle cells show low levels of apoptosis | 52 |
| 2.2 | <i>KV cell fates</i> | 57 |
| 2.2.1 | <i>No tail</i> marker co-localizes with KV cells..... | 57 |
| 2.2.2 | <i>mesogenin-1</i> partially co-localizes with KV cells | 59 |
| 2.2.3 | <i>Shh</i> marker for hypochord and floor plate | 61 |
| 3. | LONG MOTILE CILIA RETRACT WITH DEVELOPMENTAL PROGRESSION..... | 62 |
| 3.1 | <i>Kupffer’s vesicle cilia length decreases with developmental progression</i> | 62 |
| 4. | LASER ABLATION AND SUCTION OF KV CELLS | 65 |
| | DISCUSSION AND CONCLUSION..... | 68 |
| 1. | KV CELLS SHOW COLLECTIVE AND INDIVIDUAL MIGRATION | 68 |
| 1.1. | <i>The KV compact group of cells becomes part of the midline</i> | 69 |

| | |
|--|-----------|
| 1.2. <i>KV individual cell migration leads to integration in several tail structures</i> | 70 |
| 2. KV CELLS PRESENT A PROLIFERATIVE AND DEATH DYNAMICS | 74 |
| 2.1 <i>There is a proliferative window for the GFP marked cells</i> | 74 |
| 2.2 <i>The apoptosis rate varies little between developmental stages</i> | 75 |
| 3. CILIA OF THE KV CELLS RETRACT AND BECOME SHORT CILIA LATER IN THE DEVELOPMENT | 76 |
| 4. WHAT IS THE INFLUENCE OF KV CELL ABLATION IN TAIL DEVELOPMENT?..... | 77 |
| 5. CONCLUSION AND FUTURE WORK | 78 |
| REFERENCES | 79 |
| | 87 |
| APENDDIX | 87 |
| APPENDIX A..... | 87 |
| <i>Fiji Macro</i> | 87 |
| APPENDIX B..... | 88 |
| <i>Cilia Length Histograms</i> | 88 |

List of figures

Introduction

| | |
|---|----|
| <i>Figure 1. 1 - Mammalian early development.</i> | 2 |
| <i>Figure 1. 2 - Gastrulation process in the chick embryo.</i> | 3 |
| <i>Figure 1. 3 - Neurulation process.</i> | 4 |
| <i>Figure 1. 4 - Comparison of vertebrate cleavage patterns.</i> | 4 |
| <i>Figure 1. 5 - Phylogenetic tree showing the most common model organisms used in research.</i> | 5 |
| <i>Figure 1. 6 - Frog early development, gastrulation process.</i> | 6 |
| <i>Figure 1. 7 - Zebrafish early development.</i> | 6 |
| <i>Figure 1. 8 - Fate map of model organisms</i> | 7 |
| <i>Figure 1. 9 - Scheme of transverse section of different types of cilia regarding its motility and the relative position in the cell.</i> | 8 |
| <i>Figure 1. 10 - Self-enhancement and lateral inhibition mechanism</i> | 9 |
| <i>Figure 1. 11 - Asymmetry breakage mechanisms.</i> | 10 |
| <i>Figure 1. 12 – Situs solitus and Situs inversus.</i> | 11 |
| <i>Figure 1. 13 – Dorsal forerunner cell cluster at approximately 26 ss.</i> | 12 |
| <i>Figure 1. 14 - Dorsal forerunner cells tracing in the tail.</i> | 13 |
| <i>Figure 1. 15 - Scheme of dorsal forerunner cells (DFCs) formation during gastrulation phase.</i> | 14 |
| <i>Figure 1. 16 - Scheme of Kupffer's Vesicle formation.</i> | 15 |
| <i>Figure 1. 17 - Characteristic mass cell movements during tail formation in zebrafish.</i> | 16 |
| <i>Figure 1. 18 - Notochord structural aspects in a Prim-5 zebrafish embryo.</i> | 17 |
| <i>Figure 1. 19 - Axolotl Transmission electron microscopy (TEM) micrograph of a hypochord cell.</i> | 19 |
| <i>Figure 1. 20 - Mitotic indices within zebrafish tailbud.</i> | 19 |
| <i>Figure 1. 21 - Apoptotic studies in zebrafish.</i> | 20 |

Materials and Methods

| | |
|--|----|
| <i>Figure 3. 1 - Protocol used for laser ablation.</i> | 26 |
|--|----|

Results

| | |
|--|-----------|
| <i>Figure 4. 1 – KV and GFP marked cells landmarks throughout the developmental stages covered.....</i> | <i>39</i> |
| <i>Figure 4. 2 – Transgenic line foxj1a:GFP at 19-20 ss, with GFP marked cells incorporating the notochord.....</i> | <i>40</i> |
| <i>Figure 4. 3 – Transgenic line foxj1a:GFP with GFP marked cells incorporated into the notochord from 17-18 ss until 25-26 ss. A total of 12 GFP marked cells were counted in the notochord.</i> | <i>41</i> |
| <i>Figure 4. 4 – Zebrafish foxj1a:GFP line, GFP marked cells incorporated into the notochord from 25-26 ss until 29-30 ss.</i> | <i>41</i> |
| <i>Figure 4. 5 – Fixed zebrafish embryo of foxj1a:GFP transgenic line at Prim-5 developmental stage.</i> | <i>42</i> |
| <i>Figure 4. 6 - Migration of Kupffer's vesicle compact group in foxj1a:GFP zebrafish transgenic line.....</i> | <i>42</i> |
| <i>Figure 4. 7 – Movie snapshots of foxj1a:GFP zebrafish transgenic line from 17-18 ss until 29-30 ss. Ventral GFP marked cells migration.....</i> | <i>43</i> |
| <i>Figure 4. 8 – Movie snapshot of foxj1a:GFP transgenic line. GFP marked cells proliferation</i> | <i>44</i> |
| <i>Figure 4. 9 – Movie snapshot of foxj1a:GFP transgenic line. GFP marked cells incorporating the hypochord.....</i> | <i>45</i> |
| <i>Figure 4. 10 – Transgenic line foxj1a:GFP with total number of GFP marked cells incorporated into the hypochord from 23-24 ss until 27-28 ss.....</i> | <i>45</i> |
| <i>Figure 4. 11 – Transgenic line foxj1a:GFP with total number of GFP marked cells incorporated into the floor plate</i> | <i>46</i> |
| <i>Figure 4. 12 - Examples of embryo morphology after live imaging.</i> | <i>48</i> |
| <i>Figure 4. 13 - PCNA positive cells throughout development.....</i> | <i>49</i> |
| <i>Figure 4. 14 - Cell number throughout the developmental stages.</i> | <i>50</i> |
| <i>Figure 4. 15 - Summarized table with examples per developmental stages of GFP marked cells, PCNA marked cells, co-localization of the two markers and total number of embryos.....</i> | <i>51</i> |
| <i>Figure 4. 16 - Apoptotic rate throughout development.....</i> | <i>53</i> |
| <i>Figure 4. 17 - Examples of apoptosis for each somite stage. GFP marked cells, apoptotic cells, nuclei and total number of embryos</i> | <i>54</i> |
| <i>Figure 4. 18 - Examples of apoptosis for embryos used in live imaging. GFP marked cells, apoptotic cells, nuclei and total number of embryos</i> | <i>55</i> |
| <i>Figure 4. 19 - Apoptotic rates for embryos used in live imaging with two-photon microscope</i> | <i>56</i> |
| <i>Figure 4. 20 - Cell number per somite stage taking into account the apoptotic rates.</i> | <i>56</i> |
| <i>Figure 4. 21 - Summarized table with developmental stages correspondent to ntl and GFP marked cells, co-localization of the two markers and total number of embryos.....</i> | <i>58</i> |
| <i>Figure 4. 22 - Immunostaining with antibody against GFP, performed in fixed embryos with 25-26 ss. .</i> | <i>59</i> |
| <i>Figure 4. 23 - Summarized table with examples for each developmental stages correspondent GFP marked cells, mesogenin1 marked cells, co-localization of the two markers and total number of embryos.</i> | <i>60</i> |

| | |
|---|-----------|
| <i>Figure 4. 24 – Shh staining in a 19-20 ss zebrafish.....</i> | <i>61</i> |
| <i>Figure 4. 25 - Cilia length throughout the analysed somite stages.</i> | <i>63</i> |
| <i>Figure 4. 26 – Example of notochord cilia in a zebrafish embryo with 25-26 ss</i> | <i>64</i> |
| <i>Figure 4. 27 - Cilia number throughout development.</i> | <i>64</i> |
| <i>Figure 4. 28 - Kupffer vesicle at 13-14 ss stage with different magnifications.....</i> | <i>65</i> |
| <i>Figure 4. 29 – Before and after laser ablation process in a 13-14 ss stage embryo.....</i> | <i>66</i> |
| <i>Figure 4. 30 - Kupffer vesicle at 13-14s stage using foxj1a:GFP transgenic line</i> | <i>66</i> |

List of tables

Materials and Methods

| | |
|--|-----------|
| <i>Table 3.1 – Description of the In situ probes.....</i> | <i>28</i> |
| <i>Table 3.2– Description of the primary antibodies used for the immunostainings.</i> | <i>31</i> |
| <i>Table 3.3– Description of the secondary antibodies used for the immunostainings.</i> | <i>32</i> |

Results

| | |
|--|-----------|
| <i>Table 4. 1 – Summary of GFP marked cells incorporation and positions at 29-30 ss in the foxj1a:GFP transgenic line.</i> | <i>47</i> |
| <i>Table 4. 2 - Number of PCNA positive cells counted per embryo within a somite stage.</i> | <i>49</i> |
| <i>Table 4. 3 - Number of GFP marked cells counted per embryo within a somite stage.....</i> | <i>50</i> |
| <i>Table 4. 4 - Apoptotic rates (%) found for each developmental stage, in embryos used for live imaging with two-photon microscope.....</i> | <i>53</i> |
| <i>Table 4. 5 - Table with developmental stages, total number of embryos used, total number of cilia per developmental stage and cilia length average.....</i> | <i>62</i> |



Introduction

1. Embryonic development

Embryogenesis is a process whereby an embryo develops and forms. This process comprises several common developmental phases among most vertebrate organisms, being zygote stage the first. The zygote results from the egg fertilization by the sperm and fusion of paternal with maternal genetic material. In mammals, the zygote (Figure 1.1 A) enters a series of quick divisions without growth called the cleavage stage¹.

In the end of this stage, the zygote is called morula (Figure 1.1 B). Through compaction and differentiation of these cells is formed an outer layer – throphoblast – and an inner layer – embryoblast² (Figure 1.1 C). The embryoblast starts to cluster at the animal pole, forming the inner cell mass and leaving a blastocoel cavity in the vegetal pole.

At this point the embryo is called the blastocyst and the process is called blastulation (Figure 1.1 C). With differentiation of the blastocyst, the inner cell mass becomes divided in epiblast and the hypoblast (Figure 1.1 D)³. At the same time, the amniotic cavity is formed near the animal pole (Figure 1.1 E).

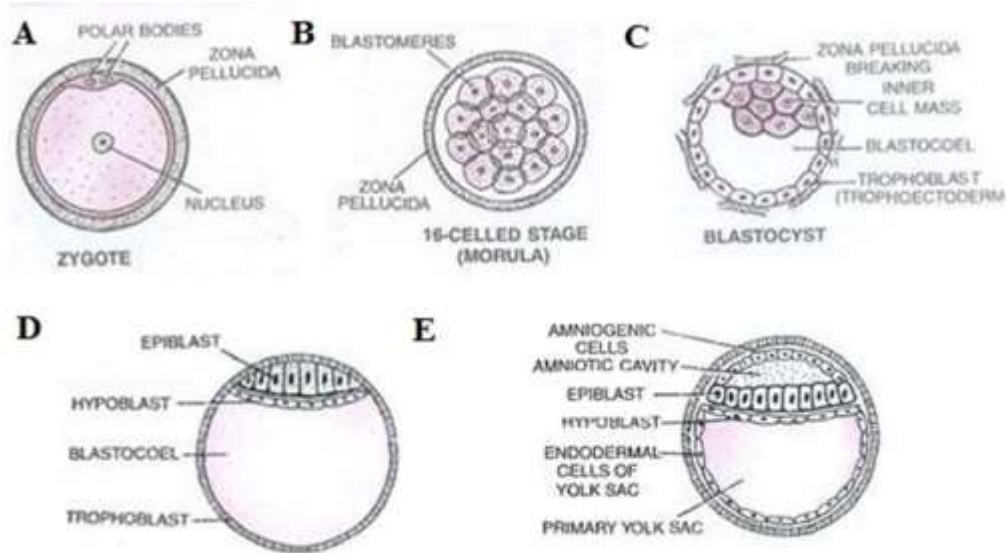


Figure 1. 1 - Mammalian early development. A – Zygote; B – Morula stage; C – Blastocyst after compaction and formation of the inner cell mass. D – Further differentiation of the inner cell mass in epiblast and hypoblast; E – Formation of the amniotic cavity. Image adapted from website <http://www.yourarticlelibrary.com/biology/>⁴

With further development, the epiblast and hypoblast form the bilateral disk. When the primitive streak is formed the gastrulation begins (Figure 1.2)⁵.

"IT IS NOT BIRTH, MARRIAGE, OR DEATH, BUT GASTRULATION, WHICH IS TRULY THE MOST IMPORTANT TIME IN YOUR LIFE." LEWIS WOLPERT (1986)

The epiblast cells migrate from the lateral sides, through the primitive streak, in the direction of the hypoblast layer³. The epiblast cells, as a consequence of ingression have a mesendoderm fate, since the hypoblast cells are replaced by ingressing cells that become endoderm³. These epiblast cells continue to migrate through the primitive streak and form an intermediate layer called mesoderm. At this point, with all the three germ layers formed, the gastrulation is complete and the earlier top epiblast layer is now the ectoderm, the intermediate layer is the mesoderm and the bottom layer is the endoderm².

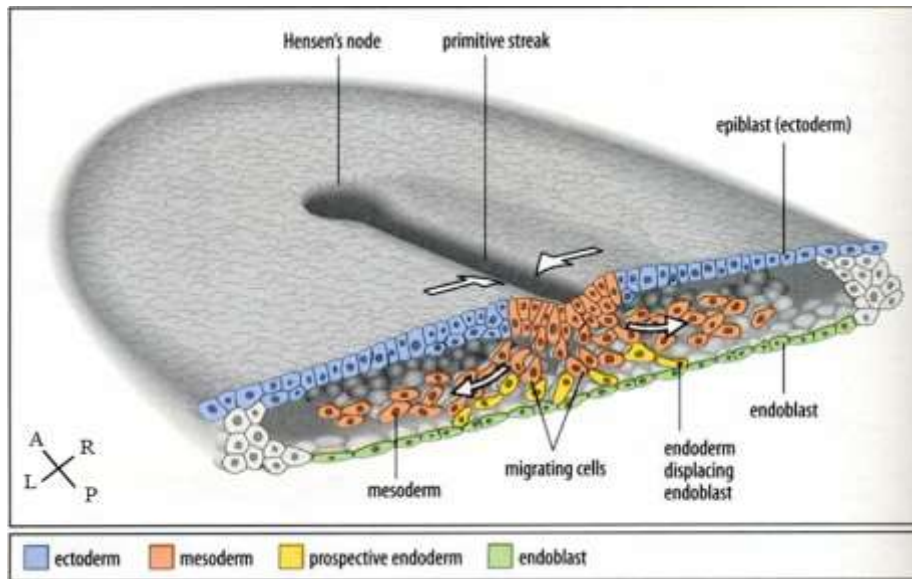


Figure 1. 2 - Gastrulation process in the chick embryo. In mouse the process occurs in the same manner, but the Hensen's node is called Node. Image taken from Wolpert, Tickle (2011), "Principles of Development"²

In the beginning of neurulation, some central cells in the mesoderm start to differentiate to form the notochord, which is a rod-like structure along the embryo responsible to signal and pattern several tissues around it⁶.

This structure will send differentiation signals to the upper tissue – ectoderm – inducing its thickening and formation of the neural plate, at whose edges are neural crest cells (Figure 1.3). The infolding of the neural plate forms the neural groove and the correspondent lateral folds. These neural folds keep converging until they touch each other and completely detach from the epidermis, forming the neural tube.

At the same time this process happens, the notochord is signalling the mesoderm. Further differentiate into paraxial or presomitic, intermediate, lateral plate mesoderm and further differentiation of presomitic mesoderm will lead to somitogenesis. The final process of the embryo development is the organogenesis, where the internal organs are formed³.

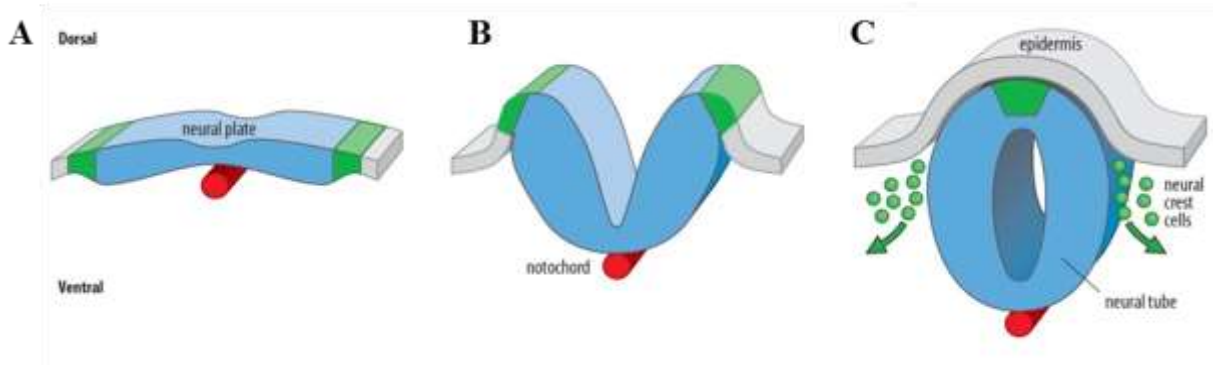


Figure 1.3 - Neurulation process. A - With differentiation signals from the notochord (red) to the ectoderm tissue, the neural plate (blue) is formed and starts to fold within. B - Further folding of the neural folds, with attention to its borders – neural crest (green). C - Total closure and detachment of the neural plate, forming the neural tube. In most vertebrates, neural crest cells migration starts upon closure of the neural tube. Image adapted from Huang et al.(2004)⁶

The processes described before are typical of mammalian embryonic development³ but in spite of the similarities⁵, specific characteristics such as the yolk amount, its distribution in the zygote, as well as the angle of the mitotic spindle, dictates distinct developmental patterns (Figure 1.4).

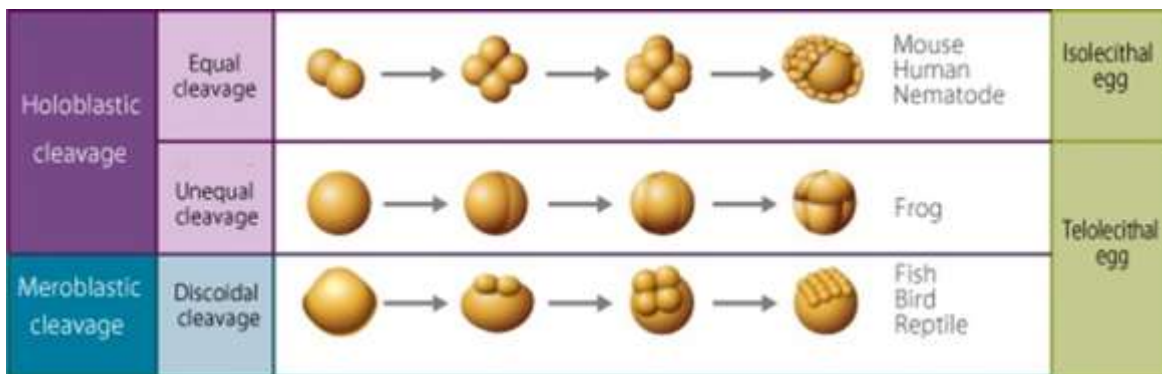


Figure 1.4 - Comparison of vertebrate cleavage patterns. Adapted figure from “A comprehensive approach to Life Science, Second Edition, University of Tokyo⁹⁴

Chicken (*Gallus gallus*) is the closest vertebrate to mouse (Figure 1.5) but the cleavage pattern is similar to the fish. Nevertheless, from the blastodisc stage on (equivalent in mouse to the bilateral disk), the developmental pattern, in spite of quicker, is much similar to the mouse embryo³.

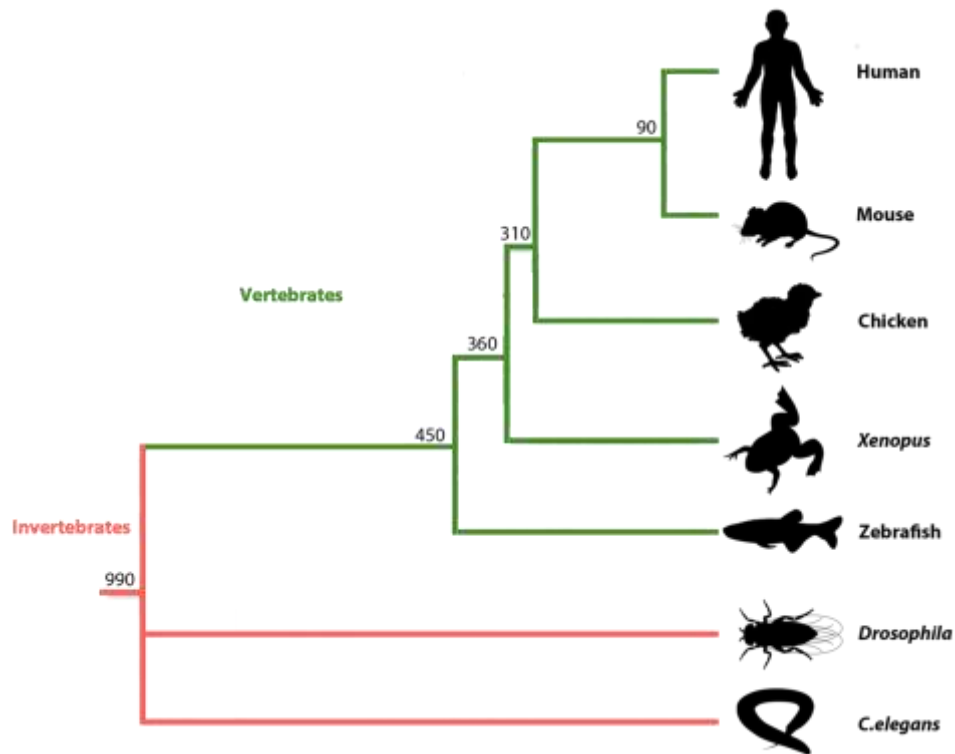


Figure 1. 5 - Phylogenetic tree showing the most common model organisms used in research. The divergence times in millions of years ago (Mya) are shown based on multigene and multiprotein studies. Branch lengths are not proportional to time. Image taken from Wheeler, Brändli (2009) ⁷

In frog (*Xenopus laevis*), there is the blastula (with the characteristic blastocoel) but with no primitive streak formation, the cellular movements observed from early gastrula, are very different from chick and mouse. In this case, the major cell movement observed is epiboly and involution (Figure 1.6 A,B), while in mouse and chick is ingression through the primitive streak. Notwithstanding, a fairly similar event to ingression is the migration of the cells through the dorsal blastopore lip. This involution will generate the endoderm and mesoderm, while the epiboly happening in the outer layer will lead to the ectoderm formation (Figure 1.6 C) ³.

Zebrafish (*Danio rerio*), being the most phylogenetically distant from the organisms described previously (Figure 1.5), is also the one with a more distinct development (Figure 1.7 A-D). Even with very different cleavages patterns (Figure 1.4) comparing with frog, there are several similarities. Both have the external epiboly of the enveloping layer, that forms the ectoderm and both have involution movements of the epiblast cells, forming the mesoderm and ectoderm.

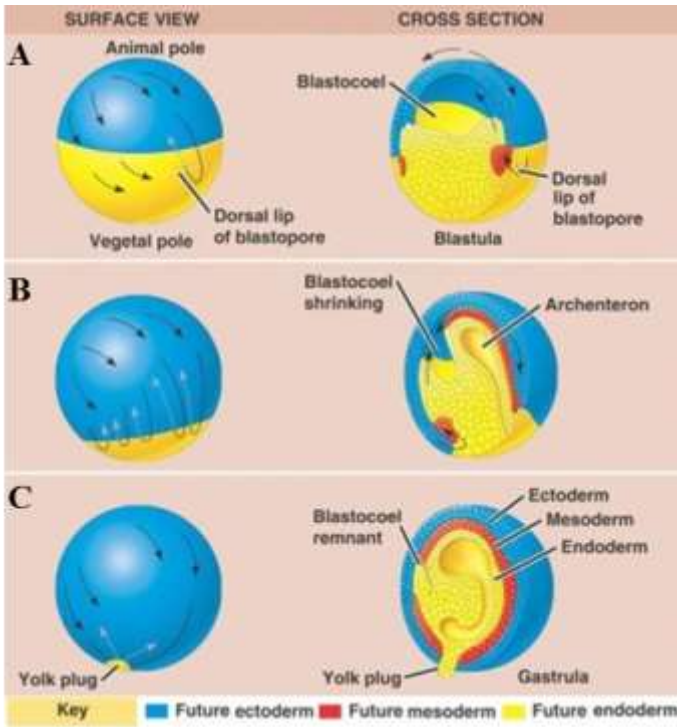


Figure 1. 6 - Frog early development, gastrulation process. A – Beginning of outer layer epiboly and involution of cells through the dorsal blastopore lip. B - Archenteron formation, C – Final phases of gastrulation, already with the three germ layers formed. Adapted from Gilbert (2008)¹

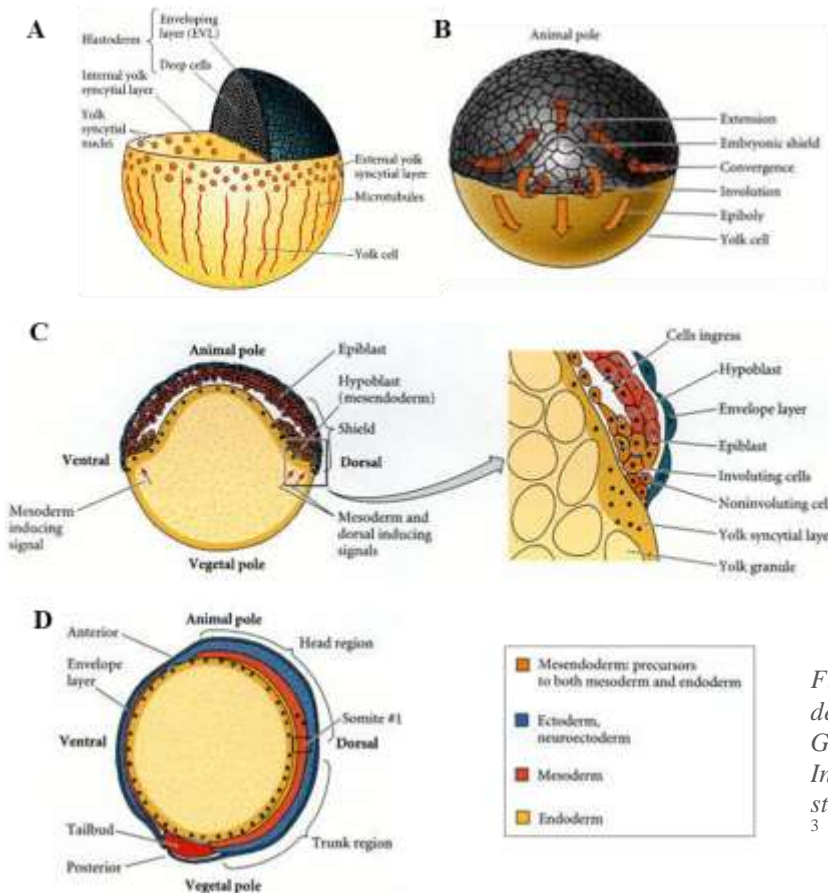


Figure 1. 7 - Zebrafish early development. A – Blastula stage; B – Gastrulation cell movements; C – Involution of epiblast cells; D – Bud stage. Image taken from Gilbert (2000)³

Although the fate map varies between organisms, there is a general agreement regarding this point. The three germ layers formed will make up all the embryonic structures and organs. It is thought that at very early stages these cells are already specified to fates like notochord, head, heart, gut, among the rest (Figure 1.8) ⁸. The ectoderm, being the most external layer, originates the outer layer of the skin, skin related structures and nervous system ³. Mesoderm, the intermediate layer, gives rise to inner layers of the skin, muscles (including the cardiac muscle), skeletal system, kidneys, circulatory system, bladder and genitalia ^{3,9}. Endoderm, the most internal layer, gives rise to the gastrointestinal track, lungs, liver, pancreas and gut ^{3,10}.

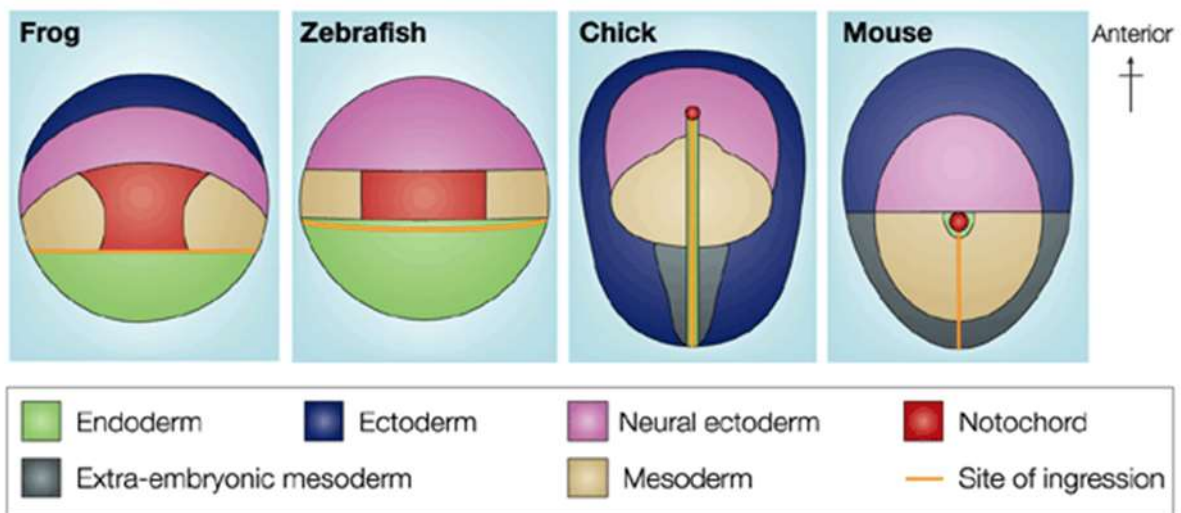


Figure 1. 8 - Fate map of model organisms (*Xenopus laevis*, *Danio rerio*, *Gallus gallus* and *mus musculus*). Image adapted from Wolpert(1998) ²

2. Left-Right Organizer

Most of these tissues and organs are organized in a bilateral way. Indeed, the axis formation is one of the first events in the embryo development. Each bilateria organism has its own axis organizer. For instances, in mouse is the node, in chick is the Hensen's node, in frog is the Nieuwkoop center and in zebrafish is the shield. In terms of gene expression, the one gene mostly associated with axis definition is Wnt ¹¹. This signalling pathway is characterized by its implication in cell-fate specification, proliferation and differentiation, cell polarity, and morphogenesis ^{12,13}.

All these organizers, pattern the embryo cells movements through physical and genetic changes in order to form the anteriorposterior (AP) and dorsolventral (DV) axis. But when considering internal organs, the symmetry pattern as evolved differently. It is generally assumed that

deuterostomes (a subtaxon of bilateria, where during development the first opening becomes the anus, in opposition to prostostomes where the first opening, during embryonic development, becomes the mouth) have an asymmetrical patterning of the internal organs. These asymmetries are governed by the left-right organizer. Which is also the node in mouse and Hensen's node in chick, but in frog is a different organ from the Nieuwkoop center, called the gastrocoel roof plate (GRP) and in zebrafish is the Kupffer's vesicle (KV). These temporary organs were collectively named the left-right organizer (LRO) in mouse, chick, frog and fish. The LRO has motile cilia (Figure 1.9), whose function is to create a flow and start a series of asymmetrical events that ultimately lead to the asymmetrical build and placement of the heart, gastrointestinal tract, liver, lungs and pancreas^{14,15}.

Asymmetry importance goes far beyond organ morphogenesis and function. It was reported, for instances, that asymmetry can also be related with animal behaviour¹⁶. Taking as an example an event occurring in all vertebrates, the nutrient recovery in the gastrointestinal tract wouldn't be so efficient if this organ wasn't asymmetrically packed¹⁷.

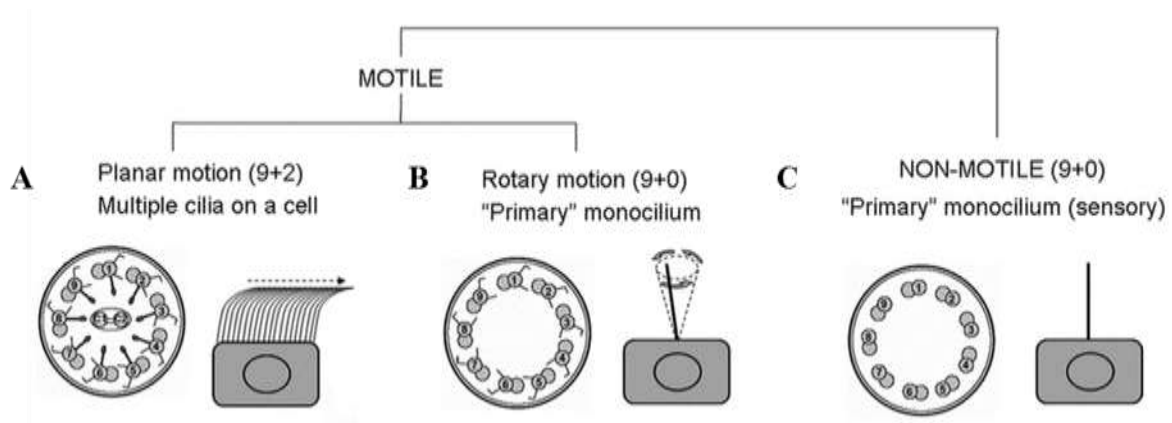


Figure 1. 9 - Scheme of transverse section of different types of cilia regarding its motility and the relative position in the cell. A – Motile cilia present in the brain, airways and reproductive tract. B – Motile cilia present the laterality organ. C – Immotile cilia present in the kidney tubules, bile duct, pancreatic duct, eye, ear and fibroblast. Image taken from Leigh et al. (2009)⁹⁵

2.1 Left-Right Asymmetry

According to Collins *et al.*¹⁸ the left-right patterning events can be summarized in four steps:

“(I) BREAKAGE OF BILATERAL SYMMETRY TO MOLECULARLY DEFINE THE LEFT AND RIGHT SIDES OF THE EMBRYO, (II) TRANSFER OF INFORMATION FROM THE SITE OF SYMMETRY BREAKAGE TO THE LEFT AND RIGHT SIDES OF THE EMBRYO, (III) MAINTAINING AND REINFORCING LEFT AND RIGHT IDENTITY IN THE LATERAL PLATE MESODERM, AND FINALLY, (IV) TRANSLATION OF THE LEFT VERSUS RIGHT INFORMATION INTO ASYMMETRIC ORGANOGENESIS. GIVEN THAT VERTEBRATES HAVE WELL-CONSERVED BODY PLANS WITH RESPECT TO THE FINAL POSITIONING AND ASYMMETRIC DEVELOPMENT OF INDIVIDUAL ORGANS, IT IS LOGICAL TO ASSUME THAT THE MOLECULAR EVENTS IN LEFT-RIGHT PATTERNING WOULD BE EQUALLY WELL CONSERVED.”

How asymmetric events start is still in debate, but the consequences of its beginning are consensual. Once the asymmetric information is transmitted to the left side of the laterality organ, the Nodal and Lefty expression are induced *in loco*. These are diffusible proteins belonging to the transforming growth factor β (TGF β) superfamily¹⁹. The self-enhancement and lateral inhibition system (Figure 1.10) is formed together by Nodal acting as an activator and Lefty as an inhibitor^{20,21}. Nodal and Lefty cascade are constricted on the left lateral plate mesoderm. Furthermore, Nodal induces the expression of several genes that will lead to asymmetric morphogenesis of internal organs¹⁸.

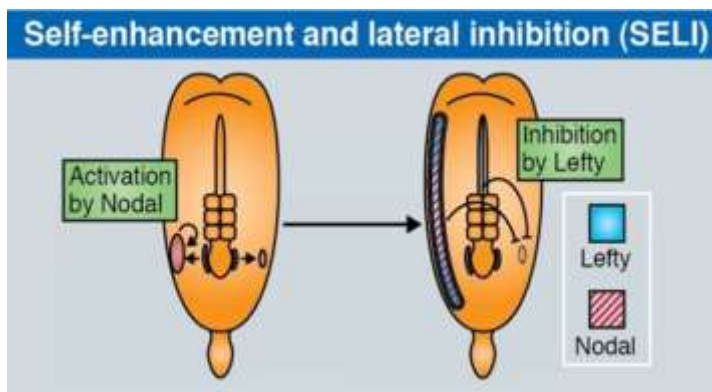
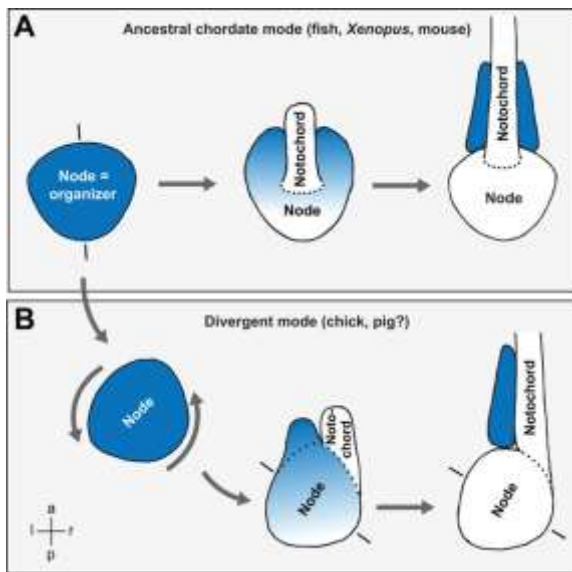


Figure 1. 10 - Self-enhancement and lateral inhibition mechanism activated with asymmetry breakage in the left-right organizer. Image taken from Nakamura *et al* (2012)²³

2.1.1 Hypothesis and Models



The breakage of symmetry through the leftward fluid flow is the most common mechanism described, but there is the curious exception of chick. Instead of a fluid flow there is the physical rotation of the Hensen's node which will create an asymmetrical Nodal expression (Figure 1.11 B) ^{17,22,23}

Figure 1. 11 - Asymmetry breakage mechanisms. A – conserved left-right asymmetry breakage with nodal flow in mouse, frog and fish. B – Divergent model for asymmetry breakage in chick with node rotation. Image taken from Blum (2014) ¹⁷

Several hypotheses have arisen to explain how leftward fluid flow would break the symmetry in the left-right organizer.

The Morphogen Gradient Model was the first model emerged ²⁴. This model suggests that morphogens released in the ventral side of the organizer would be subjected to a flow that will take them to the opposite side, leading to the creation of a gradient, and its accumulation on the left side ^{24,25}.

In 2003, McGrath et al. ²⁶ suggested that the asymmetry was exclusively created by two types of cilia – the motile and non-motile or sensory cilia. The motile cilia would create a leftward flow that the immotile cilia, acting as mechanosensors, on the left side would sense and respond with Ca^{2+} release on that side, leading to nodal asymmetrical expression. This is now known as the two-cilia hypothesis.

2.1.2 Problems with Asymmetry

This flow mechanism of symmetry breakage is error prone and consumes a lot of the gastrula embryo energy, so how did it evolve? The majority of non-chordate organisms have epidermal motile cilia adapted for locomotion and swimming. According to Blum *et al.* 2014 ¹⁷, these cilia were re-adapted upon internalization during the gastrulation phase to serve as a symmetry breakage mechanism.

If the left-right patterning occurs normally, the internal organs are placed as in Figure 1.12 - *Situs Solitus*. But when this patterning is not correctly performed, several disorders arise. *Situs inversus* is a condition where the organs are placed in a reversed order, while heterotaxia is characterized by the complete randomization of visceral organ placement. Heterotaxia is usually associated with higher death rates.

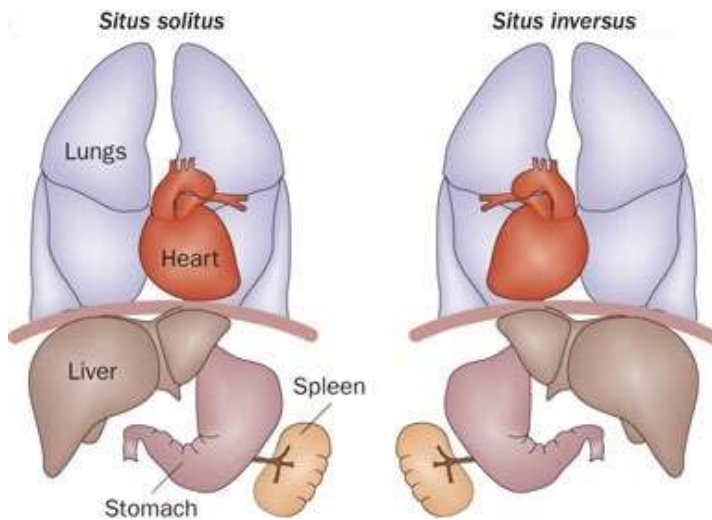


Figure 1. 12 - Scheme of normal left–right asymmetry (situs solitus) and in left-right abnormal situation (situs inversus). Image adapted from Patel et al. (2010)⁹⁶.

Particularly related with cilia, there are several pathologies like Bardet-Biedl syndrome, Joubert Syndrome, Polycystic kidney disease, among many others ^{27,28}. The study of cilia, its functions and mechanism is crucial to biomedicine in order to have better tools to fight these types of diseases.

2.2 Organizer's fates

In this study I am focused on the fate of the KV cells, in zebrafish, after their role in the left-right asymmetry patterning. In chick, frog or zebrafish these fates are not well studied. However, there are many studies regarding the mouse node cells fate.

In mouse there are several organizer populations according to the developmental stage. These populations are differentiated between each other by their lineage contributions, molecular profile, and function. The Early Gastrula Organizer (EGO) contributes to the formation of the prechordal plate, foregut endoderm, and cranial mesenchyme, according to Kinder *et al* 2001 ²⁹. With the change in function and molecular profiling of the organizer, it is formed the Mid-Gastrula Organizer (MGO). This organizer also contributes to prechordal plate and foregut endoderm but also to the

head process, notochord and the ventral midline of the neural tube. Plus differentiation of the MGO will lead to the formation of a late organizer – the Node³⁰. The node is double layered constituted by mesoderm and neuroectoderm, unlike the zebrafish which is just mesoendoderm. The cells from the ventral region of the mouse node are monociliated and will contribute to the notochord, while the cells from the dorsal region of the node will contribute to the ventral neural tube – floor plate. These contributions are essentially to the posterior trunk of the embryo²⁹⁻³¹.

It is known that in chick, the Hensen's node cells mostly integrate the notochord and the somites and at least the lateral regions of the node, have the capacity of originating more than one tissue type³². In frog, the GRP will give rise to notochord, somites and hypochord³³.

Studies regarding the KV fate were done separately by Cooper and D'Amico³⁴ and Melby *et al.* 1996¹⁰. Firstly, they described that the shield cells will mostly contribute to notochordal fates and a minority to the floor plate. Performing lineage tracing experiments they identified a specific group of forerunner cells (DFC) derived from the dorsal blastoderm margin. According to Cooper and D'Amico³⁴, approximately at 20 somite stage, part of this DFC cluster enters mesendodermal organ rudiments whereas others remain in the base of the chordal neural hinge (Figure 1.13). At later stages these cells segregate from the tissues and incorporate the notochord, somites and tail mesenchyme. However, this was not demonstrated by the authors³⁴, justifying the present work.

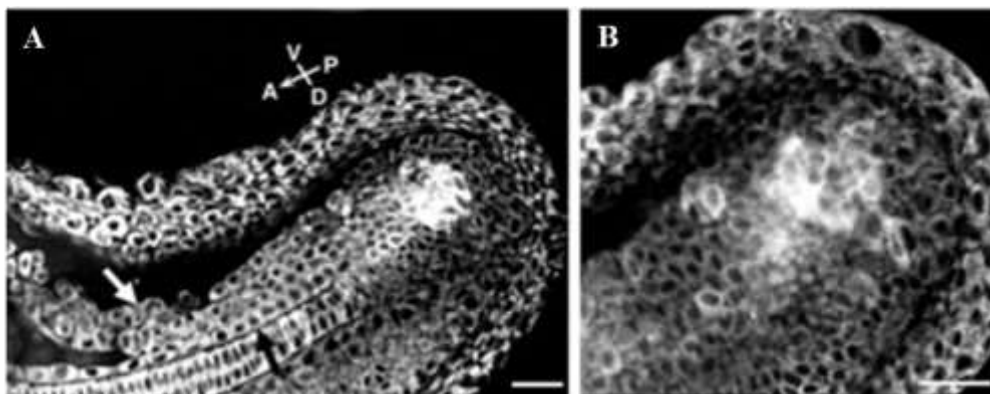


Figure 1. 13 - Embryo at approximately 26 ss. A - The Kupffer's Vesicle has disappeared by this stage and the forerunner cell cluster remains ventral to the chordal neural hinge during tail extension. Hypochordal rod (black arrow). B – Same embryo as in A at higher amplification. Scale bar - 50 μ m. Image adapted from Cooper and D'Amico (1996)³⁴.

These results are coincident with the ones from Melby *et al.*¹⁰, which according to his work, the DFCs have a tail mesodermal fate, incorporating the notochord, tail muscle and tail mesenchyme (Figure 1.14).

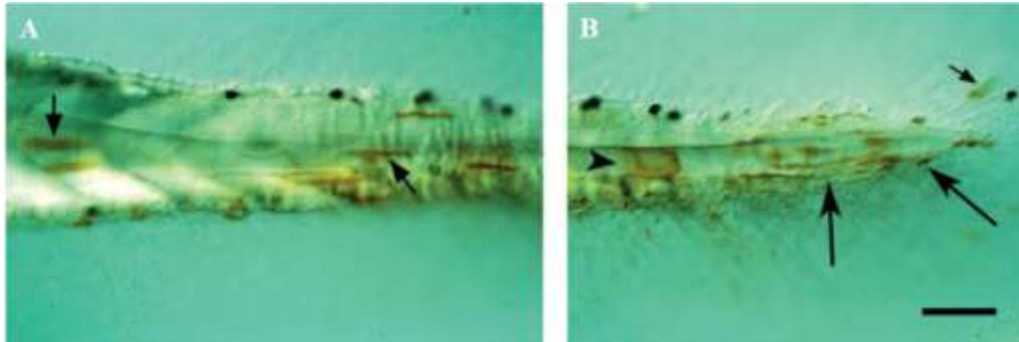


Figure 1. 14 - Dorsal forerunner cells tracing in the tail. Scale bar 50 μ m. A – Tail with labelled muscle cells (arrows), B – Posterior tail tip with labelled notochord (arrowhead), body wall mesenchyme (arrows) and fin mesenchyme (small arrow). Image and subtitle adapted from Melby (1996)¹⁰.

Knowing in detail the fates and behaviour of these cells will not only enrich the current knowledge on this topic, but will also help to make new connections and raise more important questions regarding the organisms' organizers.

3. Zebrafish Left-Right Organizer

Danio rerio, a.k.a zebrafish, is a 4-5 cm in length tropical fresh-water fish native to rivers of northern India, northern Pakistan, Nepal, and Bhutan in South Asia.

This species is a model organism that offers several advantages as a tool in research, including a short generation time, production of large clutches of eggs, external fertilization and rapid embryogenesis, which is similar to that of higher vertebrates and that, can be monitored through the transparent egg and embryo. It is a widely used model organism for genetic studies in vertebrate development, developmental biology and a variety of human congenital and genetic diseases.

The zebrafish development comprises a life cycle from fertilized egg to adult of 90 days, but in this study we only looked at the embryonic development from 9-10 until 29-30 somite stage (ss).

During this period, major events occur in the embryo such as left-right patterning by the Kupffer's vesicle, tail extension, somite formation, notochord vacuolation, among others.

3.1 Development of Kupffer's Vesicle

In 1996, Mark Cooper and Leonard D'Amico³⁴ described for the first time the dorsal forerunner cells (DFC), which we know now as the precursors of Kupffer's vesicle.

It was evident that between 50-60% epiboly a small group of cells was distinguished from the rest. These cells didn't suffer involution or ingression into the embryonic shield during germ ring formation. Instead these Noninvoluting Endocytic Cells (NEM) stayed as a cluster loosely adherent in the distal edge of the more adherent dorsal blastoderm (Figure 1.7 C).

In 2008, Oteíza *et al.*³⁵ described the complete process of KV formation. At sphere stage (4 hours post fertilization - hpf), there are the enveloping layer cells (EVL - which is an epithelial monolayer) and deep cells (DEL) (Figure 1.7 A). At this stage, there is also a group of cells called Dorsal Surface Epithelial Cells (DSE) in direct contact with the yolk syncytial layer (YSL). As the embryo develops, in the beginning of epiboly, there is a coordinated movement of EVL cells, DSE and marginal deep cells, as they start to migrate towards the vegetal pole (Figure 1.7 B). When EVL surpasses DSE (which migrates slower) these are forced to ingress. At 50% epiboly (right after formation of shield) they are totally converted to Dorsal Forerunner Cells (Figure 1.15).

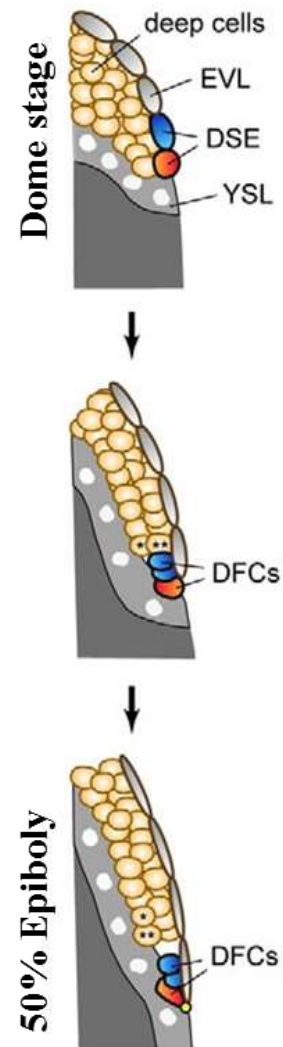


Figure 1. 15 - Scheme of dorsal forerunner cells (DFCs) formation during gastrulation phase. EVL – Enveloping layer, DSE – dorsal surface epithelium; YSL – Yolk syncytial layer. Adapted from Oteíza *et al.* (2008)³⁵

This conversion implies cell division and mesenchymal behaviours (Figure 1.16 II), like existence of protrusions. The initial number of DFC increases in this process and goes from approximately 30 to approximately 60, at 80% epiboly. With a higher cell number the wide morphology of these cluster becomes more narrow and the DFC intercalate with each other. At the end of epiboly, the DFC detach from the EVL layer. Studies revealed that the ZO-1 attachments points (tight junction) were responsible to keep these cells in touch with the upper layer. Once they detach, the ZO-1 creates multiple focal point on the apical side of the DFC and more unpolarised DFC joins the cluster to create a rosette rearrangement (Figure 1.16 III). At this point these cells suffer a mesenchymal to epithelial transition (Figure 1.16 II). This structure quickly expands, with the ZO-1 fusion, and with the lumen filling until it reaches twelve times its original size (Figure 1.16 IV, V). From tail bud to 4 ss, there is no more cell recruitment of cells and the characteristic cilia start to appear. At 9-10 ss the left-right organizer is fully formed and finishes its function around 13-14 ss.

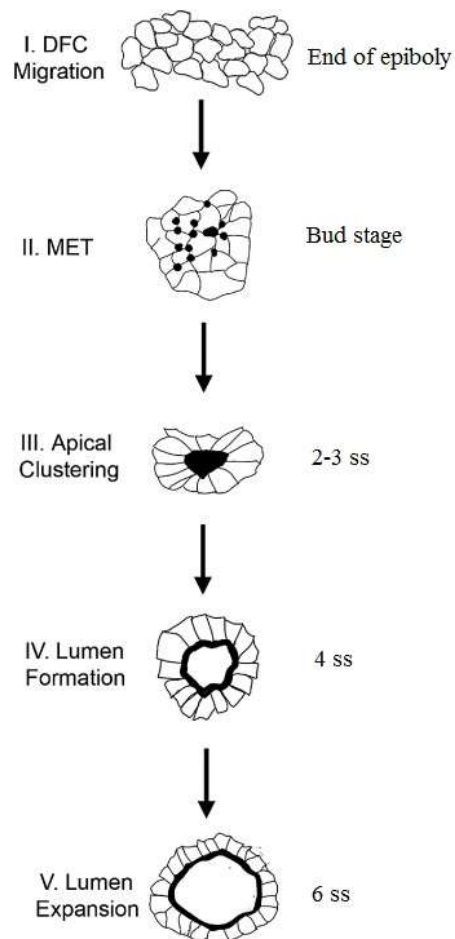


Figure 1. 16 - Scheme of Kupffer's Vesicle formation. I – DFCs migration at 80% epiboly; II – mesenchymal to epithelial transition (MET); III – Apical clustering, fusion of ZO-1 focal points; IV – Lumen formation; V – Lumen expansion. *ntl* – no tail gene, correspondent to brachyury in mouse; *tbx6* – T box 6 gene correspondent to spadetail in mouse. *ntl* and *tbx6* are required for the transitions referred in the image. Adapted from Amack 2007⁹⁷

3.2 Development of posterior body

The embryo development also comprises the growth of the posterior body. Arguments in the scientific community varied when trying to understand how this phenomenon happens.

Holmadhl, in 1925, suggested that the formation of anterior regions, like head and trunk, was ruled by a different program than the one controlling the posterior body formation ³⁶. In opposition, Pasteels, in 1943, described the tail formation as a continuation of gastrulation, not qualitatively different from the rest of the body (head and trunk) ³⁷. With research ³⁸, not just in zebrafish but also in mouse and chick, it was possible to define that several events were specific of the tail region. Mutants like *wnt3a* with severe defects in the posterior body but relatively normal head and trunk ³⁹, proved that the development of the tail has distinct processes from the anterior body ³⁸. Nevertheless, the actual posterior body formation is a combination of both hypotheses.

The tail formation in zebrafish can be described essentially in four different steps: 1) Tail bud formation, with the fusion of the marginal cells with the ventral yolk plug; 2) Extension phase, with tail elongation along the ventral side stopping when reaching the ventral side midpoint; 3) Protrusion phase, when there is an accumulation of cells in the tail bud region and 4) Tail eversion, where the tail grows away from the yolk cells. The characteristic cell movements during the tail formation are represented in Figure 1.17.

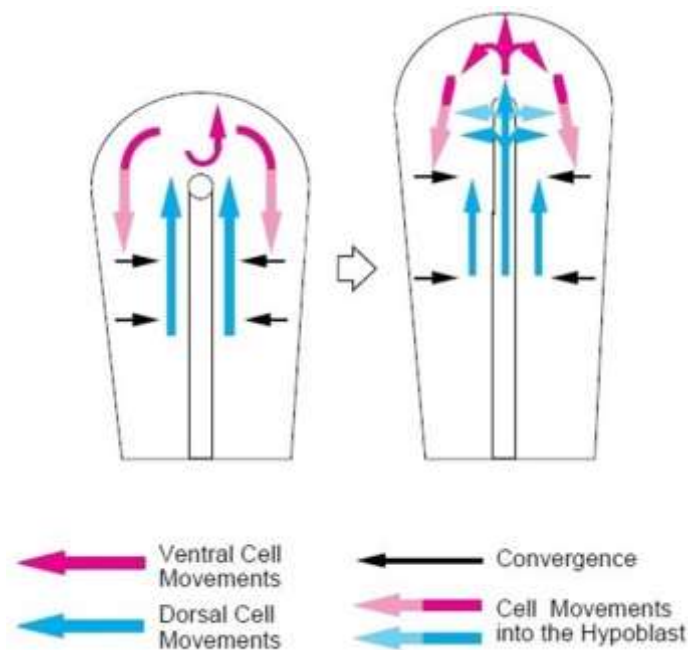


Figure 1. 17 - Characteristic mass cell movements during tail formation in zebrafish. Posterior is upwards. The two-colour arrows indicate the transition of cells from superficial regions (dark colour) into the deeper hypoblast (light colour). Top to bottom corresponds to posterior and anterior, respectively. Image and subtitle adapted from Kanki and Ho (1997).

In spite of the differences in the timing of tail formation, at late stages of neurulation in frog and at the end of gastrulation in zebrafish, is observed that the differentiation wave still occurs in the anterior to posterior direction³.

In zebrafish, the ventral midline of the tail bud anterior regions only contributes to the formation of the notochord. During early gastrula, the precursor of notochord – chordomesoderm – receives differentiation signals and suffers cellular rearrangements that force this tissue to become elongated in a rod-like shape (Figure 1.18)⁴⁰. The characteristic stiffness occurs during the segmentation period, when the central cells of the notochord acquire a large vacuole. The pressure created by these vacuoles against the surrounded tissue sheath grants this property to the notochord.

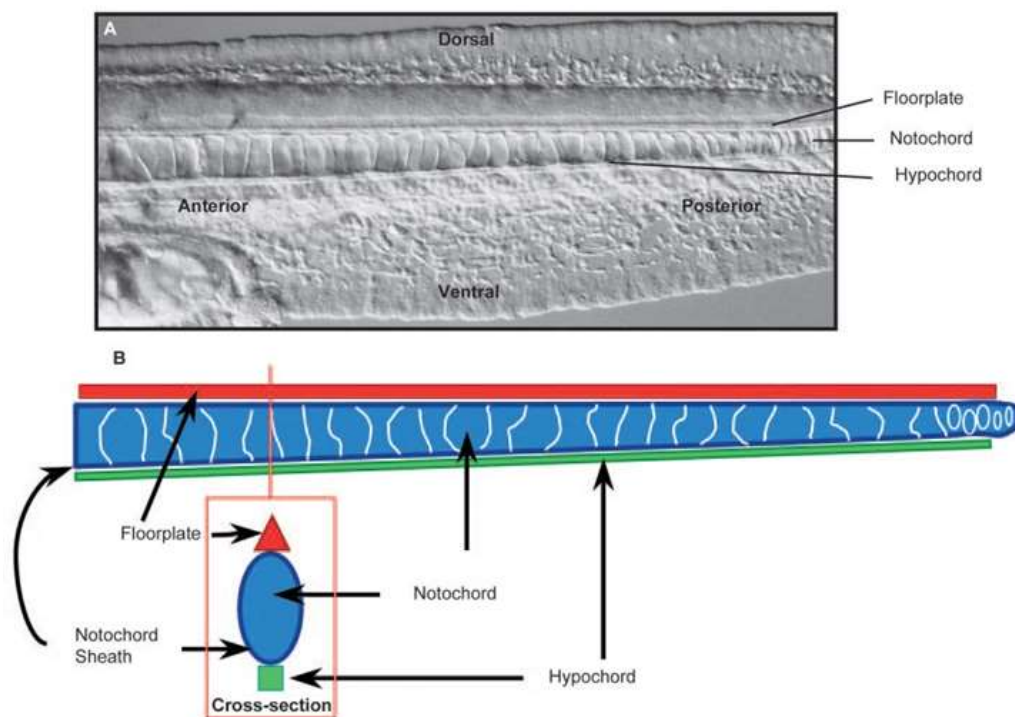


Figure 1. 18 - Notochord structural aspects in a Prim-5 zebrafish embryo. A - Tail region structures – floor plate, notochord and hypochord; B - Representative scheme with the floor plate, notochord and hypochord represented, as well as its cross-section. Image taken from Stemple et al. (2005)⁴⁰.

In zebrafish, its extension along the tail derives from ingression/involution of precursor cells in the dorsal position, formed during gastrulation⁴¹. It is described that cells at the tail demonstrate rearrangements and intercalations, which differentiate to provide the notochord extension^{42,43}. Interestingly, in *no tail* mutants, where there is no notochord formation, the tail extension is severely

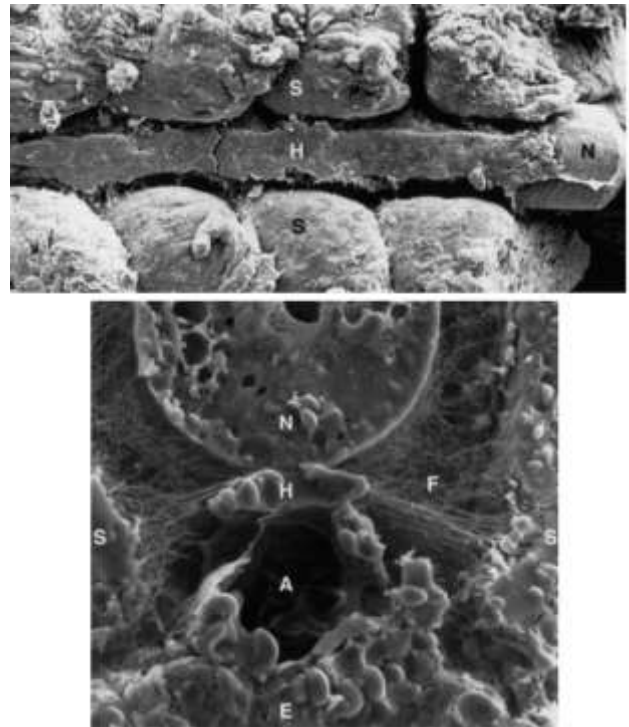
affected⁴⁴. This implies that, until some extent the notochord may contribute to the tail elongation⁴¹. In mouse and chick, the notochord is a transient signalling structure that will contribute to the nucleus pulposus in the adult (structure integrated in the intervertebral discs)⁴⁵. In zebrafish, for instances, the notochord sheath suffers mineralization during the skeleton system formation⁴⁶. A curiosity regarding this structure was reported by Bočina *et al*⁴⁷ in amphioxus where the notochord presented some cilia-like organelles. Could these cilia-like structures be present in other model organisms, like zebrafish?

In addition tail, the head is formed from the paraxial mesoderm, as well as the somites. The somites, in turn, will give rise to sclerotome (cartilage), myotome (skeletal muscle) and dermamiotome (dermis)³. It is described that at early stages of segmentation the somitogenesis begins with a clock wave like development^{48,49}. In the chick tail bud was observed that paraxial mesoderm, from the dorsal regions, gives rise to different structures like muscle precursors (somites) and neural precursors (spinal cord). In zebrafish the most dorsal cell population in the tail will give rise to the spinal cord³⁸.

While in chick and mouse the neural tube is formed by the neural folds and its closure over the neural groove, in zebrafish the neurulation process is different. Instead of creating the neural tube through the folding of the neural plate, it is first created a neural rod from epithelial sheets and with cell rearrangements and cavitation processes it becomes a tube with lumen – neural tube⁵⁰. The floor plate is the ventral region of this neural tube and it is above the notochord as shown in Figure 1.3 and 1.18. It is described that the neural tube possesses different size cilia, according to its relative position⁵¹. Particularly, the floor plate, expressing *foxj1* presents longer cilia than the lateral sides of the neural tube⁵¹, possible motile and responsible for the brain spinal fluid flow.

Beneath the notochord is another structure called the hypochord (Figure 1.18). From what it is known, this structure is well conserved among axolotls, frogs and fish (Figure 1.19)^{52,53}. In zebrafish, its derives from the lateral side of the organizer and one of its known functions is to signal to the aorta, via secretion of Vascular Endothelial Growth Factor (VEGF), to correctly differentiate and form⁵⁴. At pharyngula stage this structure starts to recede until it totally disappears⁵⁵. Cilia are spread all along the organism (Figure 1.9) and accordingly, in the hypochord cilia were also reported (in this case primary cilia)⁵⁶.

Figure 1. 19 - *Ambystoma mexicanum*. Transmission electron microscopy (TEM) micrograph of a hypochord cell (H), Notochord (N), somites (S), Prominent extracellular matrix fibrils (F), dorsal aorta (A) and endoderm (E). Image adapted from Lofberg and Collazo(1997)⁵⁷.



The proliferative profile so far described for the zebrafish tail is represented in Figure 1.20. Kanki and Ho (1997) assessed the cell proliferation in the tail at 10 ss and 18 ss. The total number of cells per defined region (Figure 1.20 – regions 1 to 5) was counted and the ratio of mitotic cell/cell nuclei counted was calculated. It was observed that the tail tip has a low proliferation rate, this results is expected since the elongation cell supply does not come from the tip.

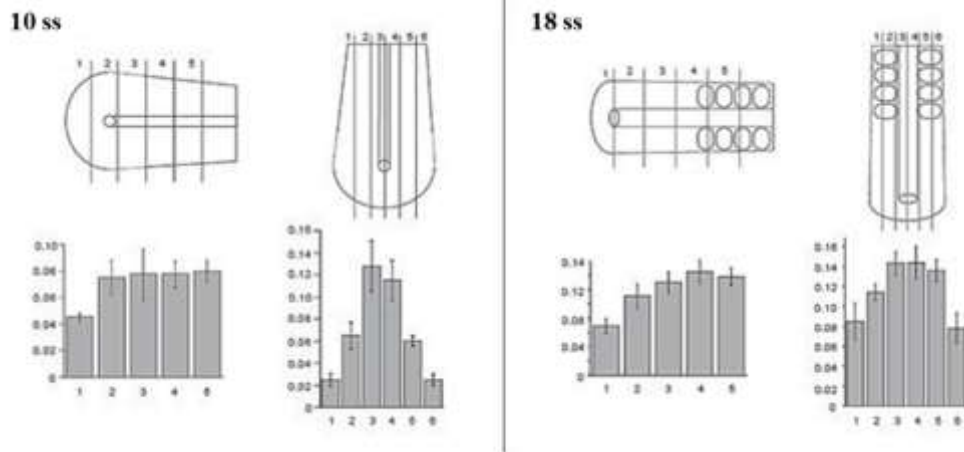


Figure 1. 20 - Mitotic indices within zebrafish tailbud. Top – dorsal views along A-P axis (left) and medial-lateral axis (right) with subdivisions 1-5. Down – Graphs with mitotic indices of each subdivision of the tail. Image adapted from Kanki and Ho (1997)³⁸

On the other side of the coin, programmed cell death is an old topic and many studies have been done in this regard⁵⁸. Glusmann defined several types of apoptosis depending on the context⁵⁹. The phylogenetic apoptosis is the elimination of a structure that has evolved with the

organism but that no longer has an active function or contribution. The morphogenetic apoptosis, happens for instances, during interdigital cell elimination along the embryo development. And the last type is the histogenetic apoptosis, that occurs when a cell is misplaced in a structure or isn't performing its function as it should, for instances, when a neuron doesn't make the appropriate synaptic connection or when a notochord cell doesn't vacuolated properly.

The deepest study regarding apoptosis in zebrafish embryos was conducted by Cole and Ross, in 2001 (Figure 1.21)⁵⁹. They described that apoptosis occurred from 18 ss to Prim-5, with a peak at 22 ss, in both ectodermal and mesodermal layers. Beyond Prim-15 stage, no more apoptosis was detected. These scientists hypothesised that the apoptosis observed in the tail could be in order to increase the space in the tail for morphogenesis of the mesenchymal cells around the notochord and spinal cord. They also assessed the notochord apoptosis rate from 10 ss until Prim-5. They noticed a peak at 26 ss, but with no specific location pattern of the apoptotic bodies. Between 14 ss and 22 ss, according to Kimmel *et al* (1995)⁴¹, at 21 ss the notochord finished the patterning of the neural ectoderm, and its cells vacuolate and swells. It could be that this elimination is representative of the cells that failed differentiation and/or vacuolation.

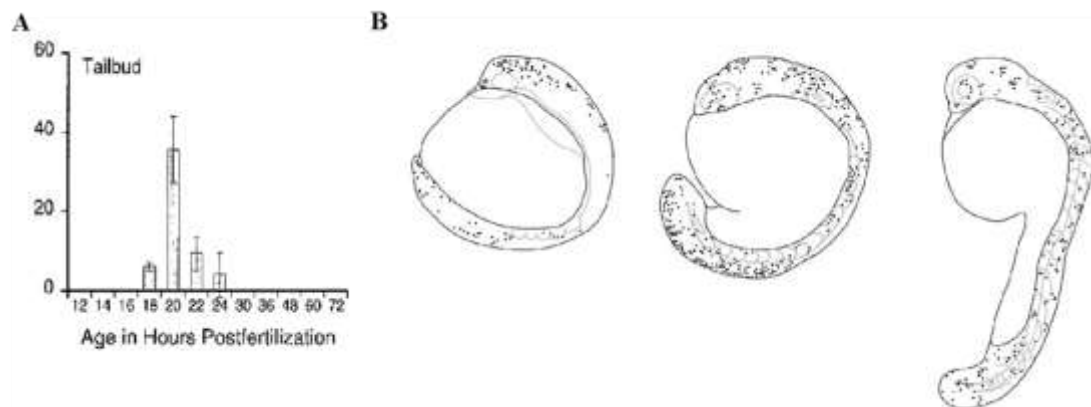


Figure 1. 21 - Apoptotic studies in zebrafish. A – Graph with zebrafish tailbud apoptotic rates throughout development; B – Each dot represents an apoptotic cell, embryo with 12, 16 and 20 hpf, respectively from left to right. Image adapted from Cole and Ross (2001)⁵⁹.

Many aspects of the zebrafish development are still unrevealed. For instances, the KV cells are crucial for the correct development of the embryo, but will they be important after the KV closes or will they die? Will they acquire and perform other functions? This thesis attempts to fulfil a gap in knowledge regarding the Kupffer's vesicle cell fates, their contribution and possible influence in the zebrafish larvae tail development..



Aims

It is known that the KV is a crucial, temporary organ that coordinates the correct embryo development. The contribution that these KV cells have in later embryonic stages is not properly studied and with the use of a transgenic line we wanted to investigate and understand the fate of these cells in zebrafish. For that purpose, I used a transgenic line (*foxj1a*:GFP) available in our laboratory, that labels the zebrafish Kupffer's vesicle cells. Using two-photon microscopy and the help from ImageJ, Huygens and Imaris software was possible to do the 3D tracking of these cells movements.

To have a detailed description of these cells and to complement the live imaging information, proliferation and death assays were performed. With a molecular approach, we aimed to determine the final position of KV cells, using immunofluorescence studies and *In situ* hybridizations to assess the co-localization of the GFP marked cells (from the *foxj1a*:GFP line) with markers for different embryonic tissues.

Considering the determinant role of cilia in the Kupffer's vesicle, the cilia length progression was studied by immunofluorescence assays to assess the potential functional contribution of the KV to the embryo tail. Through laser ablation, was also an aim to assess the potential contributions of the KV cells to the tail environment and tail structures.

Ultimately, the goal, after gathering all this information, is to better understand the fate of the KV cells, their potential functional contribution to the embryo once the left-right patterning is established; the cilia that these cells have and the overall influence and contribution to the zebrafish tail.



Materials and Methods

To meet this project aims we used *Danio rerio* (zebrafish) as a model organism. All the reagents used were from Sigma – Aldrich, except when mention otherwise.

1. Zebrafish husbandry and maintenance

Adult zebrafish were raised and maintained at 28 °C with 14h light/ 8h dark photoperiod ⁶⁰. After crossing the progenitors, embryos were collected in embryonic medium (E3) and raised at 25 °C or 28 °C incubator until they achieved the desired developmental stage, according to Kimmel et al.,1995 ⁶¹.

For this research, the transgenic reporter line Tg(0.6*foxj1a*:gfp) was used. In this transgenic zebrafish line, was introduced a 0.6 kb fragment of *foxj1a* promoter, located approximately –5.2 kb to –4.6 kb upstream of the ATG start codon, driving the expression of GFP ⁶². This line labels all ciliated cells that have a motile cilia and was used in order to distinguish the Kupffer’s vesicle (KV) cells from the remaining ones. In order to label the KV cells and cell membranes ⁶³ for the laser ablation we also used the Tg(*Ras*:mGFP) to outcross with Tg(0.6*foxj1a*:GFP).

2. Live Imaging and Microscopy

To study the movements and migration of the KV cells, we used two-photon microscopy. This type of microscopy allows a deeper penetrance in the tissues with low photo-toxicity and bleaching. This results from the usage of near-infrared radiation for excitation, which is much less absorbed by the embryo, reducing the noise and the need for a pinhole aperture for that purposes. Also, because bigger wavelengths are used the sample penetration increases, thus more fitted for whole mount live imaging. In order to understand if the KV cells have an important contribution to the tail we performed laser ablation using the Andor Spinning Disk. This microscope has the capacity of single cell ablation, allowing a more precise ablation.

2.1 Two-Photon Microscope – Migration studies

2.1.1 Whole Mount

The embryos that were fluorescent in the KV were analysed in the stereoscope and the ones with stronger fluorescence were selected. These were manually dechorionated with forceps under the stereoscope with minimum light. Five of these embryos were collected to a 1,5 mL tube, using a glass pasteur pipette. To each tube was added 1% Low Melting Agarose (LMA: 1g Low Melting Agarose - Fisher Scientific and 100 mL Embryonic Medium), previously heated and cooled down to a temperature that did not destroy the embryos. In a petri dish coated with the same 1% LMA or Agarose (1g Seakem LE Agarose – Lonza and 100 mL Embryonic Medium), each embryo was placed in an individual agarose drop and the position rearranged to allow the best. The petri dish was covered with 1X Tricaine (1 mL 25X Tricaine and 24 mL of dH₂O) at 28 °C and kept in dark until usage in the two-photon, few minutes after.

2.1.2 Image Acquisition

For time-lapse imaging the embryos were filmed with two-photon microscope (model Ultima from Praire) controlled by Prairie View v4.0.0.53 software. The 20X water lenses (Olympus XLUMPLFLN) with 1.00 numerical aperture (NA) was used and the embryos were anesthetized

with 1X Tricaine. The lens and the stage were warmed at 27,5°C, with minimum variations. The image acquisition conditions, like pocket cell throughput, photon multiplier tubes (PMT), step size, Z-stack, pixel size, optical zoom, period and repetitions, varied between embryos due to different developmental stages and fluorescence signal intensity.

After acquiring the images, as a control, some of the embryos were let to grow in a 28 °C incubator and others were fixed with PFA 4% for further analysis.

2.2 Andor Spinning Disk – Cell Ablation

2.2.1 Whole Mount

As for the two-photon, the embryos were analysed in stereoscope and the ones with stronger fluorescence in the KV were selected. These were then manually dechorionated with forceps under the stereoscope with minimum light. Several of these embryos were transferred to an agarose mold, using a glass pasteur pipette. The agarose molds were done previously using 1% agarose and after the mounting the embryos were covered in 1X Tricaine.

2.2.2 Cell laser Ablation

For KV cells ablation the embryos were analysed with Nikon Eclipse Ti-E (model Revolution XD) controlled by Andor Qi software. The 10X (PLAN FLUOR) 0.3NA and 20X (PLAN APO VC) 0.75NA objectives were used to select the best mounted embryos and the water immersion objective 60X (PLAN APO VC) 1.20NA was used to ablate the cells of interest.

The protocol used is described in Figure 2.1. The Repetition Rate, number of repeats and laser strength was variable among embryos.

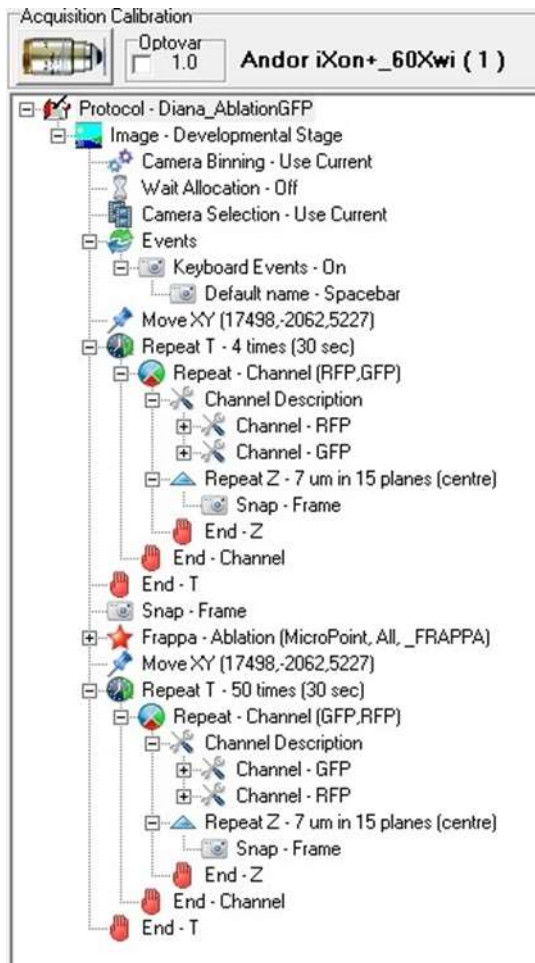


Figure 3. 1 - Protocol used for laser ablation. The program runs the protocol from up to bottom, passing through start and end of the stack position – doing a z-stack before the ablation, ablation plan and region of interest (selected in a parallel window), cell ablation (Frappa – Ablation) and repetition of the stack in order to confirm the result.

2.3 Confocal Microscopy – Fixed Samples

The embryos were mounted for an inverted microscope using a slide and a coverslip spaced by silicone (Dow Corning). The image acquisition for fixed embryos, where immunostaining or TUNEL was performed, was done using the confocal Zeiss LSM710 controlled by the Zen 2010 b SP1 software. I used a water immersion lenses 40X 1.2 NA at room temperature.

3. Molecular Techniques

The aim of the molecular techniques described below was to assess the programmed cell death and proliferation of the KV cells and evaluate the cilia length. In addition, by colocalization studies of the *foxj1a*:GFP with a few *in situ* probes, I aimed to identify the fate of subsets of KV cells.

3.1 Fixation of Embryos

All the molecular techniques were performed in fixed embryos. The criterion to choose the time window for the fixation was to cover most of the developmental stages spanning the duration of the live imaging videos. Starting from 9/10 somites and ending in Prim-5 developmental stage, the embryos were fixed hour by hour with PFA (Paraformaldehyde) 4% overnight (or even over weekend) and then dehydrated by transfer to 100% methanol. The embryos were stored at -20°C for several weeks.

3.2 *In situ* Hybridization

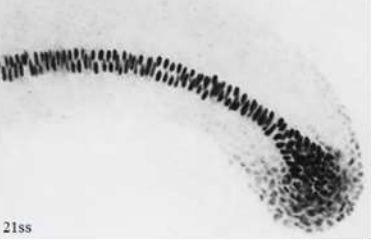
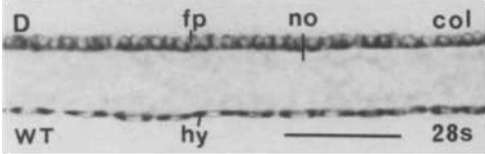
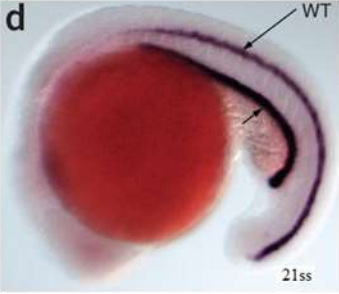



For a better understanding of the molecular signature of subsets of KV cells we performed *In situ* hybridization. This technique uses anti-sense mRNA labelled with DIG (digoxigenin) that binds to the native mRNA present in the cells that are expressing that gene, giving qualitative information about the expression pattern of a gene of interest ⁶⁴.

The following molecular markers were used: *ntl*, *Col2a1a*, *foxj1a*, *shh*, *msgn1*, *dnah7*, for original references see ⁶⁵⁻⁷³.

The probes used in this work are described in Table 1. It is important to understand that the nomenclature of the different development stages was standardized for a matter of simplicity and easy reading, i.e., if the original paper qualifies the developmental stage as 20 hpf in this Thesis it was converted to 21s, according to Kimmel et al., 1995 ⁶¹.

3.2.1. Probe information and Synthesis

Table 3.1 – Description of the In situ probes. WT – wild type; ss or s – somites; fp – floor plate; hy – hypochord; no – notochord; col – collagen.

| Name | Structure/Region Marked | Figure of the expression pattern | Reference |
|-----------------------------|-------------------------------------|--|--|
| <i>no tail (ntl)</i> | Notochord |  | Schulte et al., 1994 ⁶⁵ Essner et al. 2005 ⁶⁶ |
| <i>col2a1a</i> | Hypochord and Floor plate |  | Yan et al. 1995 ⁶⁷ Dal-Pra et al. 2011 ⁶⁸ |
| <i>foxj1a</i> | KV, floor plate and pronephric duct |  | Neugebauer et al. 2009 ⁶⁹ Yu et al., 2008 ⁷⁰ |
| <i>sonic hedgehog (shh)</i> | Floor plate |  | Essner et al. 2005 ⁶⁶ Talbot et al. 1995 ⁴¹ Krauss et al. 1993 ⁷⁴ |
| <i>mesogenin 1 (msgn1)</i> | Tail bud |  | Fior et al. 2012 ⁷¹ |
| <i>dnah7</i> | Hindbrain, tail bud |  | PS - personal communication |

The probe *Col2a1a* was kindly given by Dr. Bernard Thisse from University of Virginia. The plasmid pBSIISK+ was transformed into the DH5 α competent bacteria, multiplied and extracted by Promega Wizard Plus SV Miniprep DNA Purification System (#TB225). All steps were done as described in the protocol except the first centrifugation that was done at 4000 rpm for 10 min and in *step 3*, besides the tube inversion was also done a 5 min incubation period with Cell Lysis Solution. After the plasmid extraction, purification and quantification with Nanodrop, the sequence of interest was amplified through PCR (NZY Taq Polymerase) with the correspondent primers (forward – 5' GTA AAA CGA CGG CCA GT 3'; reverse – 5' AAC AGC ATG ACC ATG ATT AC 3'). The PCR conditions were 5 μ L NZY reaction buffer 10X ; 2 mM MgCl₂; 10 mM dNTPs; 0,4 mM Primer Mix Stock 5mM; 0,5 μ L NZY Taq polymerase 5U/ μ L; water up to 50 μ L. The cycles were done as follow: 5 min at 95 °C, 30 times repetition of 1 min 95 °C, 1 min 50 °C and 2 min 72 °C, to end the cycle 10 min 72 °C and 4 °C forever.

3.2.2. Protocol description

As a starting point, the embryos were dehydrated in 100% methanol and kept at -20°C. Embryos were rehydrated through a series of methanol dilution in a phosphate saline buffer (PBS – 80g NaCl, 2g KCl, 2g KH₂PO₄, 7.17g HNa₂O₄P.2H₂O, MiliQ Water up to 1L, adjust pH and autoclave) - 75% - 50% - 25% Methanol - waiting 5 min in between each substitution. Next, the embryos were washed 4 times in freshly made PBT (5 mL PBS, 250 μ L Tween20 10%, 44,750 mL miliQ Water) during 5 min each. In PBT the embryos were dechorionated with forceps. Accordingly to the developmental stage a solution of Proteinase K (10 mg/mL) was added to the samples during 15 min (if late somitogenesis stages), 3 min (if mid somitogenesis stages) or 1 min (if early somitogenesis stages). This is an important step since it is through protein digestion that the embryos become more permeable to the future treatment (therefore this being a common step between molecular techniques). After removing the Proteinase K solution the embryos were fixed in PFA 4% during 25 min at room temperature. This step allowed the tissue to recover hardness. The embryos were washed 5 times during 5 min with PBT and then pre-hybridized in 100% Hybridization-Mix [25 mL formamide, 12,5 mL Saline-Sodium Citrate (SSC) 20X (175,3 g NaCl, 88,2 g Sodium Citrate dehydrate, 1 L miliQ water), 500 μ L Tween20 10%, 460 μ L Citric Acid 1M pH 6.0, 4 mL Heparine 0.63 mg/mL, 7,540 mL MiliQ Water] for 2 to 5 hours at 70 °C. After this period the probe (previously diluted in Hyb-Mix in a concentration of 2 ng/ μ L) was added and the samples were incubated overnight at 70 °C.

After incubation the probe was recovered and a series of washes at 70 °C occurred. To start, a brief wash with 100 % Hyb-Mix was performed. Posteriorly, was made a wash with a solution made of 75% Hyb-Mix plus 25% SSC 2X for 15 min. This was removed and added for 15 min a solution made of 50% Hyb-Mix plus 50% SSC 2X. Next a solution made of 25% Hyb-Mix plus 75% SSC 2X was added to the samples during other 15 min, then removed and SSC 2X at 70 °C was added during 15 min. To finalize the warm washes, two washes were done, during 30 min, each with SSC 0,2 X.

All SSC 0,2X dilutions were freshly made. At room temperature a solution of 75% SSC 0.2X plus 25% PBT was added to the samples for 10 min, afterwards was added a solution made of 50% SSC 0.2X plus 50% PBT for other 10 min., and the last of the dilutions (25% SSC 0.2X plus 75% PBT) was added. The last wash was made with PBT for 10 min. After the washing steps, the blocking solution [0,1 g Bovine serum albumin (BSA), 1 mL goat serum, 49 mL PBT) was added during 2h to 5h to decrease the unspecific binding of the antibody anti-Digoxigenin (DIG). After removing it, the solution of blocking solution plus anti-DIG antibody (1 µL of antibody anti-DIG per 5 mL Blocking Solution) was added to the samples and incubated overnight at 4 °C.

The antibody staining was discarded and the samples rinsed in PBT. Afterwards the samples were washed six times with PBT during 15 min each wash. The embryos were incubated in staining buffer (5 mL TRIS 1M pH 9,5, 2,5 mL MgCl 1M, 1 mL NaCl 5M, 500 µL Tween20 10%, 41 mL MiliQ Water) at room temperature during 5 min, three times, and then transferred to a 12 well plate, carefully labelled as in the original tubes. With a glass pipette the staining buffer was gently removed and immediately replaced with substrate solution [22,5 µL Nitro-blue tetrazolium chloride (NBT), 35 µL 5-bromo-4-chloro-3'-indolyphosphate p-toluidine salt (BCIP), 10 mL Staining Buffer]. The plate was protected from bright light with foil paper and incubated at 37°C for several minutes or hours according to the probe developing times. To stop the reaction, the staining solution was removed and PFA 4% was added for 20 min. Next was performed a PBT wash during 5 min and the samples were kept in a solution made of 50%PBT and 50% Glycerol for 1h. Photograph and store at 4°C.

The embryos treated for whole mount *In situ* hybridization were mounted, photographed and stored afterwards at 4°C.

3.3 Immunostaining

Immunostaining is an antibody based technique, which allows the visualization of certain protein epitopes upon recognition by a specific antibody. In this study, this technique was used to assess the cilia length and localization in the embryo.

Embryos previously fixed in PFA 4% and dehydrated in 100% methanol for several time points were rehydrated through a series of methanol dilution in a phosphate saline buffer (PBS), as described above for *In situ* hybridization. Next, the embryos were washed 4 times in PBT during 5 min each. In PBT the embryos were dechorionated with forceps. Accordingly to the developmental stage a solution of Proteinase K (10 mg/mL) was added to the samples during 15 min (if late somitogenesis stages), 3 min (if mid somitogenesis stages) or 1 min (if early somitogenesis stages). After removing the Proteinase K solution the embryos were fixed in PFA 4% during 25 min at room temperature. As before, this step allowed the tissue to recover some hardness and resistance. The embryos were washed 5 times during 5 min with PBSX (250 μ L Triton X-100 10%, 49,750 mL PBS 1X) and then rinse in miliQ water. For additional fixation the samples were fixed with acetone for 7 min at -20°C . The samples were washed with PBSX to remove the acetone and a solution of PBDX (5 mL PBS 10X, 0,5 g BSA, 500 μ L DMSO, 500 μ L Triton X-100 10%, 44 mL miliQ water) plus fetal bovine serum (FBS - 15 μ L of serum per mL of PBDX to use) was added to block for at least 1 hour. The primary antibodies were diluted in PBDX plus FBS solution as described in Table 2 and incubated overnight at 4°C .

When performing a PCNA immunostaining, after the dechorination of the embryos it was necessary to perform extra steps before continuing to the proteinase K digestion. To the embryos I added 10 mM sodium citrate, incubated at 90°C for 5 min and washed the embryos three times in PBT, during 5 minutes.

Table 3.2– Description of the primary antibodies used for the immunostainings.

| Primary Antibody | Epitope | Host | Concentration | Supplier/ Company |
|--------------------------------|---|--------|---------------|-------------------|
| Anti - Acetylated alphaTubulin | Acetylated alpha Tubulin Monoclonal | Mouse | 1 : 400 | Sigma - Aldrich |
| Anti – GFP | GFP Polyclonal | Rabbit | 1 : 400 | Abcam Ab290 |
| Anti - PCNA | Proliferating Cell Nuclear Antigen Monoclonal | Mouse | 1 : 400 | Dako |

Next day, the samples were washed 4 times in PBDX during 30 min each. The secondary antibodies were diluted as described in Table 3, added to the samples and incubated overnight at 4 °C.

Table 3.3– Description of the secondary antibodies used for the immunostainings.

| Secondary Antibody | Fluorophore | Host | Concentration | Supplier/ Company |
|-------------------------------|----------------------------|------|---------------|----------------------|
| Anti - Mouse Alexa Fluor 546 | Alexa Fluor 546-conjugated | Goat | 1 : 500 | Invitrogen |
| Anti – Rabbit Alexa Fluor 488 | Alexa Fluor 488-conjugated | Goat | 1 : 500 | Invitrogen |
| Anti - Mouse Alexa Fluor 647 | Alexa Fluor 647-conjugated | Goat | 1 : 500 | Life Technologies |

In the third day, the samples were incubated in 4',6-diamidino-2-phenylindole (DAPI - 250 µL PBDX, 250 µL DAPI) for 2 hours. The samples were washed in PBDX 2 times for 10 min each and then washed in PBSX for 30 min. Afterwards, the embryos were fixed in PFA 4% for 5 min and washed in PBSX 3 times for 5 min each.

The embryos stained for whole mount immunostaining were mounted for confocal microscopy as mentioned before. When the results could not be analysed in the following hours after finalizing the protocol the samples were washed 3 times with PBS during 5 min each and stored at 4°C.

3.4 *In situ* Hybridization combined with Immunostaining

Since the *In situ* protocol, removes most of the fluorescent signal inherent to the Tg(0.6*foxl1a*:GFP) line, it is necessary to retrieve the staining with a GFP specific antibody. Therefore we had the need to combine these two techniques.

All the steps from *In situ* hybridization protocol were performed as described before until removal of blocking solution in the second day. Besides adding blocking solution plus anti-DIG, in this step the primary antibodies were diluted in this solution and added to the samples. Proceeding to an overnight incubation at 4 °C.

After the incubation, the solution was discarded and the samples rinsed in PBT. Was done a series of six washes, 15 min each, with PBT. Then the secondary antibodies were added (also diluted in Blocking Solution plus anti-DIG) and incubated overnight at 4 °C.

In the fourth day the antibodies were removed and the samples rinsed in PBT. I next did a series of six washes, 15 min each, with PBT and then the samples were equilibrated in staining buffer (5 mL 1 M Tris-HCl pH 9,5, 45 mL ddH₂O, final pH adjusted to 8,0) three times of 5 min each. The embryos were transferred to a 12 well plate and carefully labelled as the original tubes. The staining buffer was gently removed with a glass pipette and was immediately replaced with the staining solution (1 Fast red tablet per 2 mL of staining buffer, the tablets were dissolved in staining buffer, filtered with a 0.2 µm filter and a syringe to a new falcon). The 12 well plate was protected from bright light with foil paper and incubated at 37 °C accordingly to the probe developing time. The next steps are equal to the *In situ* hybridization protocol.

3.5 TUNEL Assay

TUNEL stands for Terminal deoxynucleotidyl transferase dUTP nick end labelling. This is a technique based on the terminal deoxynucleotidyl transferase activity, that incorporates dUTPs marked with fluorescein to the 3' end of nicked DNA, characteristic of an apoptotic cell.

As the starting point, the embryos were dehydrated in 100% methanol and kept at -20°C. The chosen stages embryos were rehydrated through a series of methanol dilution in a phosphate saline buffer (PBS) - 75% - 50% - 25% Methanol - waiting 5 min. in between each substitution. Next, the embryos were washed two times in PBS Triton 0.1% (50 mL PBS, 50 µL Triton X-100 10%) during 5 min each. In PBS Triton 0.1% the embryos were dechorionated with forceps. Then the samples were rinsed in ddH₂O and incubated in acetone for 7 min at -20 °C. Afterwards, the samples were washed in PBS 1X. Accordingly to the developmental stage a solution of Proteinase K (10 mg/mL) was added to the samples during 15 min (if late somitogenesis stages), 3 min (if mid somitogenesis stages) or 1 min (if early somitogenesis stages). After removing the Proteinase K solution the embryos were washed two times with PBS Triton 0.1% and fixed in PFA 4% during 20 min at room temperature. The embryos were washed during 5 min in PBS and then a minimum of 20 µL and a maximum of 50 µL of the TUNEL reaction solution (1:10 of Label solution and enzyme) was added. The samples were incubated overnight at 4 °C.

In the second day the samples were washed three times with PBS 1X during 5 min each. The samples could continue to immunostaining as described below or stored at 4 °C.

3.6 TUNEL followed by immunostaining

Once again, to increase the fluorescent signal of the GFP-marked cells and be able to correlate apoptosis with the cells of interest, the combination of the TUNEL Assay and the immunostaining was necessary.

To proceed from TUNEL assay to the immunostaining protocol, after the three washes with PBS 1X during 5 min each the embryos were washed 5 times during 5 min with PBSX and then rinse in miliQ water.

The remaining steps of the immunostaining protocol were performed as described before.

4. Data Analysis

All the data collected from the two-photon, spinning disk and confocal microscope were analysed in the programs described below.

4.1 Fiji / Image J software

To analyse the output data (tiff files present several times points per z-stack) from two-photon microscope, the tiff files were opened in Fiji. These files were analysed with different programs and not all of them accepted tiff files, so the tiff files were saved by time points.

A macro (Appendix A) was created and applied to the hyperstack (with the default variable order: xyczt; which means fixed z-stack and variable time points) with time points separated (under the “Plugins” tab I chose the “Bioformats” and “Stack slicer” in order to make this individualization of the hyperstack time points).

The cilia measurements were done in 3D with the plugin “Simple Neurite Tracer”. Since this plugin only accepts one channel, the one with the marked cilia was duplicated and applied the plugin too. Comparing with the hyperstack in a parallel window was possible to determine which cilia belonged to the GFP marked cells (KV cells). All the measurements were introduced in Excel and the statistical analysis done with Software Prism 5.

4.2 Huygens Professional software

Huygens professional is a software used to deconvolute images. Deconvolution is the process by which an image is trimmed to remove the noise and blurring gathered during image acquisition. There are several parameters to access the image quality that need to be taken into account when deconvoluting an image, like nyquist rate, saturation, bleaching, noise, background value and signal to noise ratio. The files saved by time points in Fiji were introduced in Huygens Professional software and the deconvolution quality parameters were accessed. The deconvolution was executed through the deconvolution wizard. The values introduced during the process were variable among images since the movies differed in quality.

4.3 Imaris Software

Imaris is a software developed for 3D image analysis, including cell tracking, filament tracer, surface detection, among others.

Once the image quality was improved and therefore, the objects under study were more prone to tracking, the data was uploaded to Imaris. The image parameters were confirmed and the luminosity, opacity and gamma factor was optimized for each video.

A spot wizard was created and the tracking was done partially by the Imaris programme. The cell average detection size was 6-7 μm and there was the need to correct the KV drifts. For that, the same spot wizard was created but the cell detection size was 80 μm in order to recognize the major group of cells as only one moving object, removing its drift afterwards, with the drift correction option.

The suggested tracking was trimmed to fit the realistic cell movement and the final tracking was recorded in .avi format.



Results

1. Live imaging revealed that KV cells incorporate the notochord, hypochord, floor plate and tail mesenchyme

In order to understand the behaviour and fate of the Kupffer's vesicle cells, after its role in the left-right body patterning, *foxj1a*:GFP line embryos were filmed with a two-photon microscope. Previous observations from our laboratory in fixed embryos (unpublished data) showed that the GFP marked cells of this transgenic line would migrate and incorporate different tail structures. Combining this information with Cooper *et al.*³⁴ and Melby *et al.*¹⁰ findings made us conclude that, live imaging studies were the best approach to the question: “*What happens to the KV cells after it closes?*”.

The movies were made from 11-12 ss to 29-30 ss (not necessarily in one movie but in a combination of sequential movies), with a total of 24 movies.

The KV at 13-14 ss is finishing its role as the left-right organizer. At this stage is observed several apoptotic cells, identifiable by the apoptotic vesicles formed (Figure 4.1 – A'*)(Movie 1 and 2).

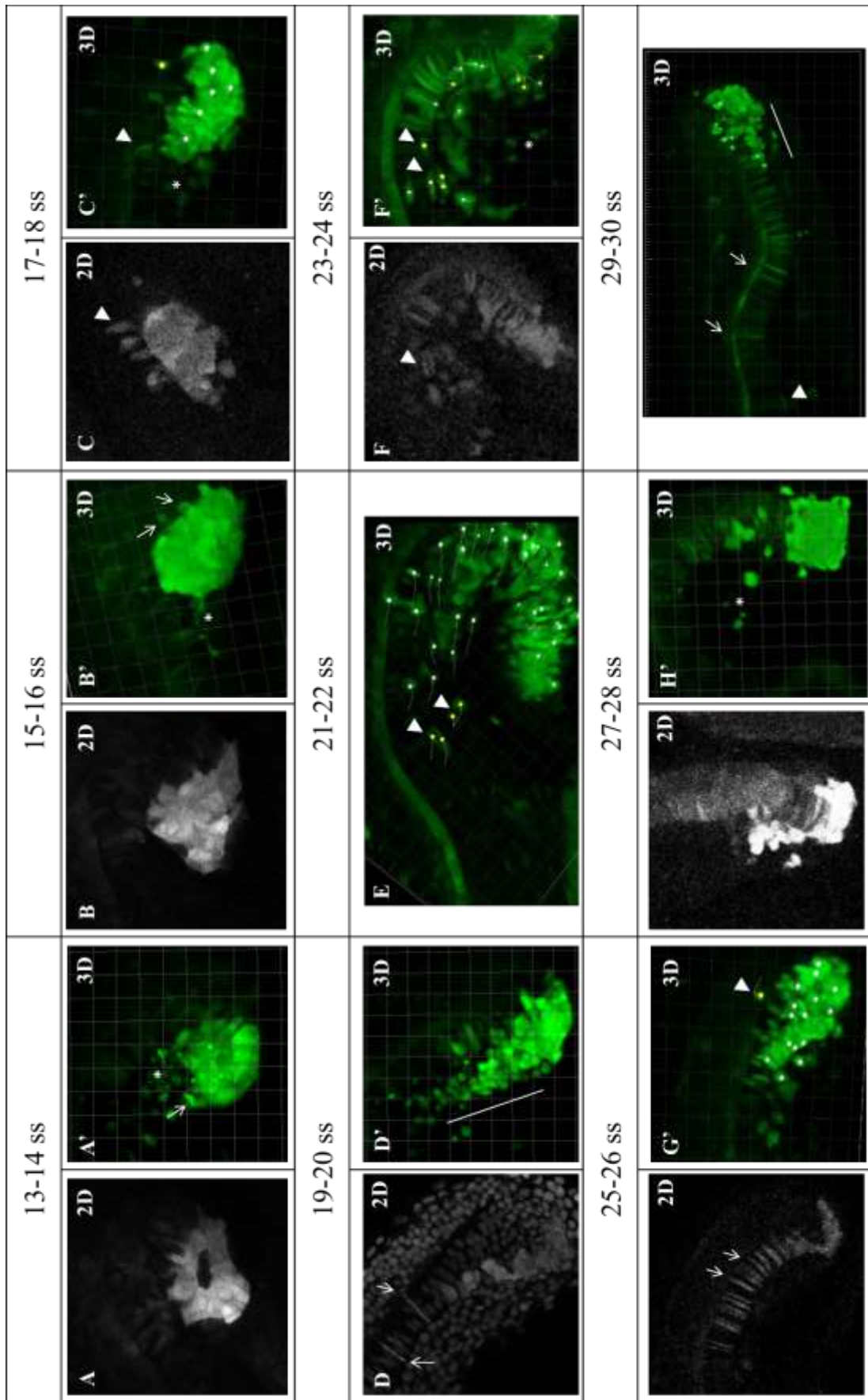


Figure 4. 1 – KV and GFP marked cells location throughout development. A and A' – Embryo at 13-14 ss. A – 2D view of the still open KV. A' – 3D view of the KV with apoptotic vesicles (). The cells exhibit exploratory movements (arrow). B and B' – Embryo at 15-16 ss. B – 2D view of the closed KV. B' – 3D view of the KV with apoptotic vesicles (*). Cells exhibit exploratory movements (arrow). C and C' – Embryo at 17-18 ss. C – 2D view showing the beginning of migration of KV cells (arrowhead). C' – 3D view with a migrating cell prior to notochord incorporation (arrowhead). D and D' – Embryo at 19-20 ss. D – 2D view of fixed embryo showing GFP marked cells incorporated into the notochord (arrow). D' – 3D view with GFP marked cells along the ventral side referred as “comet tail” (White line). E – Embryo at 21-22 ss. Cells after division (arrowhead). F and F' – Embryo at 23-24 ss. F – 2D view with GFP marked cells incorporated hypochord (arrowhead). F' – 3D view correspondent to the F, with multiple cells incorporated into the hypochord and apoptotic vesicle (*). G and G' – Embryo at 25-26 ss. G – 2D view with multiple cells incorporated into the notochord (examples: arrow). G' – 3D view with a cell incorporating the floor plate (Arrowhead). H and H' – Embryo at 27-28 ss. H – 2D view of embryo tail illustrating migration at later stages (arrow). H' – 3D view correspondent to H but emphasizing the apoptotic vesicles(*), the cells incorporated into the notochord (arrow) and migrating cells (arrowhead). I – Embryo at 29-30 ss showing the 3D view of the tail where in the notochord are visible GFP marked cells incorporated (example: arrow), GFP marked cells integrated into the hypochord (arrowhead), migrating cells (white line) and KV compact group in the tail tip.*

At 15-16 ss the KV starts to close, the lumen disappears and the once fluid filled sphere becomes a compact group (Compare Figure 4.1:A and A' with B and B') (Movie 1 and 2). During this closure, it was consistently observed some degree of apoptosis (Figure 4.1 – B' *). Strikingly, most of the KV cells that successfully migrated away from the compact group, died (Figure 4.1 – B' *) (Movie 1, 2 and 3). This type of event was observed throughout the somite stages covered, so it would be very interesting to quantify in detail the apoptosis level to understand until which degree apoptosis influences the KV cell number, ultimately leading to the understating of their contribution to the tail structures.

At 17-18 ss was observed for the first time the migration away from the KV compact group without apoptosis occurrence (Figure 4.1 – C and C'). When the migration started, it was not easy to discern a migrating cell from one that is just left behind due to tail elongation. Imaris drift correction was not sufficient to correct this error. Therefore it will be assumed that these cells have two types of movements: 1) passive movement - left behind due to tail elongation and 2) migration away from the KV compact group.

The cells that migrated first, readily started to incorporate the notochord (Figure 4.1 – C and C' arrowhead). On one hand, this incorporation was executed as a collective behaviour, where a group of cells incorporated the notochord from the ventral towards the dorsal side (Figure 4.2; Movie 4). On the other hand, was also observed individual incorporations into this structure from the same direction (Movie 6). I also observed incorporation from the tip of the notochord (posterior) towards the anterior side. It is indistinguishable if it is a group or an individual incorporation (Movie 7), since the high fluorescence intensity did not allow this characterization.

The cells left the KV compact group with a round cell shape with protrusions, but prior to incorporation into the notochord. As expected, the cell shape became very elongated, and they squeeze in the notochord, vacuolating after incorporation (Figure 4.2). To understand the molecular profile of the GFP marked cells, would be interesting to perform an *In situ* hybridization with a notochord marker and see if there is a co-localization with the GFP marked cells.

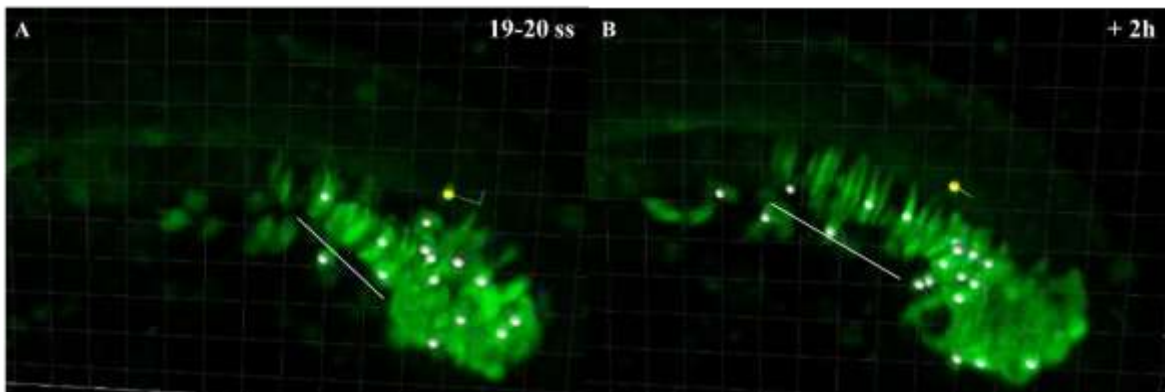


Figure 4. 2 – Transgenic line *foxj1a:GFP* at 19-20 ss, with GFP marked cells incorporating the notochord. A – Collective migration of GFP marked cells towards the anterior region through the ventral side (white line). B – Collective incorporation into the notochord (white line), where the cells acquire a elongated shape.

In a total of 8 movies, where the notochord is clearly seen, a maximum of 12 cells were counted from 17-18ss until 25-26 ss (Figure 4.3) and from the 25-26 ss until 29-30 ss other 25 cells were counted incorporating this structure (Figure 4.C; Movie 7, 18, 19).

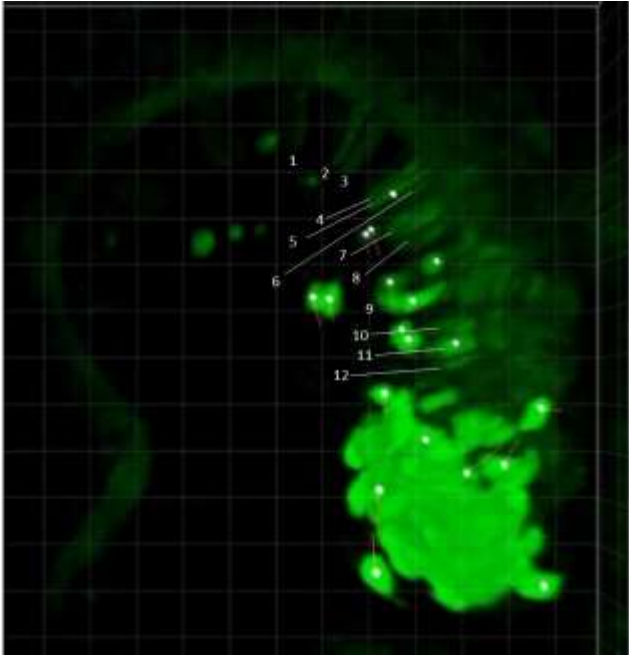


Figure 4. 3 – Transgenic line *foxj1a:GFP* with GFP marked cells incorporated into the notochord from 17-18 ss until 25-26 ss. A total of 12 GFP marked cells were counted in the notochord.

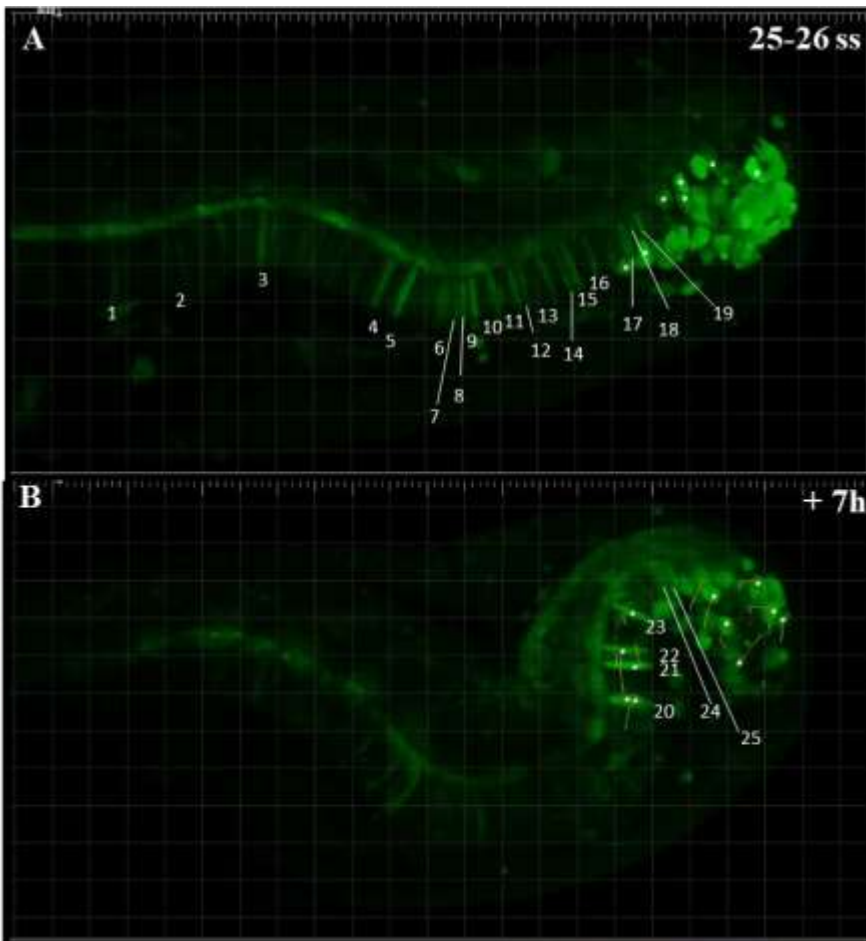


Figure 4. 4 – Zebrafish *foxj1a:GFP* line, GFP marked cells incorporated into the notochord from 25-26 ss until 29-30 ss. A – At 25-26 ss were counted a total of 19 GFP mared cells. B – In the latest stage covered were counted 25 GFP marked cell in the notochord.

At this stage, the KV compact group was located in the ventral side of the chordal neural hinge (CNH). From this region, the cells migrated in the anterior direction along the midline, mostly through the ventral side.

As tail elongation occurred, the KV compact group became more central, until it reached a position totally aligned with the end of the notochord (Figure 4.5). A later position of the KV compact group was better seen in fixed samples, at Prim-5 (Figure 4.6).

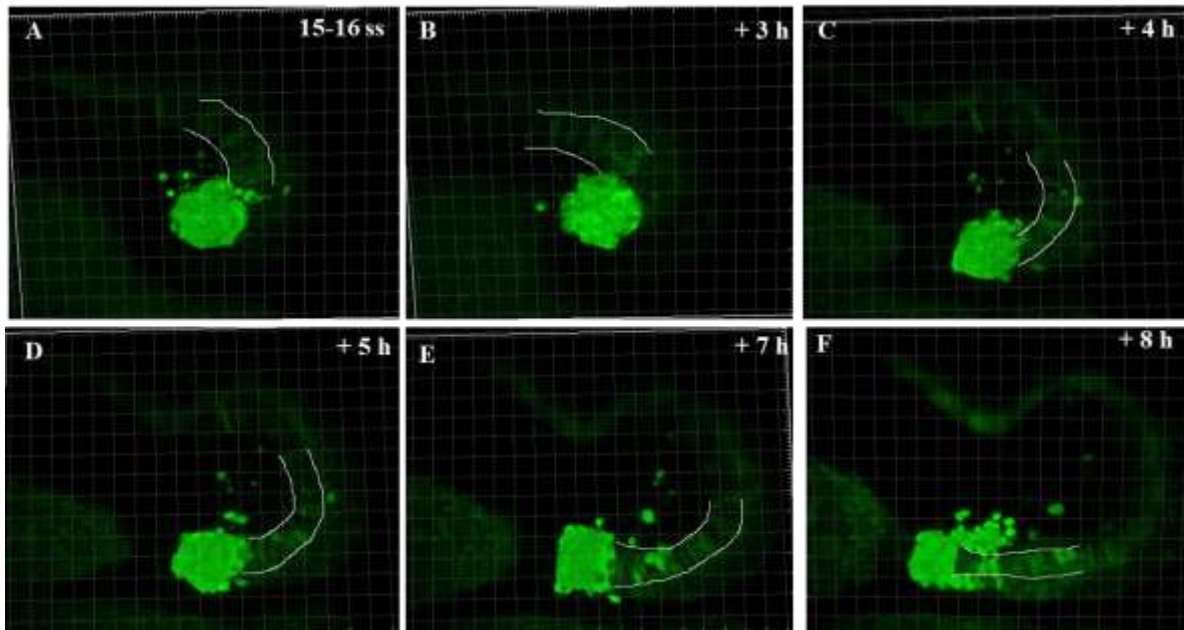


Figure 4. 6 - Migration of Kupffer's vesicle compact group in *foxj1a:GFP* zebrafish transgenic line. KV cells (green). Lines draw represent the notochord position. Scale bar 40 μ m.

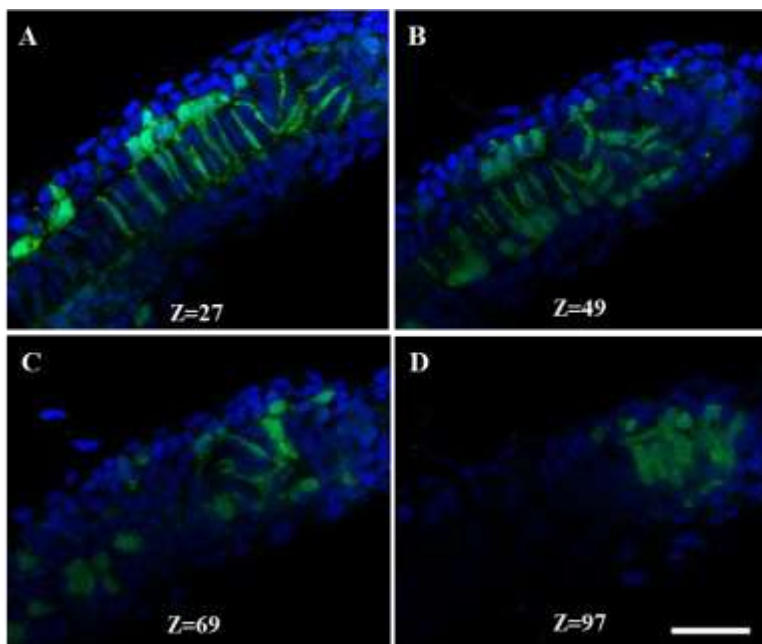


Figure 4. 5 - Image acquired with confocal microscope, 40X. Embryo in Prim-5 developmental stage. Nuclei – DAPI (blue); GFP marked cells – green. A – D: Same embryo tail showed in different z position. It's evident the presence of GFP marked cells and their different positions and orientations over the tail region and along z. Clear presence of GFP marked cells incorporated in the notochord cells (arrow) and floor plate (arrowhead). Scale bar 30 μ m.

Curiously, apoptosis continued to occur to some of the cells that left the KV compact group. This cells, together with the migrating ones and the cells left behind, created a “comet tail” display (Figure 1 – D white line). A number of cells remained in the ventral area (Figure 4.7). These cells started migrating away from the KV compact group at 17-18 ss along with the others, but instead of incorporating any structure or die, these cells persisted in the ventral region (Movie 11 and 12), ending up losing their fluorescence.

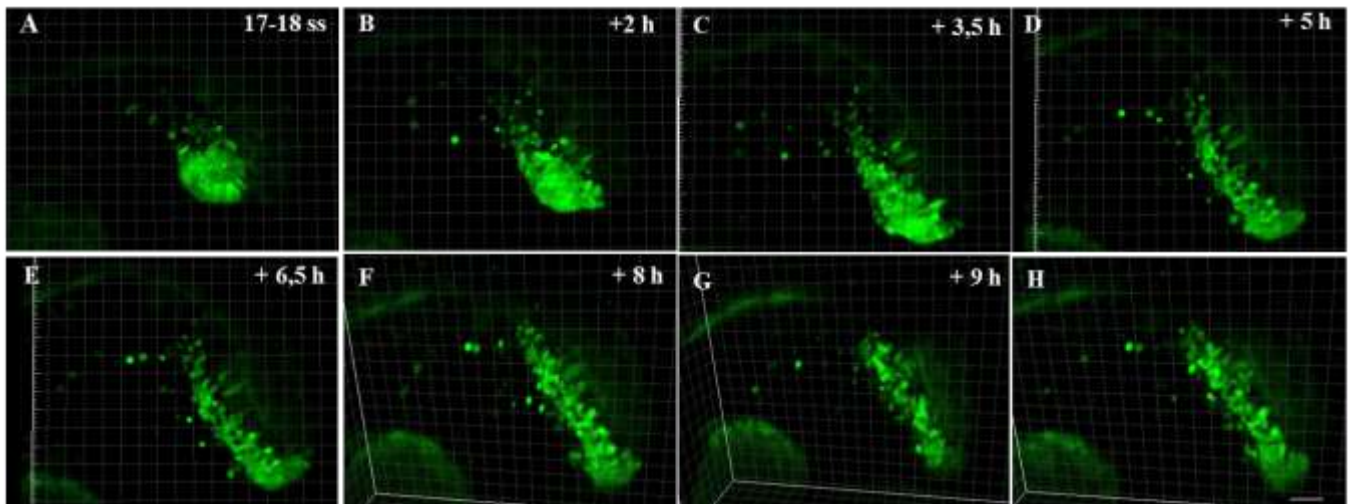


Figure 4. 7 – Movie snapshots of *foxj1a:GFP* zebrafish transgenic line from 17-18 ss until 29-30 ss. Migration of GFP marked cells (green) towards the anterior region through the ventral side of the embryo. Scale bar 50 μ m.

As embryo development continued and tail elongation was more evident, more cells integrated the notochord (Figure 4.1 –D and D’) and at 21-22 ss cell division was observed for the first time (Figure 4.1 – E and E’ arrowhead) (Figure 4.8)(Movie 13 and 14).

This event was not registered in all movies that covered this somite stage, so another approach to assess the number of dividing cells was needed (see section 2.1). Moreover, in live imaging the cell number increase was not, overall, obvious. For instances, and like mentioned before, within the KV compact group was not possible to discern individual cells to be able to count them.

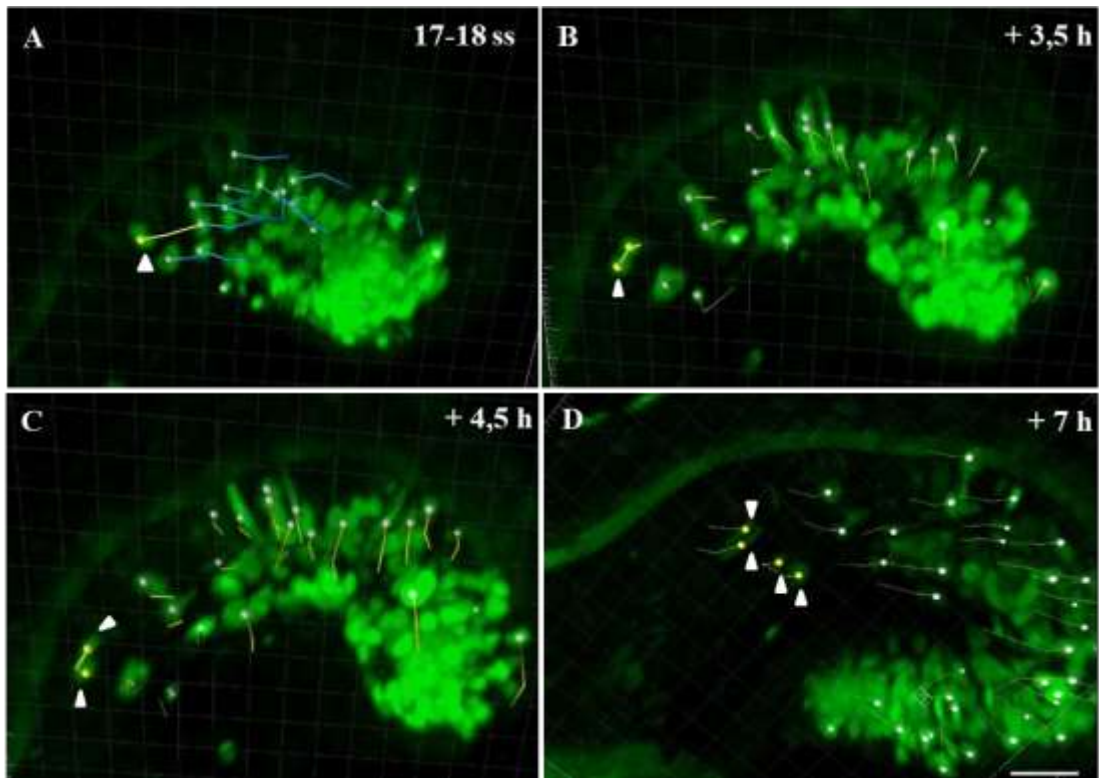


Figure 4. 8 – Movie snapshot of *foxj1a:GFP* transgenic line. Starting at 21-22 ss the arrowheads indicate GFP marked cells dividing from A to D. Scale bar 30 μm .

At 23-24 ss occurred the first incorporation into the hypochord (Figure 4.1 – F and F'; Movie 8). This incorporation was done both through the ventral and dorsal sides of the embryo (Figure 4.9 - Arrowhead). In a total of 4 movies where this incorporation was clear, 6 cells were counted to integrate this structure (Figure 4.10). The cell shape acquired was similar to the structure that they incorporate (Figure 4.9), meaning elongated, as a single row of cells and in the ventral side of the notochord. In Figure 4.9, some of the cells with an elongated shape were not yet placed under/ventral to the notochord, so it was assumed that these cells may still be migrating. Was also observed collective (Figure 4.H - arrowhead) and individual (Figure 4.H - arrow) migration.

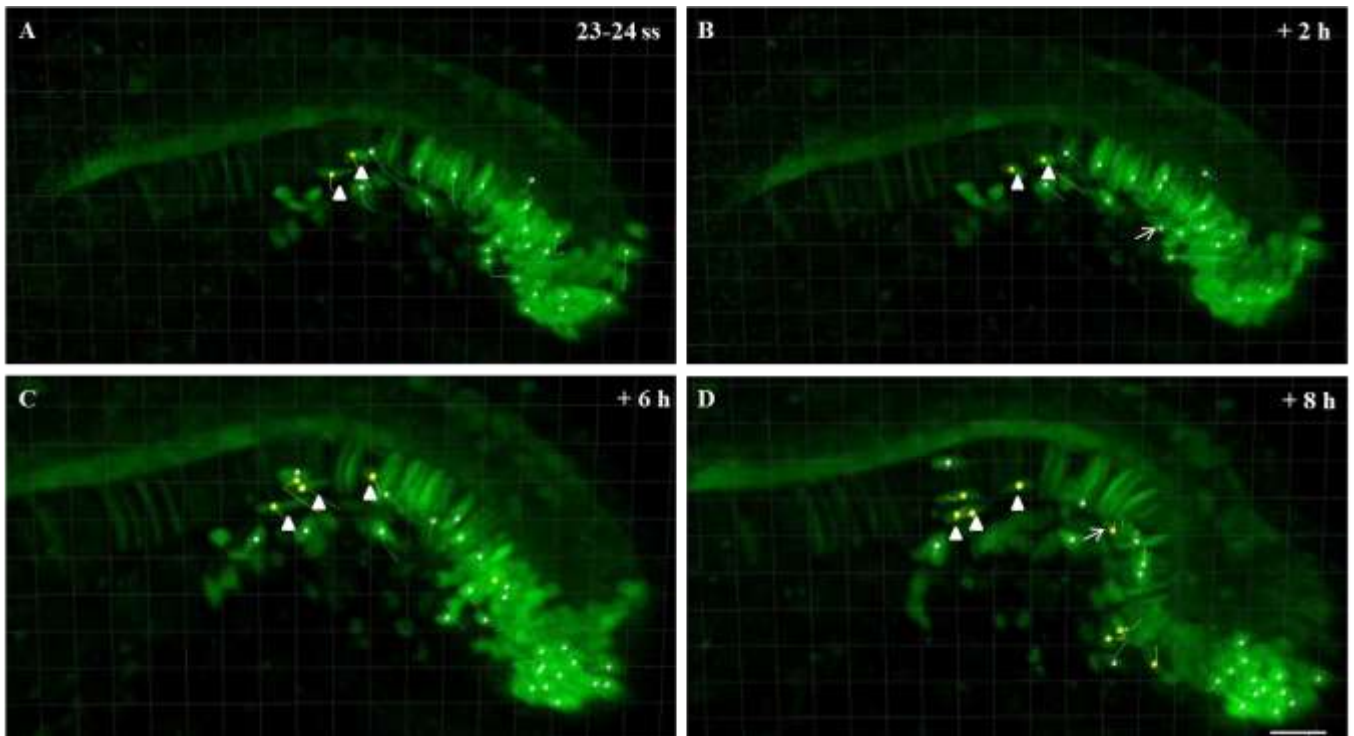


Figure 4. 9 – Movie snapshot of *foxj1a:GFP* transgenic line. Starting at 23-24 ss the arrowheads indicate GFP marked cells incorporating the hypochord. Scale bar 30 μ m.

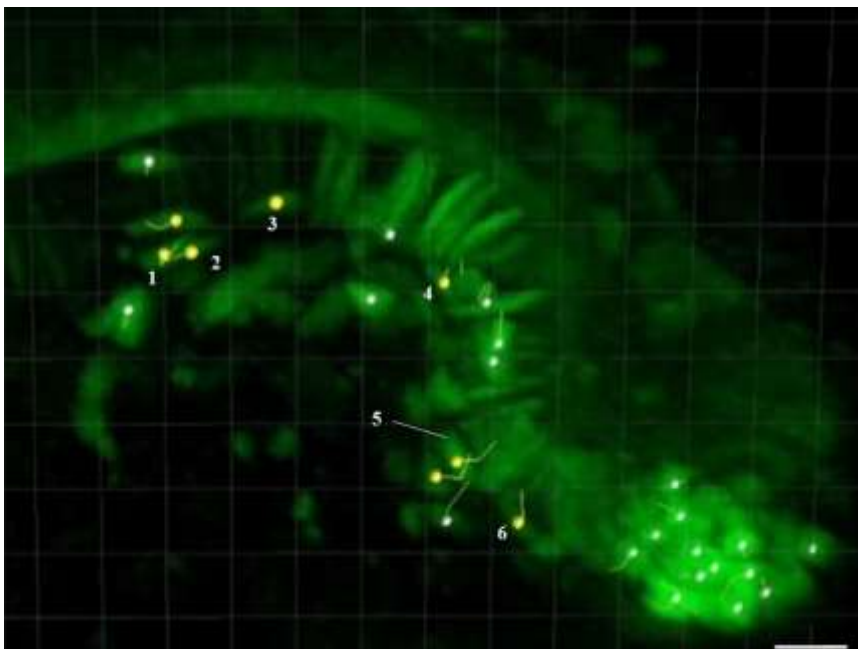


Figure 4. 10 – Transgenic line *foxj1a:GFP* with GFP marked cells incorporated into the hypochord from 23-24 ss until 27-28 ss. A total of 6 GFP marked cells were counted in the hypochord.

At 25-26 ss occurred the first incorporation into the floor plate (Figure 4.1 – G and G’; Movie 9,10). The cells incorporating this structure were just two in a total of 6 movies (Movie 9 and 10). These can also be seen in fixed samples, with the exception that in fixed samples it was possible to observe more cells in this structure (Figure 4.6 – Arrowhead). The first event of cell incorporation happened at 25-26 ss (Movie 5) through the ventral region (ventral towards dorsal) (Figure 4.11). The cells conserved their round shape characteristic of this structure.

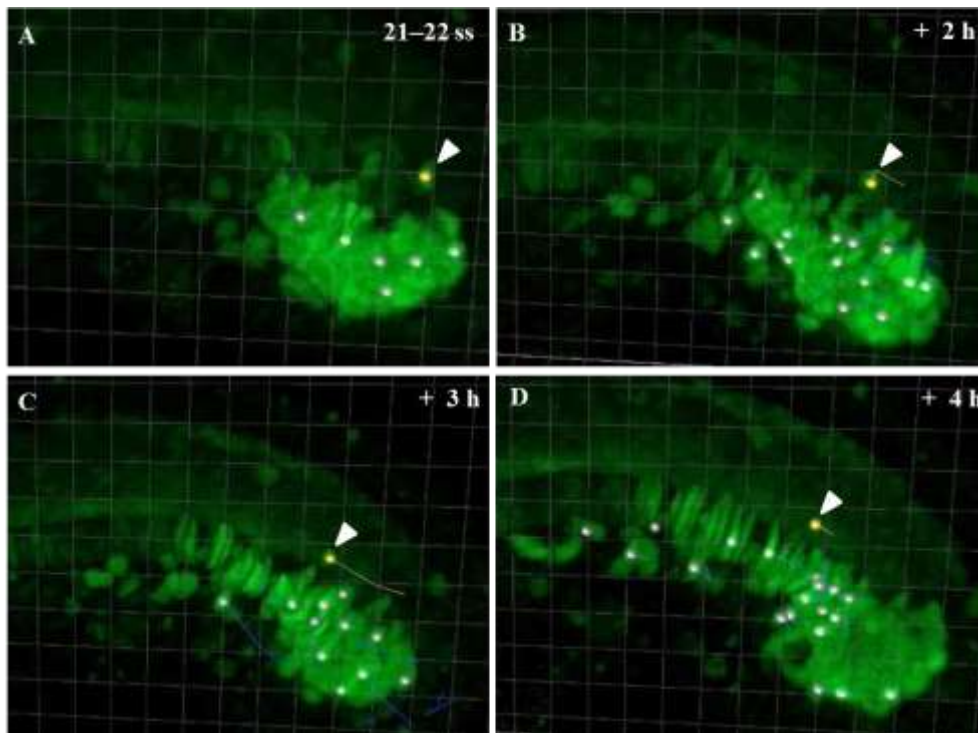


Figure 4. 11 – Transgenic line *foxj1a:GFP* with GFP marked cells incorporated into the floor plate. A maximum of two GFP marked cells were counted in the floor plate.

By live imaging was not possible to observe incorporation in the somites once the stack did not include these structures. Nevertheless, it was shown in fixed embryos the presence of GFP marked cells in the somites (Figure 4.22). Also, in an *In situ* hybridization using presomitic markers one would expect to see co-localization if the GFP marked cells would be prone to incorporate the somites

Several aspects were taken into consideration regarding the GFP-marked cells. These cells fluorescence decreased after incorporating the notochord, while the fluorescence of the ones that

remained outside the notochord, stayed equally strong to the rest of the GFP marked population (Figure 4.1 – A to I'; Movie 15). This fact is a hint to answer the question: “*Do cells lose fluorescence over time and therefore is not possible to trace them properly?*” Once the fluorescence is decreased only after incorporation, probably the fluorescence of these cells remains long enough to allow a complete tracking until their final position.

Overall, the KV cells incorporated the notochord, hypochord, floor plate and tail mesenchyme. Part of the KV population also remained in the ventral region of the embryo and in fixed samples was also observed GFP marked cells in the somites.

Table 4. 1 – Summary of GFP marked cells incorporation and positions at 29-30 ss in the foxj1a:GFP transgenic line.

| Structure | Maximum n° of cells | N_{embryos} |
|------------------------|----------------------------|--|
| Notochord | 25 | 8 |
| Hypochord | 6 | 4 |
| Floor plate | 2 | 6 |
| Ventral region | Several | 15 |
| Somites | 3 (in fixed samples) | 3 |
| Tail and notochord tip | Several | 18 |

The embryos mounted for live imaging with two-photon microscope were fixed after filming in order to perform more experiments.

A distinction was made between the filmed embryos (defined from now on as “Filmed”), the agarose embedded (defined from now on as “Agarose”) and the embryos that were mounted but that during the process were released from the agarose (defined from now on as “Released”).

This distinction was necessary because the tail extension was somewhat altered in the embryos that developed while embedded in agarose and even more in the embryos filmed, i.e. in direct exposure to the laser (Figure 4.12). Nevertheless, and in spite of the difficult development stage classification, the live imaging results can be confirmed when compared to the fixed samples results.

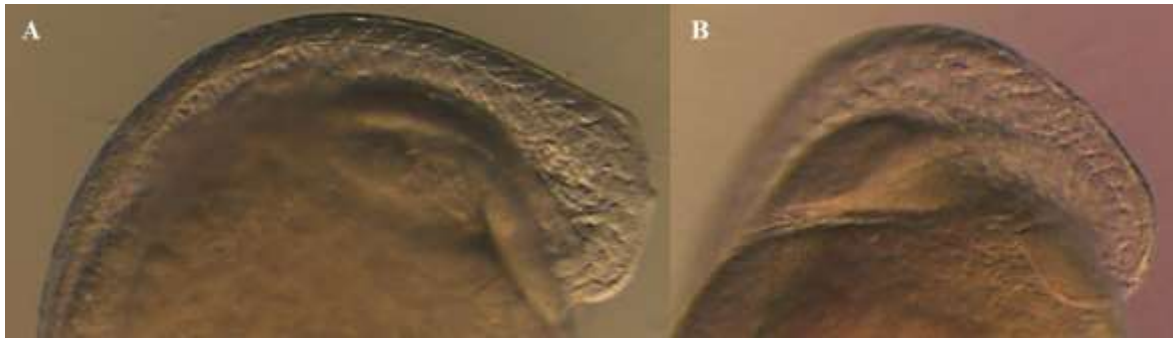


Figure 4.12 - Examples of embryos after live imaging. A – Embryo filmed during 3,30h with two-photon microscope. B – Embryo embedded in agarose during 3,30h but not directly exposed to the laser and therefore to photo toxicity.

2. Complementary information from fixed samples

To characterize in more detail the Kupffer's vesicle cell behaviour, several molecular techniques were performed. Accordingly, from the same batch of filmed embryos, several were let to grow in the incubator and fixed in groups of 20 as they developed.

2.1 Kupffer's vesicle cells undergo proliferation and programmed cell death

In a cell tracking study, for a more complete characterization, it is important to know the dynamics of proliferation versus apoptosis along the migratory process. In that regard, estimation of this population contribution to the embryo development can be estimated.

The PCNA (Proliferating cell nuclear antigen) is a protein that binds to the DNA and is essential for replication, being highly expressed during the S phase⁷⁵. Performing an immunostaining with an antibody against PCNA allowed us to see which cells are in that phase. In this particular case, I also used an antibody against GFP so that KV cells could be seen, to assess the co-localization with PCNA. Thereby, understanding the proliferative profile of the KV cells after their function in left-right patterning.

2.1.1 KV cell proliferation occurs between 21-22 and 25-26 somite stage

The PCNA immunostaining was performed at several time-points with a minimum of 5 embryos per developmental stage. I have recorded 34 stained embryos acquired with two-photon microscope. One example per developmental stage is summarized in Table 5, the correspondent population size and the co-localization of GFP marked cells with PCNA antibody.

At 21-22s, 23-24s and 25-26s the GFP marked cells co-localized with the PCNA antibody and were counted on average 8,25, 16,5 and 6,5 proliferating cells, respectively (Table 4.2). The PCNA positive cells are shown in Figure 4.13. In any other developmental stage dividing cells were not found.

Table 4. 2 - Number of PCNA positive cells counted per embryo within a somite stage (Ss). Total number of embryos – N.

| Ss | 9-10 | 11-12 | 13-14 | 15-16 | 17-18 | 19-20 | 21-22 | 23-24 | 25-26 | 27-28 | 29-30 |
|-----------------------------|------|-------|-------|-------|-------|-------|-------|-------|-------|-------|-------|
| N | 2 | 4 | 6 | 2 | 3 | 2 | 4 | 4 | 2 | 2 | 3 |
| Counted PCNA positive cells | 0 | 0 | 0 | 0 | 0 | 0 | 15 | 23 | 8 | 0 | 0 |
| | 0 | 0 | 0 | 0 | 0 | 0 | 0 | 10 | 5 | 0 | 0 |
| | | 0 | 0 | | 0 | | 0 | 0 | | | 0 |
| | | 0 | 0 | | | | 0 | 0 | | | |
| Mean | 0 | 0 | 0 | 0 | 0 | 0 | 8,25 | 16,5 | 6,5 | 0 | 0 |

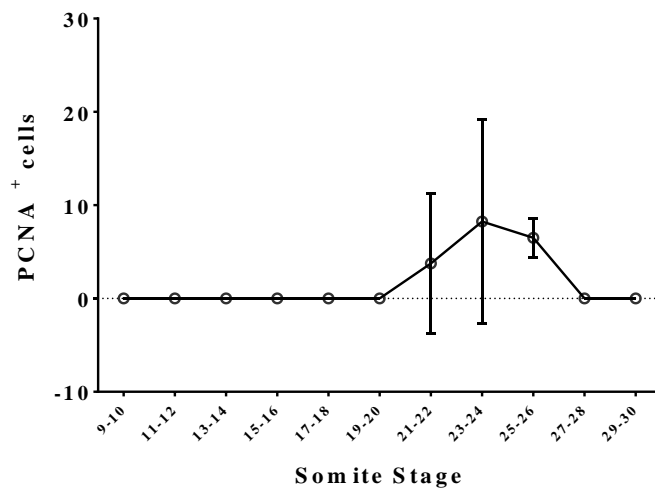


Figure 4. 13 - PCNA positive cells throughout development. Each value represents the mean of PCNA positive cells counted per developmental stage.

After perceiving that the GFP marked cells divide we wanted to see if it was reflected in the total number of GFP marked cells. By that logic, the total number of GFP marked cells per developmental stage was counted (Table 4.3 and Figure 4.14). Using this approach was possible to see an overall increase in cell number. We used the t-test for statistical analysis, where it was observed a significant increase at 11-12 ss, 21-22 ss and 29-30 ss. The increase in cell number at 21-22 ss is expected once at this stage we counted PCNA positive cells thus, cells entering S-phase (as seen in Figure 4.13). Contrary to the 29-30 ss, the increase at 11-12 ss was not expected. This could be explained by low sample number or by less likely reactivation of the *foxj1a* promotor. The cell number fluctuations, in spite of non-significant could be explained due to biological variance.

Table 4. 3 - Number of GFP marked cells counted per embryo within a somite stage (Ss). Total number of embryos – N and the mean values for each somite stage.

| Ss | 9-10 | 11-12 | 13-14 | 15-16 | 17-18 | 19-20 | 21-22 | 23-24 | 25-26 | 27-28 | 29-30 |
|------------------------------------|------|-------|-------|-------|-------|-------|-------|-------|-------|-------|-------|
| N | 7 | 5 | 6 | 8 | 3 | 7 | 7 | 5 | 4 | 5 | 4 |
| Number of cells counted per embryo | 35 | 70 | 46 | 32 | 38 | 31 | 76 | 68 | 34 | 61 | 80 |
| | 52 | 40 | 33 | 34 | 37 | 21 | 89 | 36 | 32 | 60 | 89 |
| | 43 | 50 | 33 | 28 | 38 | 36 | 65 | 42 | 51 | 63 | 60 |
| | 24 | 55 | 38 | 28 | | 36 | 46 | 37 | 80 | 54 | 58 |
| | 33 | 48 | 24 | 40 | | 45 | 61 | 26 | | 28 | |
| | 27 | | 45 | 37 | | 29 | 34 | | | | |
| | 29 | | | 45 | | 38 | 50 | | | | |
| | | | | 37 | | 83 | | | | | |
| Mean | 34,7 | 52,6 | 36,5 | 35,1 | 37,7 | 39,9 | 60,1 | 41,8 | 49,3 | 53,2 | 71,8 |

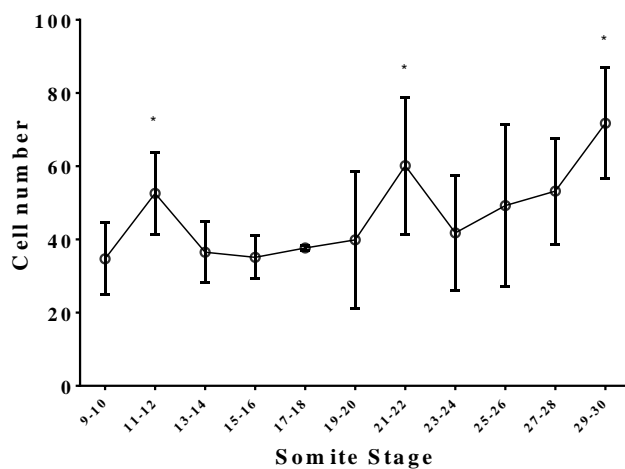


Figure 4. 14 - Cell number throughout the developmental stages. Within a somite stage each value represents the average number of GFP marked cells per embryo. * Significantly different with $p > 0,05$.

| Somite Stages | | GFP - Green | PCNA - Red | Merge | N |
|---------------|-------|-------------|------------|-------|---|
| | 9-10 | | | | 2 |
| | 11-12 | | | | 5 |
| | 13-14 | | | | 4 |
| | 15-16 | | | | 3 |
| | 17-18 | | | | 2 |
| | 21-22 | | | | 4 |
| | 23-24 | | | | 4 |
| | 25-26 | | | | 2 |
| | 27-28 | | | | 2 |
| 29-30 | | | | 3 | |

Figure 4. 15 - Summarized table with examples per developmental stages of GFP marked cells (green), PCNA marked cells (Red), co-localization of the two markers (Merge) and total number of embryos (N). Images acquired with 20X magnification in two-photon microscope. Anterior to the left and dorsal to the top.

Comparing cell number throughout development (Figure 4.14) with PCNA positive cells (Figure 4.15) we could observe that the increase in PCNA around 23-24 ss was reflected in the increase of cell number towards the end of the experimental period.

2.1.2 Kupffer's vesicle cells show low levels of apoptosis

In opposition to the proliferation we wanted to analyse the apoptosis of the GFP marked cells, understanding in that regards the population dynamics. The TUNEL assay marks the nicked DNA, characteristic of apoptotic cells. With this technique plus the immunostaining to enhance the GFP signal was possible, through co-localization, to understand which GFP marked cells were dying and when.

This assay was performed at several time-points with a minimum of 5 to 10 embryos in each developmental stage. The developmental stages covered a window from 9-10 ss to 29-30 ss. I have recorded 80 fixed embryos acquired with a confocal microscope.

The number of TUNEL marked cells dying was variable between developmental stages. A certain number of these apoptotic cells were also variable between replicates in the same developmental stage.

For evaluation of apoptotic rates in each developmental stage, see Table 4.4. The formula used to calculate the apoptotic rates was: total number of TUNEL marked cell per stage / total number of GFP marked cells per somite stage. For apoptosis examples per developmental stage, see Figure 4.17.

In addition, embryos mounted for live imaging with the two-photon microscope were fixed after filming in order to understand if the photo toxicity was inducing abnormal levels of apoptosis. As mentioned before the terms 'filmed', 'agarose' and 'released' were used. For description of apoptotic rates in embryos subjected to live imaging, see Table 4.4. For examples of apoptosis also for these embryos, see Figure 4.18.

Table 4. 4 - Apoptotic rates (%) found for each developmental stage, in embryos used for live imaging with two-photon microscope and total number of embryos (N).

| Somite stage | Apoptotic Rate (%) | N | Somite stage | Apoptotic Rate (%) | N |
|--------------|--------------------|---|---------------------|---------------------------|----------|
| 9-10 | 3,29 | 7 | 25-26 | 8,45 | 4 |
| 11-12 | 3,04 | 5 | 27-28 | 3,38 | 5 |
| 13-14 | 4,11 | 6 | 29-30 | 1,74 | 4 |
| 15-16 | 4,63 | 8 | | | |
| 17-18 | 1,77 | 3 | Live Imaging | Apoptotic Rate (%) | N |
| 19-20 | 1,57 | 7 | Filmed | 1,31 | 4 |
| 21-22 | 1,90 | 7 | Agarose | 2,52 | 7 |
| 23-24 | 3,83 | 5 | Released | 1,38 | 8 |

Regarding these data, t-test analyses indicated that the apoptotic rates were overall not significantly different from each other (Figure 4.16), but had some fluctuation in significance that may be solve with population size increase and biological variance. With a ROUT test no outliers were identified.

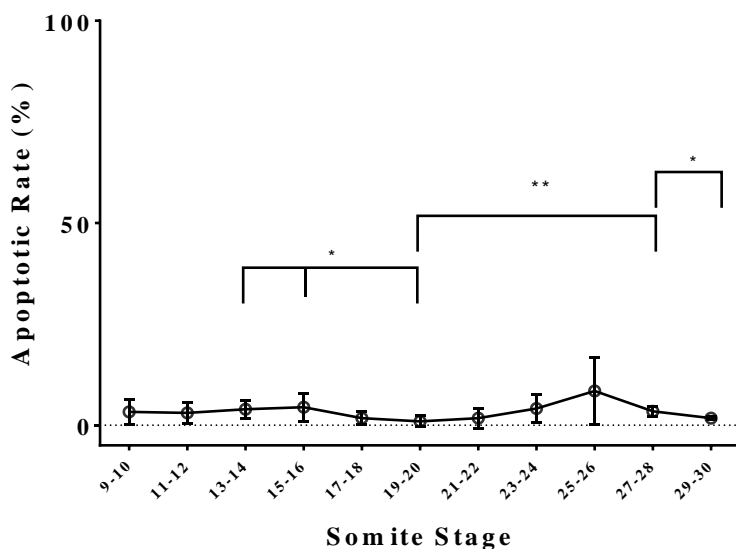


Figure 4. 16 - Apoptotic rate throughout developmental. Each value is calculated as follows: total number of TUNEL marked cell per stage / total number of GFP marked cells per stage. * significantly different with $p > 0,05$; ** significantly different with $p > 0,01$.

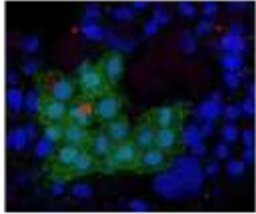
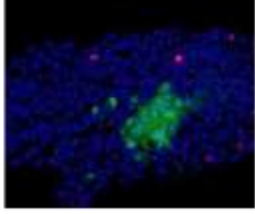
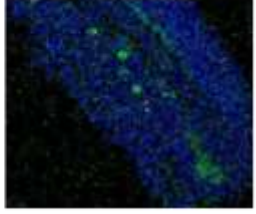
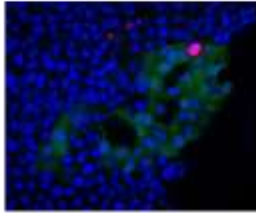
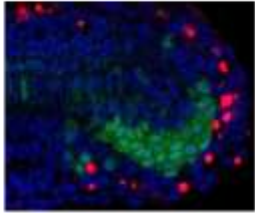
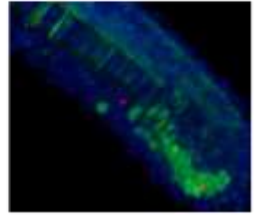
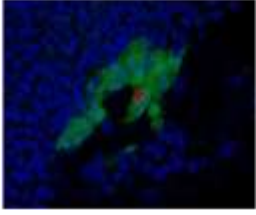
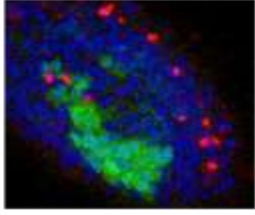
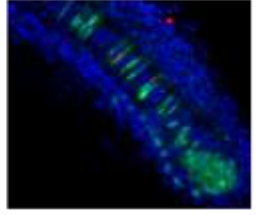
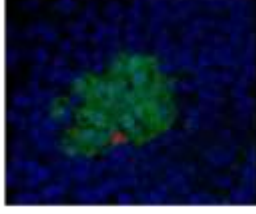
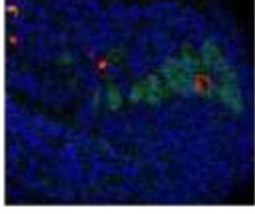
| Ss | Example | N | Ss | Example | N | Ss | Example | N |
|-------|---|---|-------|---|---|-------|--|---|
| 9-10 |  | 7 | 17-18 |  | 3 | 25-26 |  | 4 |
| 11-12 |  | 5 | 19-20 |  | 7 | 27-28 |  | 5 |
| 13-14 |  | 6 | 21-22 |  | 7 | 29-30 |  | 4 |
| 15-16 |  | 8 | 23-24 |  | 5 | | | |

Figure 4. 17 - Examples of apoptosis for each somite stage. GFP marked cells (green), apoptotic cells (TUNEL – red), nuclei (DAPI – blue). ss – somite stage. N – Total number of embryos. Anterior to the left and dorsal to the top.

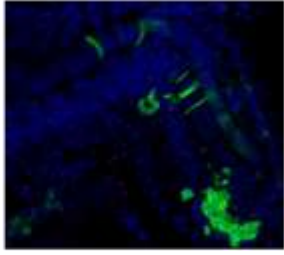
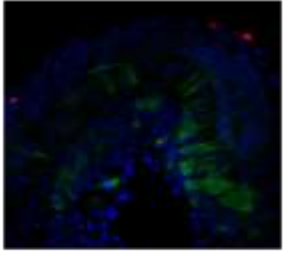
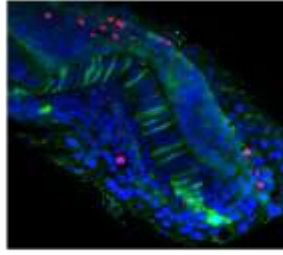
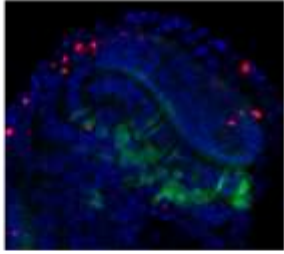
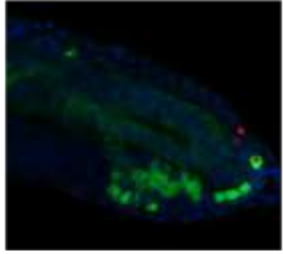
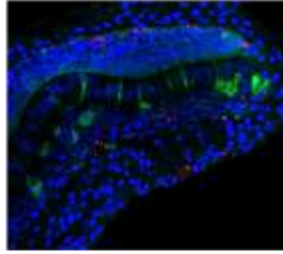
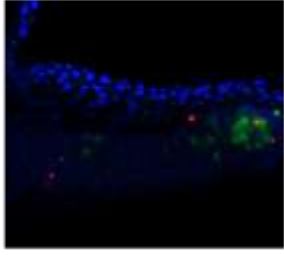
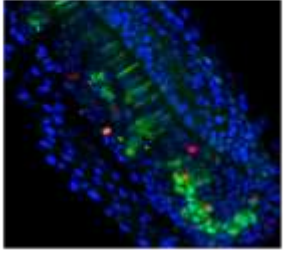
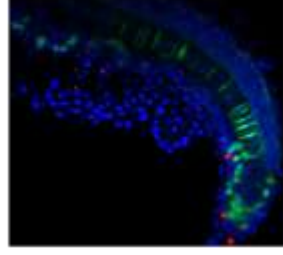
| | Example | | Example | | Example | N |
|-------------------|--|-------------------|--|-------------------|--|---|
| Filmed 25-26 ss |  | Filmed 27-28 ss |  | Filmed 29-30 ss |  | 4 |
| Agarose 27-28 ss |  | Agarose 27-28 ss |  | Agarose 29-30 ss |  | 7 |
| Released 25-26 ss |  | Released 25-26 ss |  | Released 29-30 ss |  | 8 |

Figure 4. 18 - Examples of apoptosis for embryos used in live imaging. GFP marked cells (green), apoptotic cells (TUNEL – red), nuclei (DAPI – blue). ss – somite stage. N – Total number of embryos. Anterior to the left and dorsal to the top.

The apoptotic rates of these embryos were not significantly different within the categories “Filmed”, “Agarose” or “Released”, using t-test analyses. With the same statistical analyses, the values of these categories were also not significantly different from the apoptotic rates found in several developmental stages (Table 4.4 and Figure 4.19). Regarding the live imaging embryos, no outlier was found.

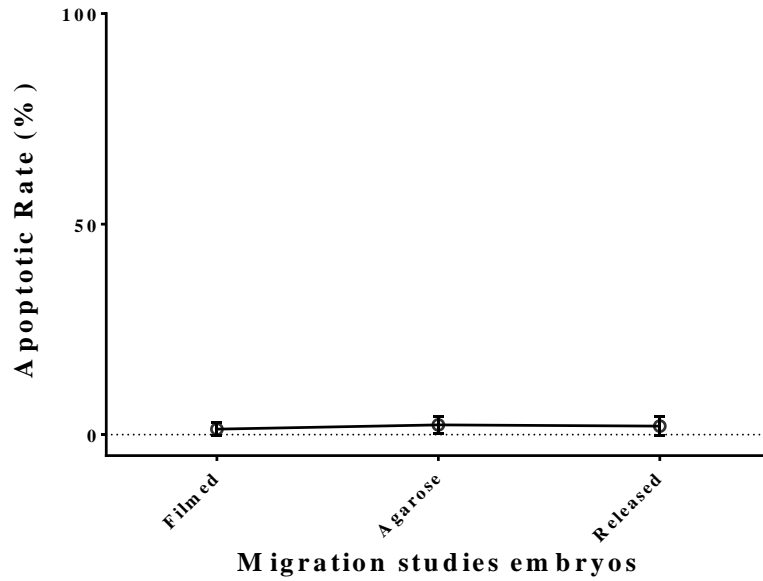


Figure 4. 19 - Apoptotic rates for embryos used in live imaging with two-photon microscope. The “Filmed” embryos used were 25-30 ss. The “Agarose” embryos were 27-30 ss and the “Released” were 25-30 ss. Each value represents the mean of the apoptotic rates found for these stages.

Recalling the proliferation and cell number throughout development the apoptotic rates were very low all over the experimental period (Figure 4.16). Subtracting the apoptotic rate to the number of cells counted is observed the same curve pattern where the cell number increases slowly over time (Figure 4.17). In conclusion, apoptosis was not high enough to affect it.

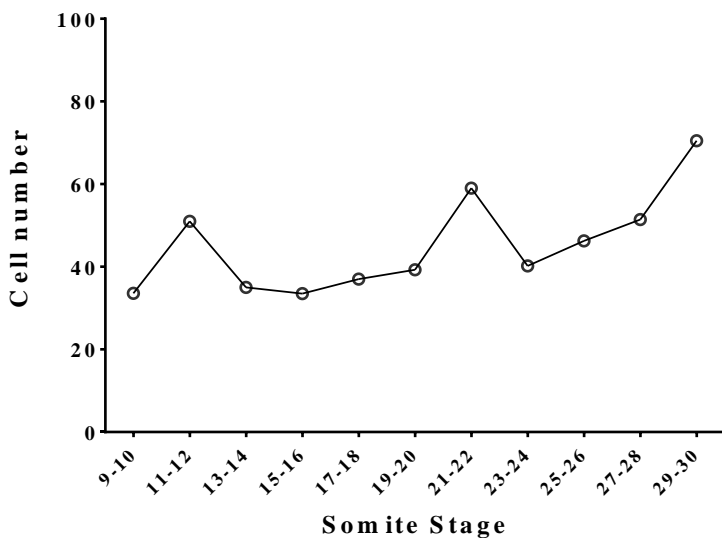


Figure 4. 20 - Cell number per somite stage taking into account the apoptotic rates. Within a somite stage each value represents the average number of GFP marked cells per embryo after subtracting the apoptotic rate for that stage.

2.2 KV cell fates

Besides the proliferation and death dynamics, one major aim of this thesis was to discover the fates of the KV cells and their molecular profile. As said before, the question was firstly addressed with Live Imaging where we understood which structures in the tail the GFP marked cells would incorporate. Having this in mind, with the fixed samples, we wanted to complement this information through co-localization of the GFP marked cells with specific tail structure markers.

The markers used were notochord marker (*no tail*), a presomitic mesoderm marker (*mesogenin1*), a hypochord and floor plate marker (*shh*) and a cilia motility marker (*dnah7*) (Table 3.1 *Materials and Methods*).

In situ hybridization is a technique used, through hybridization of an antisense mRNA probe, to assess the presence of specific mRNAs in a cell, tissue or individual. In this way, it is possible to study the molecular profile of KV cells by characterize the genes they express.

2.2.1 *no tail* marker co-localizes with KV cells

The *no tail* marker expression pattern is described in Figure 4.21.

It was possible to observe that *ntl* co-localized with KV marked cells in all the studied developmental stages. This co-localization may indicate that these cells have a higher probability of incorporating the notochord, as it was indicated by the live imaging results.

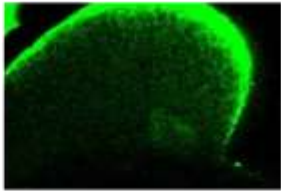
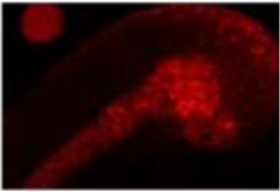
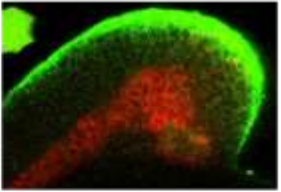
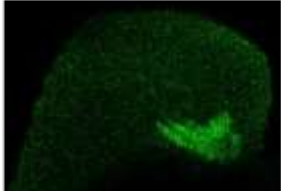
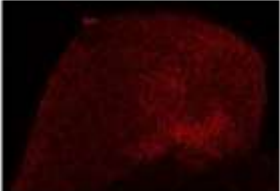
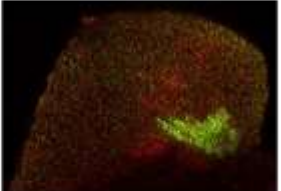
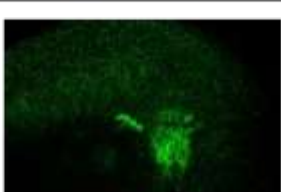
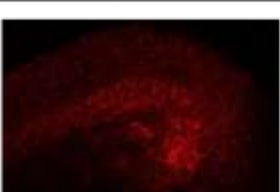
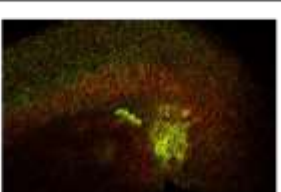
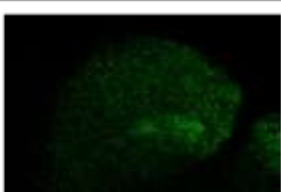
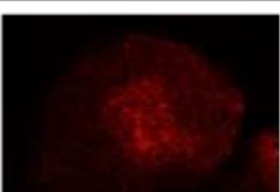
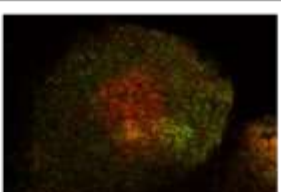
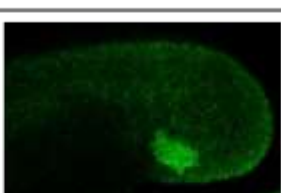
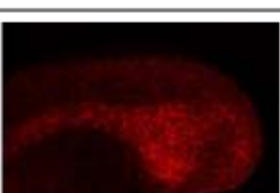
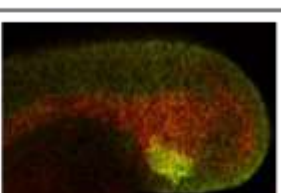
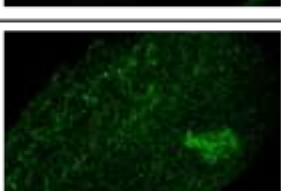
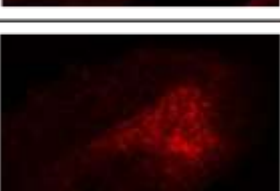
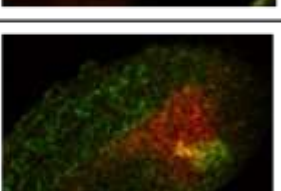
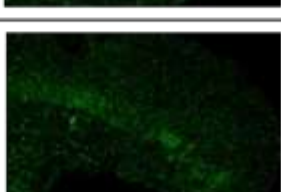
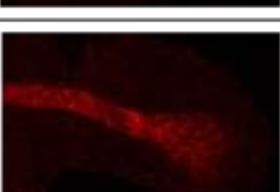
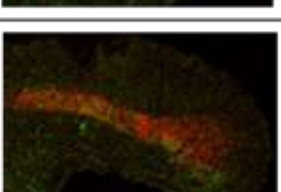
| Somite Stages | | GFP - Green | <i>ntl</i> - Red | Merge | <i>N</i> |
|---------------|-------|---|---|---|----------|
| | 13-14 |  |  |  | 1 |
| | 17-18 |  |  |  | 2 |
| | 21-22 |  |  |  | 2 |
| | 23-24 |  |  |  | 1 |
| | 25-26 |  |  |  | 1 |
| | 27-28 |  |  |  | 3 |
| | 29-30 |  |  |  | 1 |

Figure 4. 21 - Summarized table with developmental stages correspondent to *ntl* (red) and GFP marked cells (green), co-localization of the two markers (Merge) and total number of embryos (*N*). Images were acquired with 20X magnification in the two-photon microscope. Anterior to the left and dorsal to the top.

2.2.2 *mesogenin-1* partially co-localizes with KV cells

The co-localization with *mesogenin1* may indicate that these cells are fated to integrate the presomitic mesoderm⁷¹ and later on the somites (Figure 4.22). As it is described in Figure 4.24, the co-localization with this probe is partial in all the developmental stages. This partial overlap is progressively less from 25-26 ss until 29-30 ss. Very few cells incorporated the somites (Figure 4.22).

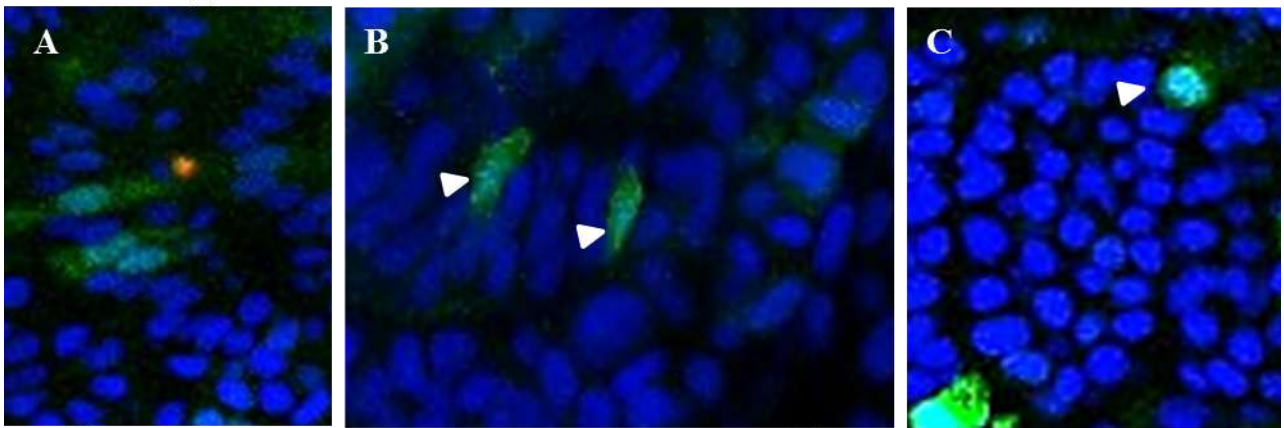


Figure 4. 22 - Immunostaining with antibody against GFP, performed in fixed embryos with 25-26 ss. GFP marked cells (green) and DAPI staining (blue).

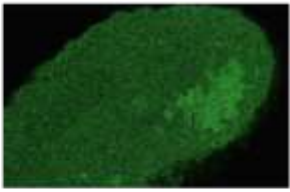

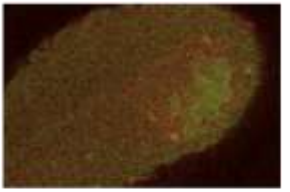
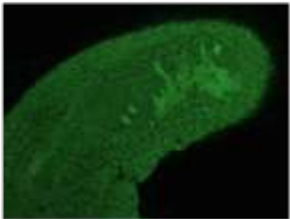
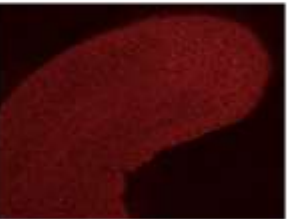
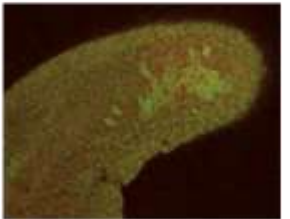
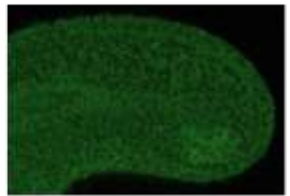

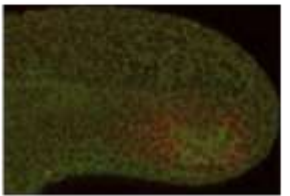
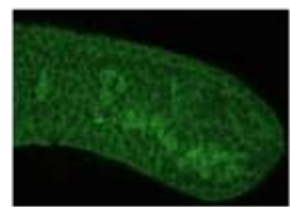
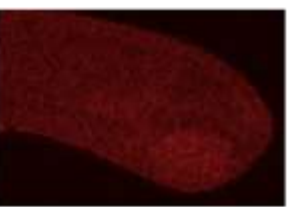
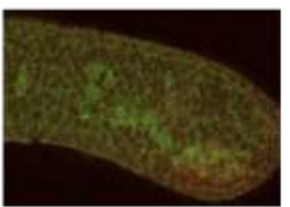

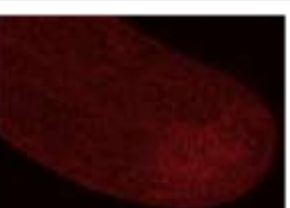

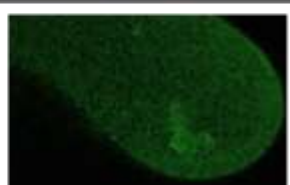

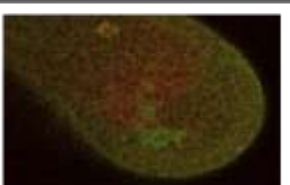
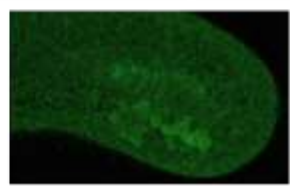


| Somite Stages | | GFP - Green | <i>msgn1</i> - Red | Merge | <i>N</i> |
|---------------|-------|---|---|---|----------|
| | 15-16 |  |  |  | 2 |
| | 17-18 |  |  |  | 2 |
| | 19-20 |  |  |  | 2 |
| | 23-24 |  |  |  | 2 |
| | 25-26 |  |  |  | 2 |
| | 27-28 |  |  |  | 2 |
| | 29-30 |  |  |  | 1 |

Figure 4. 23 - Summarized table with examples for each developmental stages correspondent GFP marked cells (green), mesogenin1 marked cells (*msgn1* - red), co-localization of the two markers (Merge) and total number of embryos (*N*). Images acquired with 20X magnification in two-photon microscope. Anterior to the left and dorsal to the top.

2.2.3 *Shh* marker for hypochord and floor plate

The *shh* marker would mark the hypochord and floor plate^{41,66,74}, as showed in Table 3.1 *Materials and Methods*. It would be expected some co-localization with this marker once some of the KV cells integrate these structures. However, this marker did not work (Figure 4.25), probably due to human error, more experiments will be needed to assess this gene expression.

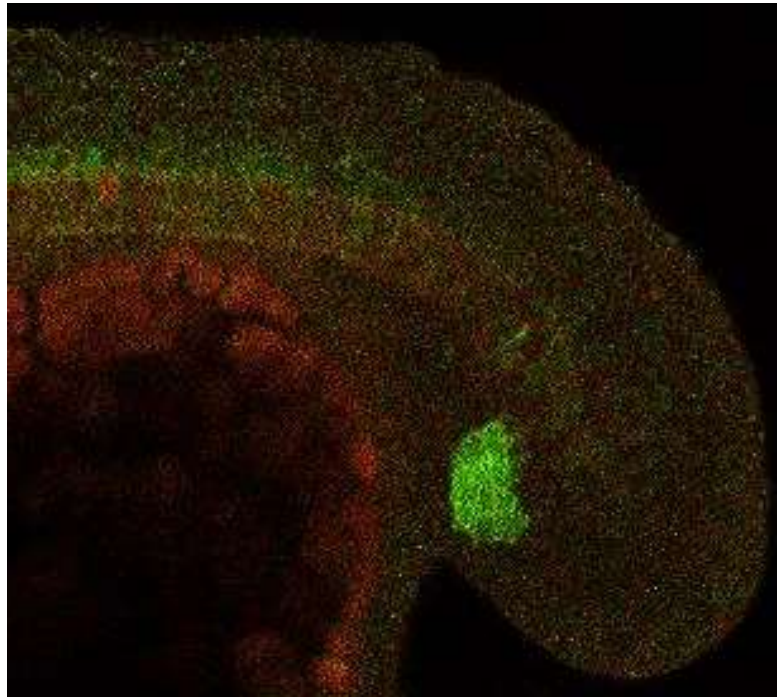


Figure 4. 24 - Image acquired with two-photon microscope, 20X. Embryo at 19-20 ss. It is possible to observe a very faint *shh* staining (red) and GFP marked cells (green).

As an alternative marker for hypochord and floor plate, *Col2a1a* has been developed, but still needs optimization.

In conclusion, the notochord marker *ntl* was very helpful and allowed to confirm the notochordal fate of the majority of cells that once were part of the KV. The *msgn1* probe showed that some cells are more prone to incorporate the PSM (presomitic mesoderm) but more live imaging studies are needed. On the other hand, the hypochordal and floor plate fates were not yet confirmed by molecular markers but were confirmed by their position in the embryo.

3. Long motile cilia retract with developmental progression

One of the main characteristics of the Kupffer's vesicle is the fact that it is made of monociliated cells. The majority of these cells having long and thick motile cilia ⁷⁶. These beating cilia produce a fluid flow that ultimately will lead to the left-right patterning of internal organs ¹⁷. These cilia are specialized and different in length from the primary cilia that surround the KV. For this reason, as the KV closes and becomes a compact group we asked whether cilia become shorter and similar to the surrounding ones. So, we analysed the cilia length progression throughout several developmental stages.

3.1 Kupffer's vesicle cilia length decreases with developmental progression

In the KVs from embryos with 12-14 ss cilia length is on average 6-7 μm , but once the KV lumen starts to disappear and the KV starts to close, these long cilia also start to retract. The cilia length per developmental stage is possible to assess in Figure 4.25. The histograms correspondent to each developmental stage are in annexe B.

At each somite stage, several embryos were observed and the cilia were measured using "Simple Neurite Tracer", allowing a 3D measurement. A pool of cilia per developmental stage was assessed and the statistical analysis was performed over these pools (Table 4.5 and Figure 4.26).

Table 4. 5 - Table with developmental stages, total number of embryos used, total number of cilia per developmental stage and cilia length average.

| Somite stage | N _{total embryos} | N _{total cilia} | Cilia Length(Average) |
|--------------|----------------------------|--------------------------|-----------------------|
| 11-12 | 5 | 158 | 7,23 μm |
| 13-14 | 5 | 129 | 6,90 μm |
| 15-16 | 10 | 297 | 3,45 μm |
| 17-18 | 3 | 57 | 3,44 μm |
| 19-20 | 3 | 86 | 2,48 μm |
| 21-22 | 4 | 253 | 2,85 μm |
| 23-24 | 10 | 434 | 2,96 μm |
| 25-26 | 5 | 223 | 2,63 μm |
| 27-28 | 3 | 180 | 2,99 μm |
| 29-30 | 5 | 282 | 1,95 μm |

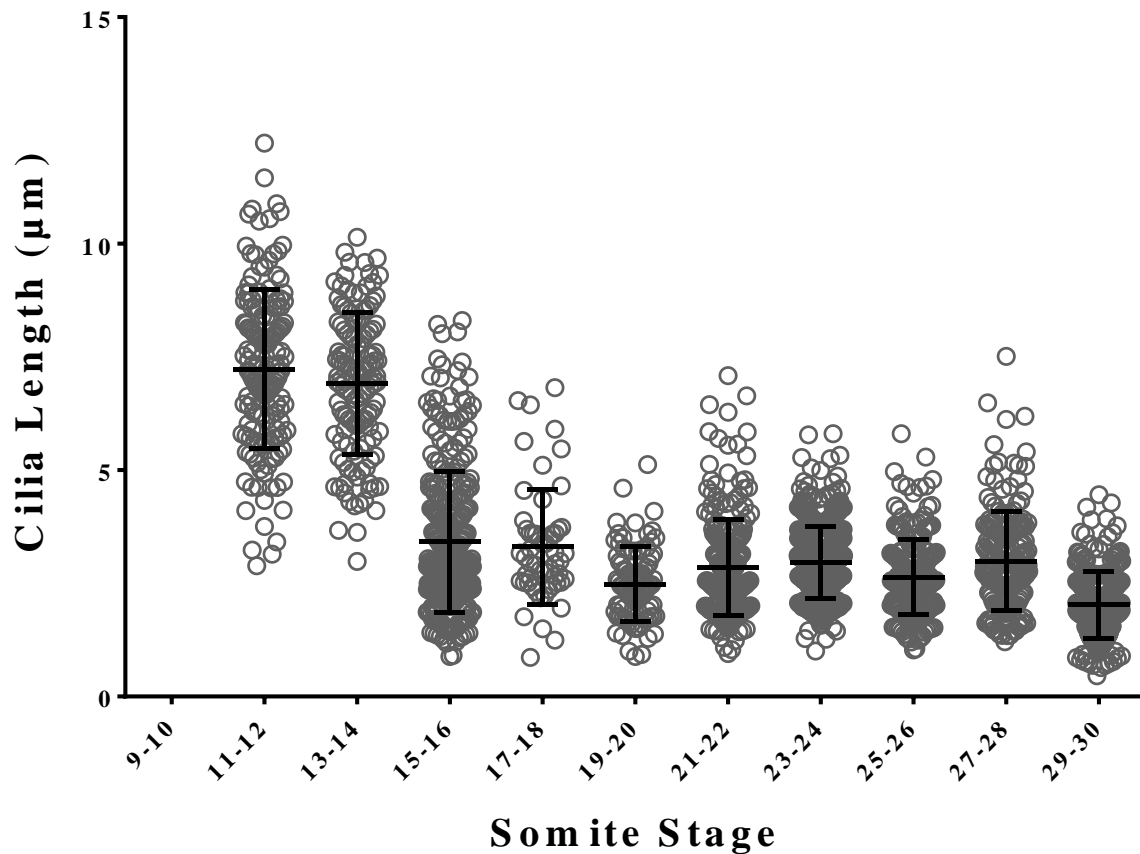


Figure 4. 25 - Cilia length throughout the analysed somite stages. Within a somite stage is represented a pool of cilia lengths from several embryos and each value represents one cilia length. These values are all significantly different from each other.

After statistical analysis using the t-test, the cilia length throughout development was found to be significantly different from each other. At 15-16 ss, there is a pool of long and short, as well as retracting cilia; this is a clear intermediate stage. There are slightly differences among developmental stages due to natural sample variation.

After careful observation it was possible to understand that overtime cilia from the (once) KV cells will resemble the cilia length range of the population of surrounding cells. For instance, the cells incorporating the notochord had long cilia at 13-14 ss, these retracted and once they incorporate the notochord, the cilia length is similar to the adjacent cells (Figure 4.26), which is on average 2,78 μm ⁴⁷.

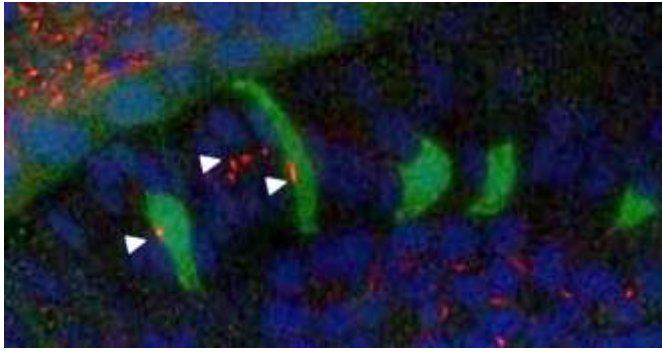


Figure 4. 26 - Image acquired with confocal microscope, 40X. Embryo with 25-26 ss. GFP marked cells (green), cilia (acetylated tubulin – red), nuclei (DAPI – blue). Notochord cilium (arrow head).

With the possibility of increased cell number due to the existing proliferative window, we investigated the number of cilia along development (Figure 4.27). The similarities between cilia and cell number (Figure 4.14 or 4.17) are obvious. As expected, the cilia number reflects the cell number, confirming that these cells are monociliated. These two aspects were addressed independently with different techniques and in different embryos. Nevertheless, there is a consistent peak at 21-22s and 29-30s (Figure 42). For more details read *Discussion*.

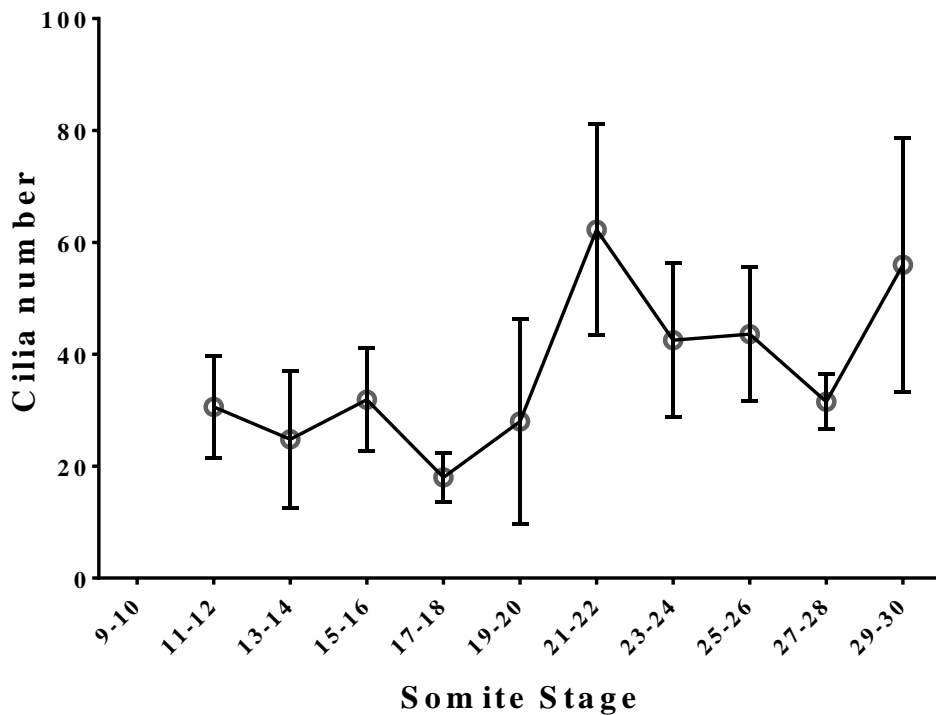


Figure 4. 27 - Cilia number throughout development. Each value represents the mean of cilia number within a somite stage. Using the t-test, all values were overall significantly different from each other. As an exception where identified pairs of non-significance between: 11-12 ss and 13-14 ss; 15-16 ss and 17-18 ss; 21-22 ss and 23-24 ss; 23-24 ss and 25-26 ss; 27-28 ss with 17-18 ss, 21-22 ss and 23-24 ss.

4. Laser ablation and suction of KV cells

The general contribution of the KV cells to the tail and to the structures they integrate can be assessed in several ways. For instances, through more detailed gene expression analysis or further studies of KV specific genes. Another way, is to understand what happens to the development of the embryo once these cells are ablated, removed by suction and/or transplanted into another embryo.

Thus, we ablated KV cells between 13-14 ss, when it was morphologically possible to visualize the Kupffer's vesicle, using the transmitted light of the Andor Spinning Disk (Figure 4.28 A-C). For this set of experiments we used the transgenic line *Ras:mGFP* in order to better visualize the cell membranes (Figure 4.29 A). As described before in the *Materials and Methods* Section, several laser conditions were tried but neither gave the desired result since only two or three cell membranes were destroyed while the remaining cells suffered from photo bleaching (Fig 4.29 A, B).

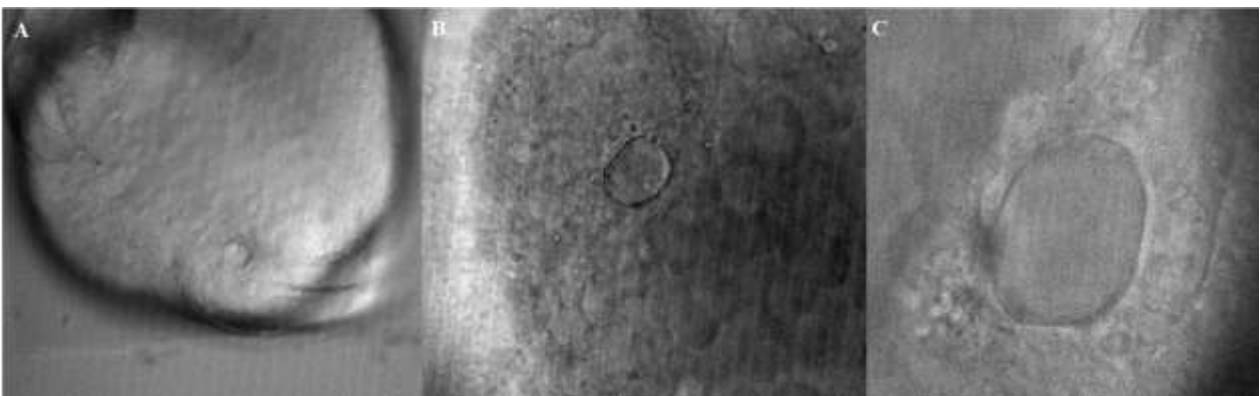


Figure 4. 28 - Kupffer vesicle at 13-14 ss stage. Visualize with andor spinning disk, transmitted light. A – Kupffer vesicle with 10X magnification. B – Kupffer vesicle with 20X magnification. C - Kupffer vesicle with 60X magnification.

One possible explanation for this frustrating result is that the distance between the surface of the embryo and the KV is too large. In fact, from measurements in 6 embryos we concluded that on average there was 70 μm from the surface of the embryo to the KV. This depth is too large and did not allow the efficient laser ablation.

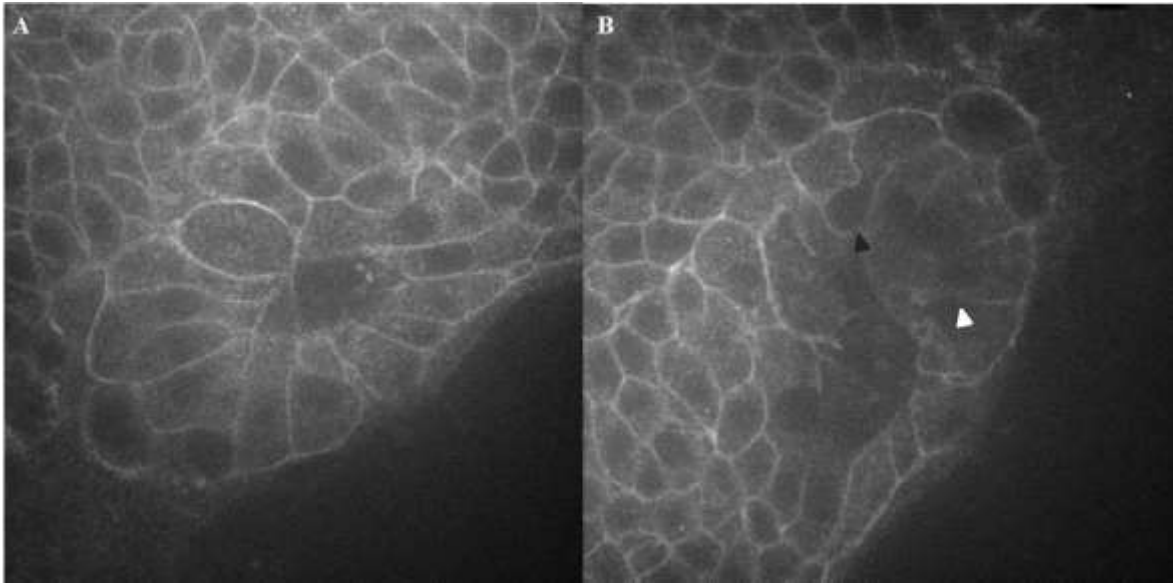


Figure 4. 29 - Laser ablation process in a 13-14 ss stage embryo. A – Kupffer vesicle before ablation. B – Kupffer vesicle after ablation. Because the Ras:mGFP was used it was possible to see the membrane retraction after the ablation (black arrow). Nevertheless, some of the membranes just showed bleaching (white arrow) as it is possible to understand from the unaltered membrane structure.

Ideally, the ablation should be performed at 15-16 ss stage. At this stage the KV already executed its left-right function and cell migration did not start yet.

Therefore, the ablation was also tried at 15-16 ss, where the KV is a compact group of cells, only distinguishable with *foxj1a*:GFP transgenic line. However, since this transgenic line has a very weak fluorescence (Figure 4.30) even the minimum bleaching effect from the laser caused these cells to be no longer detectable and ablation efficiency could not be assessed.

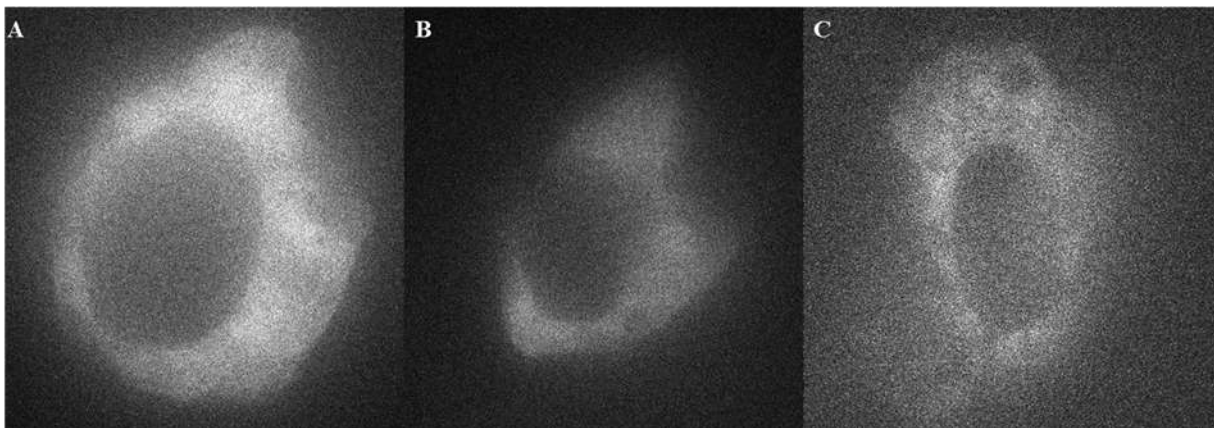


Figure 4. 30 - Kupffer vesicle at 13-14s stage using *foxj1a*:GFP transgenic line. Visualization with fluorescence light Andor Spinning Disk. A – C Several examples of the Kupffer vesicle with 60X magnification.



Discussion and Conclusion

KV cells have a function in left-right asymmetry but surprisingly these cells persist after LR function finishes. Why? In this project we set out to investigate what is the fate and the contribution of the (once) KV cells to the fish larvae.

Two attempts to describe the fate of the KV after its closure were done in 1996³⁴, but in spite of the elegant techniques employed for the time, the developmental stages covered were only until 26s. Nowadays, better tools are available to study this topic. No more attempts were done to validate the information provided by these scientists or to understand the importance of KV cells after its closure.

In this research study the KV cell fates were addressed with a specific transgenic line – *foxj1a*:GFP, which labels very well KV cells. There was an alternative line, *sox17*:GFP but the cells marked by this gene included also the endoderm around the KV. The *foxj1a* is a ciliogenesis transcriptional factor associated with motile cilia fate specification⁶². This transgenic line allowed the tracking of KV cells after its closure.

1. KV cells show collective and individual migration

Among many cells tracked, some of them could be followed along the whole movie duration, but others go out of the stack plane, depending on the embryo position and stack size. The difference

between time points is a fine balance between a time interval that is small enough (15 to 20 min) to allow the correct tracking of the cell and not too much laser intensity that would cause photo bleaching and photo toxicity to the embryos.

In this project two-photon live imaging allowed the observation of different types of cell movements. With this in mind, we observed collective migration of KV cells after its closure (Figure 4.5) and also individual cell migration. Within individual cell migration, there is the passive cell movement away from the KV compact group due to tail elongation and the actual migration of KV cells, once again, away from the compact group and into structures (Figure 4.3, 4.4, 4.10 and 4.11). Special emphasis was put into this individual cell migration to better understand the variety of KV cells fates.

1.1. The KV compact group of cells becomes part of the midline

Regarding the collective migration, it was very interesting to analyse that there is always a group of cells that stays together (Figure 4.5). Around this group there are exploratory movements of cells, which are described as a single cell movement away from the KV compact group that consistently return to it (Figure 4.1 arrow). During the optimization of live imaging conditions, when the warming system was not available, the embryo developed at a much slower rate and these types of movements were more evident. At 15-16 ss, when a cell managed to leave the group it would be entering an apoptotic phase shortly after (Figure 4.1 *). With a normal growth rate at 27-28 °C temperature this was also observed.

It is hypothesized here that there is an attractant responsible for this group of cells cohesion and that when the cells are specified for a certain fate, this attractant effect no longer works. Attractants in the KV cells have been reported⁷⁷ and may be responsible for this behaviour during KV formation. The same type of cohesive mechanism would be expected to act in this group during tail elongation. To test this hypothesis, antibody detection of several reported chemokines, such as Cxcr4 would be an option.

The KV compact group, throughout development, became more central to the midline and the apparent cell number that constitutes it decreases. In fixed samples was observed a later position of these cells is in the tail tip (Figure 4.6). In the tail tip there is no *foxj1a* reported expression, at this developmental stage, so the fluorescence seen must be from the GFP perdurance, detected with the

immunostaining anti-GFP. Not necessarily meaning that the cells have a KV origin but rather a *foxj1a* expressing background. Obviously, more live imaging movies should be done to cover later developmental stages.

Extrapolating information from frog, studies say that the cells of the dorsal margin of the blastopore (equivalent of the shield), during tail elongation retain their organizer capacity and are located at the chordal neural hinge⁴³. Curiously in zebrafish, the KV compact group was observed in the chordal neural hinge during development. If this was evolutionarily conserved, as it seems, one would hypothesise that these cells retain their organizer capacity. Transplantation experiments should be performed with these cells to further investigate their capacity. In chick and mouse transplantation experiments with the chordal neural hinge cells, showed that these cells could induce notochordal and floor plate fates^{78,79}.

1.2. KV individual cell migration leads to integration in several tail structures

Regarding the individual cell migration it was observed three distinct situations: death (Figure 4.18), incorporation into a structure or fluorescence decay (Figure 4.7 and Movie 15).

In our study *no tail* (*ntl*) marker was used to identify KV cells that incorporated the notochord. As reported by Amacher⁴⁴ *ntl* marker is a transcriptional factor related with mesoderm formation, anterior somite patterning, among others⁶⁵. It is known that since sphere stage the region where the shield and the DFC will rise co-localizes with *no tail*, it is also known that the KV cells at 13-14s express *no tail*⁶⁵, but further on in development it was not assessed. From our studies it is possible to say that the (once) KV cells co-localize with *no tail* in more developmental stages than the ones described before (Figure 4.21).

Equally informative as a molecular marker to determine the cell fate, is cell shape and position (Figure 4.3 and 4.4). The cells that leave the compact group as round cells and completely change their shape into thin elongated cells are clearly differentiating into notochord cells. This cell shape fate is in accordance with mouse, chick and frog, as also its LRO cells fates include incorporation in the notochord. Also the shield in zebrafish was previously incorporated into the anterior notochord⁵⁴.

If we look from an organizer point of view, it is nonetheless curious that part of the first organizer (shield) will constitute part of the notochord¹⁰ and that the cells from the second organizer

formed (KV), that is induced by this notochord, will, once its function ends, mainly “return” to the notochord. Do the KV cells have two main fates, one temporary (KV) and one permanent (notochord)? Or these cells unique fate is the notochord with transient formation of temporary organizers?

An interesting observation is that the KV – a signalling center, is displaced along the development but the majority of its cells incorporate other signalling center – the notochord. This result was expected if we compare it with previous research in other model organisms^{10,34}. Besides the notochord, it is known that the tail bud is a progenitor region governed mainly by the expression of *fgf*, *ntl* and *wnt*⁷¹. From this region notochord, somites, hypochord and floor plate cells are originated. The GFP marked cells in the tail bud co-localize with *ntl*, this may indicate that the GFP marked cells in this region have, to some extent, a role in progenitor maintenance.

It was so far described in amphioxus, the presence of cilia-like structures⁴⁷, but in zebrafish or other model organisms no study revealed their present in the notochord. With our research, it was possible to state that also in zebrafish, there is a cilia-like structure in the notochord, with a specific orientation towards the center of this structure (Figure 4.26). The study of its function and motility would be of interest.

Although in different proportions, the next most common fate we detected was incorporation of GFP marked cells into the hypochord (Figure 4.9). It was reported that a *ntl* positive cell can also become hypochordal fated^{52,53}. Since most of the GFP marked cells throughout development co-localize with *ntl*, these findings support the two most common fates among KV cells, which are notochord and hypochord. Like with the notochord, the hypochord cell shape and localization is the best marker we can use. The cells integrating this structure acquire a perpendicular orientation to the notochordal cells and are positioned below the notochord, as described by Eriksson *et al* (2000)⁵⁵. These cells start migrating with a round cell shape with protrusions, but once incorporated in this structure they become elongated⁵² (Figure 4.10). In the live imaging movies it is possible to observe several transversal cells to the notochord, not exactly in the hypochord region but in parallel with it (Figure 4.9 and 4.10). It is known that the hypochord is made of a single line of cells, so the parallel cells are most probably still migrating to integrate the hypochord. Regarding fates, the origin of the hypochord is still debated since there is evidence that point to a mesodermal origin^{52,53} and others point to an endodermal origin^{12,55}. Once all the KV cells co-localize with *no tail*, we can propose that the hypochord cells are of mesodermal origin⁹.

In spite of *ntl* expression correlates with notochord and hypochord fates, cells expressing this gene can even adopt other fates, therefore a more specific probe marking each structure would be required to understand the specification and differentiation timings of these cells. For notochordal

fates it could be used the lysyl oxidases, particularly *lox15b* that is robustly expressed in the tail tip at least at 20s stage ⁸⁰. For hypochordal fates it could be used the hairy-related gene *her 4* ⁵³ or Collagen, type II alpha I, *col2a1* ^{67,68}.

The contribution of the KV cells to the floor plate is very small and it is not visible in all the movies. Even so, the cell shape and location recapitulates the one described for floor plate ⁸¹. These GFP marked cells are also present in fixed samples. Until 29-30 ss they are observed in several embryos in the same quantity (one or two cells, Figure 4.11), but in Prim-5 an embryo presented ten cells in the floor plate location (Figure 4.6). Unfortunately this stage was not included in our live imaging study. Prolonged live imaging with coverage of Prim-5 developmental stage would solve this question. In spite of the few cells incorporating the floor plate, this number agrees to what is described in other organisms ⁸². It is known that the shield contributes to the floor plate, but also the shield itself is constituted by ectoderm. In this case, the KV being mostly of mesodermal origin, we do not expect to acquire high numbers of cells fated to become floor plate.

In all the model organisms described, the organizers incorporated the paraxial mesoderm, from where the somites are formed. In the case of the zebrafish shield, it is known that it contributes to these tissues but from the (once) KV cells, this integration seems rather restricted. Although the colocalization with *msgn1* was positive for some cells expressing *foxj1a*, in the zebrafish embryo the KV contribution to somitic fates is not so evident. More specific markers could also be tested in the future, such as *myoD* ⁷¹.

One curious unknown cell fate is formed by the group of ventral cells that end up losing fluorescence (Figure 4.7). These cells seem to be an example of passive cell movement; since comparing its relative position towards the notochord, it looks that they are just left behind when the KV compact group of cells moves with tail elongation.

It is described that the juvenile fin is constituted of mesenchymal cells involved in a thin epithelial sheet. In spite of the similarities, the juvenile fin is a transient structure. From the tail ventral region (somites or notochord), a population of proliferating cells emerge. With the notochord bend and tilt toward the dorsal side, the fin-ray precursors move in the caudal and dorsal direction, replacing the larval finfold ⁸³. In the adult tail fin, there is a source of stem cells, thought to be responsible for fin regeneration, called hypural cells. These cells belong to the tail mesenchyme described before, as the bone that is attached to spiny rays of the caudal fin ⁸⁴. For a long time the tail mesenchyme was thought to have a neural crest origin, but recent findings by Carney et al (2013) ⁸⁵, claimed that the fin mesenchyme is exclusively of mesodermal origin.

So, can these ventral cells be the precursors of the hypural cells, whose origin is unknown? Later developmental stages would need to be assessed and probably a different type of KV cell labelling, such as Kaede photo conversions, should be used. Also, laser ablation of these cells and regeneration studies in adult caudal fin could be an interesting project.

As mentioned before, a distinction was made between filmed, agarose embedded and embryos released from the agarose (Figure 4.12). Several differences were noticed, like the developmental velocity - which is faster in released - and tail morphology - which is deformed in agarose embedded embryos (either filmed or not). The minimum possible agarose density was used (0,5%) once lower than that would not immobilize the embryos, so other techniques should be tried to avoid this effect.

It is known that specific pressures or forces can change gene expression in embryos through mecanosensation ⁸⁶. Hypothetically, the pressure done by the agarose could provoke or alter cell migration or even lead to its arrest. Once the ventral cells found in live imaging were not often encountered in fixed samples, these could result of defective development due to truncations in tail elongation. As said before, laser ablation of KV cells and testing different embryo mounting settings, where the tail is not constricted in agarose would elucidate this matter.

On the other hand, these 'agarose' studies were complemented with fixed samples, which were never exposed to the laser and have grown freely in E3 medium. In general the results were similar. The fates observed in live imaging - notochord, hypochord, floor plate and tail mesenchyme - were also observed in fixed samples. The comparison between these two techniques allows us to have a high degree of confidence in stating that, in general, the development of the embryo and cell migration is not affected by the deformed tail growth.

But there are some differences worth mentioning between live and fixed embryos, such as the meaning of a GFP marked cell. In live imaging it's possible to see the cells migrating from/to a region/structure and therefore we promptly see its KV origin. On the other hand, in fixed samples, the migration path of a GFP marked cell, already incorporating a structure, or in a certain region is not known and thus it is not possible to be sure that it is a KV cell. A very powerful technique that could be used would be the Kaede injections at 1 or 2 cell stage and photo conversion of DFC at shield stage. This would allow us to know the cells origin even in fixed samples.

Several setbacks were encountered during this study, such as low fluorescence intensity and its highly sensitivity to light. One such drawback is if KV cells are not followed from the begging of its closure (where these cells are the only ones expressing *foxj1a*) it is not possible to discern if the GFP marked cells observed, are originated from the KV or if they just started expressing *foxj1a*. In spite

of KV cells are not the only cells expressing *foxj1a*⁸⁷, they are the first cells to express this gene and GFP intensity in these cells is visibly higher than in the others.

An advantage of GFP is the high protein life time, i.e. even if *foxj1a* is no longer being expressed, the GFP will remain in the cell, allowing a longer tracking due to perdurance. In live imaging it was possible to observe that after 40-60min of KV cells incorporate new tissues, cell fluorescence started to decrease. The GFP half-life varies according to the context but it's generally very stable⁸⁸.

Nevertheless, there are alternative tools to this line, like *foxj1a:CreER*^{T2} transgenic line crossed with a heat shock induced loxP line. This line was available for this study and an optimization was carried out. Unfortunately, it was unsuccessful since the promoter sequence of the Cre line was incorrect. The Kaede injection and photo-conversion of DFC was also considered but due to time limitations only *foxj1a:GFP* line was used.

Overall, we could answer some interesting questions. Even within the KV population the fates differ, there are notochordal fates, hypochordal fates, floor plate fates, tail mesenchyme and maybe hypural cell fates. What determines which cell follows which fate, is still a very intriguing and exciting developmental question.

2. KV cells present a proliferative and death dynamics

2.1 There is a proliferative window for the GFP marked cells

Kanki and Ho³⁸ reported the proliferative profile of the tail region at 14 ss and 18 ss (Figure 1.20). As it is easily observed the proliferation is higher as closer to the midline the cells are. In accordance with this information and, since the position of the KV cells is in this region; there is a short window of proliferation from 21-22 ss to 25-26 ss. The total number of cells per developmental stage was counted and there was a significant increase in cell number at 11-12 ss, 21-22 ss and 29-30 ss. Nevertheless, the total estimated number of cells is not expected to be much higher since most of the observed cells along the development present a cilium, which is indicative that these cells are not

dividing since for that, the cilium should be retracted ⁸⁹. The initial KV cohort is composed of 30-60 cells ⁷⁶ and with our detailed study we conclude that overall the cell number significantly increases from 9-10 ss until 29-30 ss (Figure 4.15).

2.2 The apoptosis rate varies little between developmental stages

As defined by Glucksmann and explained previously, there are three different contexts of apoptosis. The one observed in the KV cells is histogenetic, since it's generally low along the developmental stages and seemingly random.

The apoptotic rate is slightly (but not significantly) higher at 15-16 ss, and this was also corroborated by live imaging movies (Figure 4.1 *). Indeed at this stage, while the KV is closing and the cells did not yet start migrating, several cells die (distinguished by the characteristic apoptotic small round vesicles ⁹⁰). It was curious to observe that most of the cells that enter apoptosis first migrated away from the KV compact group and shortly after the apoptotic vesicles were formed. In the live imaging, at 17-18 ss, with the “comet tail” formation and migration away from the KV compact group it was also possible to verify the formation of apoptotic vesicles (Figure 4.7). However, this was not reflected in the apoptotic rates obtained (Table 4.4). According to Cole and Ross ⁵⁹, apoptosis is a quick process, cleared in a maximum of 2 hours. On one hand, it could be that some of the embryos fixed for this assay, had already cleared the apoptotic vesicles. We consider this option not likely due to the short 1h time intervals between embryo fixation. On the other hand, it could be that at 17-18 ss there was an increase in apoptosis due to photo toxicity. This would not be revealed in the apoptotic rates, because this study was performed in embryos after filming and not at that specific stage. This doubt could be solved with in vivo marking of apoptosis with annexin V detection ⁹¹. In spite of detection of apoptotic cells, due to the principle of TUNEL assay it does not discriminate between apoptotic, necrotic or autolysis death. As an alternative technique to identify apoptosis we could target the active form of effector caspases (for instances, Caspase 3).

Comparing the apoptotic rates between embryos used for live imaging and the ones directly fixed, there was no significant difference. With the data obtained we conclude that overall apoptosis is low and constant throughout the somites stages covered (Figure 4.16 and 4.20).

3. Cilia of the KV cells retract and become short cilia later in the development

In zebrafish, it is known that Kupffer vesicle^{66,92} cells are monociliated and mainly motile, their influence in embryo development is crucial for left right patterning, as explained before.

With KV closure, the cilia start to retract until their average length is similar to the immotile cilia in the tail region (Figure 4.25). From 17-18 ss, along the developmental stages, their size doesn't change significantly, where most of the cells keep a short cilia. Looking at the histograms (annexe B) it is possible to conclude that the shapes of the curves obtained are different between some developmental stages. At 11-12 ss and 13-14 ss the curves shape is similar to a normal distribution, slightly deviated to the right, i.e. more long cilia measured. From that stage on, most of the histograms show a curve deviated to the left and present a higher slope from 2-3 μm class. Taking into account the population surrounding the KV cells, with the progression of developmental stage, the cilia length becomes more and more similar to the cells around it (Figure 4.26).

It is known that KV cilia are mostly motile⁷⁶ and that *foxj1a* gene is usually associated with motile cilia. So, are these shorter cilia motile? Is it possible that these cells are no longer expressing *foxj1a* and the fluorescence seen is due to a delay degradation of GFP? These doubts are easily answered with live imaging using a high speed video camera or by a simple *In situ* hybridization with *dnah7* probe, which will inform us of the cilia motility.

Comparing cell number (Figure 4.17) with cilia number (Figure 4.27), it is possible to see that before the proliferative window, the cilia number is inferior to the cell number. This could be explained by the cilium retraction that needs to happen before the cell enters a division stage. On the other way around, at 25-26 ss the increase number of cilia and decreased cell number could be due to small population size in the cell number data (N=2) or that some cells acquired a multiciliated profile. The increase in population size would be advisable. Nevertheless, the curve profile is similar between cell number and cilia number, as expected once these cells are monociliated.

4. What is the influence of KV cell ablation in tail development?

Besides some contribution to the tail tissues what is the influence of these cells in larvae development? And what consequences would have its absence? These questions attempted to be answered with laser ablation of the KV cells at 16 ss, where the results would only be due to the ablation and missing KV cells, in opposition to 13-14 ss KV ablation, where left-right defects would also be present and potentially mask KV cells expected smooth effects.

The laser used for ablation had the tremendous precision of ablating only one cell. This feature proved, in this particular case, not to be an advantage but a weakness, since with a weak transgenic line (*foxj1a:GFP*) and the need of approximately 30 point ablation, most certainly resulted in bleaching instead of ablation.

A more aggressive and wide field ablation should be tried, not just to overcome the difficult tissue penetration but to maintain the efficiency of the laser at deep regions of the embryo. Once optimized the ablation at 16s, the morphology of the tail region would be verified and compared with control embryos. In particular, the number of notochord cells would be counted since most of the KV cells incorporate this structure.

As an easy correlation with hypural cells, the ablated embryos would be let to grow until 48h, when the pigmentation is well established and the hypural coincident pigmentation gap is clearly present. Hypothesizing that some of the KV cells are the precursors of the hypural cells; we could then ask whether this pigmentation gap still exists after ablation.

An important consideration when analysing the ablation results, is that the KV cells have a proliferative window beginning at 21-22 ss, i.e. after the laser ablation at 16 ss. So, at 21-22 ss would there be a compensatory mechanism of the ablated KV cells? A solution to this situation would be to perform the ablation after the proliferative window but at that stage the cell migration already started. As an alternative, a system like the nitro-reductase mediated cell ablation would be worth trying⁹³. Either way we need to ensure that no compensatory proliferation occurs.

5. Conclusion and future work

This research study served not only as a validation of the hypothesized KV cells fates by Cooper and D'Amico³⁴, but also allowed the assessment of these fates with cutting edge live imaging technologies. Was possible to understand that Kupffer's vesicle cells proliferate, die, migrate and incorporate structures in the zebrafish tail. Furthermore, it is in accordance with distinct left-right organizers of other model organisms.

In spite of all the information added to the previous knowledge about the KV, still many questions remain unanswered. For instances, *what is the function of these cells in the structures they incorporate? Will these cells be important for the embryo development from Prim-5 stage on? Once they are expected to have a role in signalling the surrounding cells, how do these cells influence the cells around?*

To elucidate the fates of the KV cells more molecular markers should be tested. For somite incorporation analysis a targeted live imaging and markers would be a good approach. While for ventral cells analysis a different mounting should be tried, as well as regeneration studies once these cells removed.

The proliferation and death assay should be repeated for some time points to increase the results confidence and the cilia motility needs to be assessed.

To clarify the KV contributions and interactions between cells, knowing that laser ablation does not work at this stages and deepness, could be executed the nitroreductase-mediated cell ablation⁹³ or using the CellTram, suction of the precursors of Kupffer's vesicle cells.



References

1. Gilbert, S. F. *Developmental Biology*. (2008).
2. Wolpert, L. & Tickle, C. *Principles of Development*. (2011).
3. Gilbert, S. F. *Developmental Biology*. (Sinauer Associates, 2000). at <http://www.ncbi.nlm.nih.gov/books/NBK10052/>
4. Mondal, P. Notes on Embryonic Development in Human. at <http://www.yourarticlelibrary.com/biology/notes-on-embryonic-development-in-human-explained/11891/#comment-10822>
5. Solnica-Krezel, L. Conserved patterns of cell movements during vertebrate gastrulation. *Curr. Biol.* **15**, 213–228 (2005).
6. Huang, X. & Saint-Jeannet, J.-P. Induction of neural crest and opportunities of life on the edge. *Dev. Biol.* **275**, 1–11 (2004).
7. Wheeler, G. N. & Brändli, A. W. Simple vertebrate models for chemical genetics and drug discovery screens: lessons from zebrafish and *Xenopus*. *Dev. Dyn.* **238**, 1287–308 (2009).
8. Kimmel, C. B., Warga, R. M. & Schilling, T. F. Origin and organization of the zebrafish fate map. *Development* **108**, 581–594 (1990).
9. Warga, R. M. & Nüsslein-Volhard, C. Origin and development of the zebrafish endoderm. *Development* **126**, 827–838 (1999).
10. Melby, a E., Warga, R. M. & Kimmel, C. B. Specification of cell fates at the dorsal margin of the zebrafish gastrula. *Development* **122**, 2225–37 (1996).

11. Hikasa, H. & Sokol, S. Y. Wnt signaling in vertebrate axis specification. *Cold Spring Harb. Perspect. Biol.* **5**, (2013).
12. Cleaver, O., Seufert, D. W. & Krieg, P. a. Endoderm patterning by the notochord: development of the hypochord in *Xenopus*. *Development* **127**, 869–879 (2000).
13. Amerongen, R. Van *et al.* Frat is dispensable for canonical Wnt signaling in mammals service Frat is dispensable for canonical Wnt signaling in mammals. *Genes Dev.* 425–430 (2005). doi:10.1101/gad.326705
14. Fliegauf, M., Benzing, T. & Omran, H. When cilia go bad: cilia defects and ciliopathies. *Nat. Rev. Mol. Cell Biol.* **8**, 880–893 (2007).
15. Nonaka, S., Shiratori, H., Saijoh, Y. & Hamada, H. Determination of left-right patterning of the mouse embryo by artificial nodal flow. *Nature* **418**, 96–99 (2002).
16. Rogers, L. J., Zucca, P. & Vallortigara, G. Advantages of having a lateralized brain. *Proc. Biol. Sci.* **271 Suppl** , S420–S422 (2004).
17. Blum, M., Feistel, K., Thumberger, T. & Schweickert, A. The evolution and conservation of left-right patterning mechanisms. *Development* **141**, 1603–13 (2014).
18. Collins, M. M. & Ryan, A. K. Are there conserved roles for the extracellular matrix, cilia, and junctional complexes in left-right patterning? *Genesis* **52**, 488–502 (2014).
19. Hirokawa, N., Tanaka, Y. & Okada, Y. Cilia, KIF3 molecular motor and nodal flow. *Curr. Opin. Cell Biol.* **24**, 31–39 (2012).
20. Meinhardt, H. & Gierer, A. Pattern formation by local self-activation and lateral inhibition. *BioEssays* **22**, 753–760 (2000).
21. Nakamura, T. *et al.* Generation of robust Left-Right asymmetry in mouse embryo requires Self-Enhancement and Lateral-Inhibition System. *Dev. Cell* **11**, 495–504 (2006).
22. Mendes, R. V., Martins, G. G., Cristovão, A. M. & Saúde, L. N-cadherin locks left-right asymmetry by ending the leftward movement of hensen's node cells. *Dev. Cell* **30**, 353–360 (2014).
23. Nakamura, T. & Hamada, H. Left-right patterning: conserved and divergent mechanisms. *Development* **139**, 3257–3262 (2012).
24. Nonaka, S. *et al.* Randomization of left-right asymmetry due to loss of nodal cilia generating leftward flow of extraembryonic fluid in mice lacking KIF3B motor protein. *Cell* **95**, 829–837 (1998).

25. Okada, Y., Takeda, S., Tanaka, Y., Belmonte, J. C. I. & Hirokawa, N. Mechanism of nodal flow: A conserved symmetry breaking event in left-right axis determination. *Cell* **121**, 633–644 (2005).
26. McGrath, J., Somlo, S., Makova, S., Tian, X. & Brueckner, M. Two populations of node monocilia initiate LR asymmetry in mouse. *Cell* **114**, 61–73 (2003).
27. Powles-Glover, N. Cilia and ciliopathies: Classic examples linking phenotype and genotype—An overview. *Reprod. Toxicol.* (2014). doi:10.1016/j.reprotox.2014.05.005
28. Manojlovic, Z., Earwood, R., Kato, A., Stefanovic, B. & Kato, Y. RFX7 is required for the formation of cilia in the neural tube. *Mech. Dev.* **132**, 28–37 (2014).
29. Kinder, S. J. *et al.* The organizer of the mouse gastrula is composed of a dynamic population of progenitor cells for the axial mesoderm. *Development* **128**, 3623–3634 (2001).
30. Sulik, K. *et al.* Morphogenesis of the murine node and notochordal plate. *Dev. Dyn.* **201**, 260–278 (1994).
31. Beddington, R. S. Induction of a second neural axis by the mouse node. *Development* **120**, 613–620 (1994).
32. Selleck, M. a & Stern, C. D. Fate mapping and cell lineage analysis of Hensen’s node in the chick embryo. *Development* **112**, 615–626 (1991).
33. Shook, D. R., Majer, C. & Keller, R. Pattern and morphogenesis of presumptive superficial mesoderm in two closely related species, *Xenopus laevis* and *Xenopus tropicalis*. *Dev. Biol.* **270**, 163–185 (2004).
34. Cooper, M. S. & D’Amico, L. a. A cluster of noninvoluting endocytic cells at the margin of the zebrafish blastoderm marks the site of embryonic shield formation. *Dev. Biol.* **180**, 184–98 (1996).
35. Oteíza, P., Köppen, M., Concha, M. L. & Heisenberg, C.-P. Origin and shaping of the laterality organ in zebrafish. *Development* **135**, 2807–13 (2008).
36. Holmdahl, D. E. Experimentelle Untersuchungen über die Lage der Grenze primärer und sekundärer Körperentwicklung beim Huhn. *Anat. Anz.* **59**, 393–396 (1925).
37. Pasteels, J. Proliférations et croissance dans la gastrulation et la formation de la queue des Vertébrés. *Arch. Biol.* **54**, 1–51 (1943).
38. Kanki, J. P. & Ho, R. K. The development of the posterior body in zebrafish. *Development* **124**, 881–93 (1997).

39. Takada, S. *et al.* Wnt-3a regulates somites and tailbud formation in the mouse embryo. *Genes Dev.* **8**, 174–189 (1994).
40. Stemple, D. L. Structure and function of the notochord: an essential organ for chordate development. *Development* **132**, 2503–12 (2005).
41. Talbot, W. S. *et al.* A homeobox gene essential for zebrafish notochord development. *Nature* **378**, 150–157 (1995).
42. Sausedo, R. a & Schoenwolf, G. C. Cell behaviors underlying notochord formation and extension in avian embryos: quantitative and immunocytochemical studies. *Anat. Rec.* **237**, 58–70 (1993).
43. Gont, L. K., Steinbeisser, H., Blumberg, B. & de Robertis, E. M. Tail formation as a continuation of gastrulation: the multiple cell populations of the *Xenopus* tailbud derive from the late blastopore lip. *Development* **119**, 991–1004 (1993).
44. Amacher, S. L., Draper, B. W., Summers, B. R. & Kimmel, C. B. The zebrafish T-box genes *no tail* and *spadetail* are required for development of trunk and tail mesoderm and medial floor plate. *Development* **129**, 3311–3323 (2002).
45. McCann, M. R., Tamplin, O. J., Rossant, J. & Seguin, C. a. Tracing notochord-derived cells using a *Noto-cre* mouse: implications for intervertebral disc development. *Dis. Model. Mech.* **5**, 73–82 (2012).
46. Bensimon-Brito, A., Cardeira, J., Cancela, L., Huysseune, A. & Witten, E. Distinct patterns of notochord mineralization in zebrafish coincide with the localization of Osteocalcin isoform 1 during early vertebral centra formation. *BMC Dev. Biol.* **12**, 28 (2012).
47. Bočina, I., Ljubešić Nikola, N. & Saraga-Babić, M. Cilia-like structures anchor the amphioxus notochord to its sheath. *Acta Histochem.* **113**, 49–52 (2011).
48. Palmeirim, I., Henrique, D., Ish-Horowicz, D. & Pourquié, O. Avian hairy gene expression identifies a molecular clock linked to vertebrate segmentation and somitogenesis. *Cell* **91**, 639–648 (1997).
49. Tenin, G. *et al.* The chick somitogenesis oscillator is arrested before all paraxial mesoderm is segmented into somites. *BMC Dev. Biol.* **10**, 24 (2010).
50. Clarke, J. Role of polarized cell divisions in zebrafish neural tube formation. *Curr. Opin. Neurobiol.* **19**, 134–138 (2009).
51. Cruz, C. *et al.* *Foxj1* regulates floor plate cilia architecture and modifies the response of cells to sonic hedgehog signalling. *Development* **137**, 4271–4282 (2010).

52. Latimer, A. J., Dong, X., Markov, Y. & Appel, B. Delta-Notch signaling induces hypochord development in zebrafish. *Development* **129**, 2555–2563 (2002).
53. Latimer, A. J. & Appel, B. Notch signaling regulates midline cell specification and proliferation in zebrafish. *Dev. Biol.* **298**, 392–402 (2006).
54. Shih, J. & Fraser, S. E. Characterizing the zebrafish organizer: microsurgical analysis at the early-shield stage. *Development* **122**, 1313–1322 (1996).
55. Eriksson, J. & Löfberg, J. Development of the hypochord and dorsal aorta in the zebrafish embryo (*Danio rerio*). *J. Morphol.* **244**, 167–176 (2000).
56. Wloga, D. *et al.* TTLL3 Is a Tubulin Glycine Ligase that Regulates the Assembly of Cilia. *Dev. Cell* **16**, 867–876 (2009).
57. Löfberg, J. & Collazo, A. Hypochord, an enigmatic embryonic structure: Study of the axolotl embryo. *J. Morphol.* **232**, 57–66 (1997).
58. Yamashita, M. Apoptosis in zebrafish development. *Comp. Biochem. Physiol. - B Biochem. Mol. Biol.* **136**, 731–742 (2003).
59. Cole, L. K. & Ross, L. S. Apoptosis in the developing zebrafish embryo. *Dev. Biol.* **240**, 123–142 (2001).
60. Westerfield. Westerfield, 2000. The Zebrafish Book. A Guide for the Laboratory Use of Zebrafish (*Danio rerio*). *Zebrafish Book. A Guid. Lab. Use Zebrafish (Danio rerio)* (2000). at <<http://zfin.org/ZDB-PUB-101222-52>>
61. Kimmel, C. B., Ballard, W. W., Kimmel, S. R., Ullmann, B. & Schilling, T. F. Stages of embryonic development of the zebrafish. *Dev. Dyn.* **203**, 253–310 (1995).
62. Caron, A., Xu, X. & Lin, X. Wnt/ β -catenin signaling directly regulates Foxj1 expression and ciliogenesis in zebrafish Kupffer's vesicle. *Development* **139**, 514–24 (2012).
63. Cooper, M. S. *et al.* Visualizing morphogenesis in transgenic zebrafish embryos using BODIPY TR methyl ester dye as a vital counterstain for GFP. *Dev. Dyn.* **232**, 359–368 (2005).
64. Thisse, C. & Thisse, B. High-resolution in situ hybridization to whole-mount zebrafish embryos. *Nat. Protoc.* **3**, 59–69 (2008).
65. Schulte-Merker, S., van Eeden, F. J., Halpern, M. E., Kimmel, C. B. & Nüsslein-Volhard, C. no tail (ntl) is the zebrafish homologue of the mouse T (Brachyury) gene. *Development* **120**, 1009–1015 (1994).

66. Essner, J. J., Amack, J. D., Nyholm, M. K., Harris, E. B. & Yost, H. J. Kupffer's vesicle is a ciliated organ of asymmetry in the zebrafish embryo that initiates left-right development of the brain, heart and gut. *Development* **132**, 1247–60 (2005).
67. Yan, Y. L., Hatta, K., Riggleman, B. & Postlethwait, J. H. Expression of a type II collagen gene in the zebrafish embryonic axis. *Dev. Dyn.* **203**, 363–376 (1995).
68. Dal-Pra, S., Thisse, C. & Thisse, B. FoxA transcription factors are essential for the development of dorsal axial structures. *Dev. Biol.* **350**, 484–495 (2011).
69. Judith M. Neugebauer, Amack, J. D., Peterson, A. G., Bisgrove, B. W. & H. Joseph Yost. FGF signalling during embryo development regulates cilia length in diverse epithelia. *Nat. Lett.* **458**, 651 – 655 (2009).
70. Yu, X., Ng, C. P., Habacher, H. & Roy, S. Foxj1 transcription factors are master regulators of the motile ciliogenic program. *Nat. Genet.* **40**, 1445–53 (2008).
71. Fior, R. *et al.* The differentiation and movement of presomitic mesoderm progenitor cells are controlled by Mesogenin 1. *Development* **139**, 4656–65 (2012).
72. Sampaio, P., Rafael, P. & Almeida, M. De. Using cilia mutants to study left-right asymmetry in zebrafish. (2014).
73. Thisse, B. & Thisse, C. Fast Release Clones: A High Throughput Expression Analysis. *ZFIN Direct Data Submiss.* (<http://zfin.org>). (2004).
74. Krauss, S., Concordet, J.-P. & Ingham, P. W. A functionally conserved homolog of the Drosophila segment polarity gene hh is expressed in tissues with polarizing activity in zebrafish embryos. *Cell* **75**, 1431–1444 (1993).
75. Kisielewska, J., Lu, P. & Whitaker, M. GFP-PCNA as an S-phase marker in embryos during the first and subsequent cell cycles. *Biol. Cell* **97**, 221–229 (2005).
76. Sampaio, P. *et al.* Left-right organizer flow dynamics: how much cilia activity reliably yields laterality? *Dev. Cell* **29**, 716–28 (2014).
77. Mizoguchi, T., Verkade, H., Heath, J. K., Kuroiwa, A. & Kikuchi, Y. Sdf1/Cxcr4 signaling controls the dorsal migration of endodermal cells during zebrafish gastrulation. *Development* **135**, 2521–2529 (2008).
78. Cambray, N. & Wilson, V. Axial progenitors with extensive potency are localised to the mouse chordoneural hinge. *Development* **129**, 4855–4866 (2002).
79. Teillet, M. a, Lapointe, F. & Le Douarin, N. M. The relationships between notochord and floor plate in vertebrate development revisited. *Proc. Natl. Acad. Sci. U. S. A.* **95**, 11733–11738 (1998).

80. Gansner, J. M., Mendelsohn, B. a., Hultman, K. a., Johnson, S. L. & Gitlin, J. D. Essential role of lysyl oxidases in notochord development. *Dev. Biol.* **307**, 202–213 (2007).
81. Odenthal, J., van Eeden, F. J., Haffter, P., Ingham, P. W. & Nüsslein-Volhard, C. Two distinct cell populations in the floor plate of the zebrafish are induced by different pathways. *Dev. Biol.* **219**, 350–363 (2000).
82. Patten, I., Kulesa, P., Shen, M. M., Fraser, S. & Placzek, M. Distinct modes of floor plate induction in the chick embryo. *Development* **130**, 4809–4821 (2003).
83. Yoshinari, N. & Kawakami, A. Mature and juvenile tissue models of regeneration in small fish species. *Biol. Bull.* **221**, 62–78 (2011).
84. Geraudie, J., Monnot, M. J., Brulfert, a. & Ferretti, P. Caudal fin regeneration in wild type and long-fin mutant zebrafish is affected by retinoic acid. *Int. J. Dev. Biol.* **39**, 373–381 (1995).
85. Lee, R. T. H., Knapik, E. W., Thiery, J. P. & Carney, T. J. An exclusively mesodermal origin of fin mesenchyme demonstrates that zebrafish trunk neural crest does not generate ectomesenchyme. *Development* **140**, 2923–32 (2013).
86. Freund, J. B., Goetz, J. G., Hill, K. L. & Vermot, J. Fluid flows and forces in development: functions, features and biophysical principles. *Development* **139**, 3063–3063 (2012).
87. Tian, T., Zhao, L., Zhang, M., Zhao, X. & Meng, A. Both foxj1a and foxj1b are implicated in left-right asymmetric development in zebrafish embryos. *Biochem. Biophys. Res. Commun.* **380**, 537–42 (2009).
88. Clontech Laboratories, I. *Living Colors - User Manual*. **1**, (2005).
89. Wang, W., Wu, T. & Kirschner, M. W. The master cell cycle regulator APC-Cdc20 regulates ciliary length and disassembly of the primary cilium. *Elife* **3**, 1–12 (2014).
90. Rojo, C. & González, E. Apoptosis in zebrafish embryos: removing cells from inappropriate locations. *Zebrafish* **5**, 25–37 (2008).
91. Van Ham, T. J., Mapes, J., Kokel, D. & Peterson, R. T. Live imaging of apoptotic cells in zebrafish. *FASEB J.* **24**, 4336–42 (2010).
92. Kramer-Zucker, A. G. *et al.* Cilia-driven fluid flow in the zebrafish pronephros, brain and Kupffer's vesicle is required for normal organogenesis. *Development* **132**, 1907–1921 (2005).
93. Curado, S., Stainier, D. & Anderson, R. Nitroreductase-mediated cell/tissue ablation in zebrafish: a spatially and temporally controlled ablation method with applications in developmental and regeneration studies. *Nat. Protoc.* **3**, 948–954 (2008).

94. A comprehensive approach to Life Science. *Univ. T* (2011). at <<http://csIs-text3.c.u-tokyo.ac.jp/inactive/allcontents.html>>
95. Leigh, M. W. *et al.* Clinical and genetic aspects of primary ciliary dyskinesia/Kartagener syndrome. *Genet. Med.* **11**, 473–487 (2009).
96. Patel, A. & Honoré, E. Polycystins and renovascular mechanosensory transduction. *Nat. Rev. Nephrol.* **6**, 530–8 (2010).
97. Amack, J. D., Wang, X. & Yost, H. J. Two T-box genes play independent and cooperative roles to regulate morphogenesis of ciliated Kupffer's vesicle in zebrafish. *Dev. Biol.* **310**, 196–210 (2007).



Appendix

Appendix A

Fiji Macro

```
print("\\Clear");
dir = getDirectory("Choose directory to save images: ");

for (i=1; i<=nImages; i++) {
    selectImage(i);
    //title = File.nameWithoutExtension();
    title = getTitle();
    pos = indexOf(title, ".");
    new_title = substring(title, 0, pos);
    print(title);
    print(new_title+" T = "+i);
    saveAs("Tiff", dir+"\\ "+new_title+" T = "+i+"");
    close(title);
}
//run("Close All");
```

Appendix B

Cilia Length Histograms

